UNIVERSITY OF CALIFORNIA,
IRVINE

Visualizing Calcium Dynamics in the Regulation of T Lymphocyte Motility and Activation

DISSERTATION

submitted in partial satisfaction of the requirements
for the degree of

DOCTOR OF PHILOSOPHY

in Biomedical Sciences

by

Tobias Xiao Dong

Dissertation Committee:
Professor Michael D. Cahalan, Chair
Professor Ian Parker
Professor Albert Zlotnik
Professor Edwin S. Monuki
Professor Grant MacGregor

2017

DEDICATION

To my family.

My parents,
for instilling in me a passion for the intellectual pursuit of scientific knowledge,
for all the sacrifices they have made selflessly,
and for all the obstacles they have overcome,
just to provide the best they could for my brother and I.

And my brother, little Jack,
for always giving me a reason to be better,
so I can be a worthy big brother for you to look up to,
(and set high standards for you).

TABLE OF CONTENTS

LIST OF FIGURES

Page

ACKNOWLEDGMENTS

I would like to express my deepest gratitude to my thesis advisor, Dr. Michael Cahalan, for all his support and guidance during my time in the lab. I have always admired his tireless passion for science, and his constant excitement for immunoimaging has been contagious and rejuvenating. His mentorship has provided me with invaluable experience as a future physician scientist.

I would like to thank my committee members, Dr. Ian Parker, Dr. Albert Zlotnik, Dr. Edwin Monuki, and Dr. Grant MacGregor, for all their time and contributions, even on the shortest of notices. Dr. Parker has been an irreplaceable source of expertise, and many of our imaging studies would not have been possible without him. Dr. Zlotnik has been a refreshing presence, and never hesitated to ask the tough questions. Dr. Monuki's wisdom and insight have been an integral part of my training as a physician scientist. And finally, without Dr. MacGregor's transgenic expertise, the Salsa6f mouse would not even exist.

I most graciously thank all past and current members of the Cahalan lab, for they have been like a family to me. Thanks to Dr. Sabrina Leverrier and Dr. Ying Yu for their initial work on T cell motility. Thanks to Dr. Melanie Matheu for her friendly energy and vital guidance in training me during the start of my time in the lab. Thanks to Dr. Lu Forrest and Dr. Olga Safrina for being the lab moms and for always helping me learn new techniques. Thanks to Dr. Milton Greenberg for being a close friend, a valuable colleague, and even now a constant source of mentorship. Thanks to Dr. Anna Amcheslavsky for your friendly presence and all your help with molecular biology. Thanks to Dr. Andy Yeromin and Dr. Joseph Dynes for being invaluable sources of scientific advice and technical assistance, both of you have saved me from despair countless times. A special thanks to Dr. Shiva Othy for literally everything, from scientific discussions to food runs. Thanks to Dr. Jonathan Skupsky for all your advice and wisdom as a physician scientist. Thanks to Dr. Amit Jairaman for your welcome new energy in the lab. And lastly, thanks to Angel Zavala for being MVP taking care of all my mice issues.

I thank the Department of Physiology and Biophysics, the Institute of Immunology, and the Medical Scientist Training Program at UC Irvine for providing an exceptionally nurturing scientific environment for my graduate research education. A special thanks to my classmates in the department, Clinton Yu, Lisa Baik, Dr. Logan Roberts, and Dr. Galina Schmunk for that special bond we shared.

I would like to thank the UCI Transgenic Mouse Facility, Jon Neumann, Tom Fielder, Shuling Wang, and Kai-Xuan Shi for all your repeated efforts to bring the Salsa6f mouse to life. I thank Dr. Audrey Gerard and the Max Krummel Lab at UCSF for so willingly teaching me the microchannel fabrication technique. I thank Dr. Hugh Bender and the Chris Hughes Lab at UCI for allowing me to use their equipment in microfabrication.

During these studies, I had the opportunity to use several types of microscopy including conventional epifluorescence imaging, TIRF microscopy, confocal microscopy, and two-photon microscopy. The world of microscopes is expanding and I have been fortunate to have access to a range of instrumentation that have made this work possible. I wish to once again express my profound gratitude to Dr. Parker and Dr. Dynes for their excellent help.

I thank all my friends who have supported me through this long and difficult journey. You have dealt with all my struggles and listened to all my sorrows, asking for nothing in return and yet giving me endless laughter, good food, your company, and warm memories to keep me going. There are too many of you to name but know that every single one of you has helped in getting me to where I am today. A particular thanks to the Prototypes and the Corps Dance Crew, for your existences have constantly given me a place to destress and renew my energy. I feel like my whole life these past few years has been nothing but either late nights in lab or late nights in parking lots and studios with you guys.

And once again, I would like to thank my family. Words cannot describe what you mean to me, and I truly could not have come this far without your constant love and support. You have raised me well, and I am who I am because of you.

CURRICULUM VITAE

Tobias Xiao Dong

EDUCATION

Ph.D. in Biomedical Sciences 2017	**University of California, Irvine** Department of Physiology and Biophysics
B.S. in Biochemistry and Cell Biology 2009	**University of California, San Diego** Division of Biological Sciences
B.A. in Psychology 2009	**University of California, San Diego** Department of Psychology

RESEARCH EXPERIENCE

Graduate Student Researcher 2011-2017	**University of California, Irvine** Cahalan Lab
Undergraduate Research Assistant 2006-2010	**University of California, San Diego** Dong Lab

SELECT HONORS AND AWARDS

1st Place Poster Award 2016	**American Physician Scientist Assoc. West Regional Meeting** University of Southern California
3rd Place Poster Award 2014	**XII Immunology Fair** University of California, Irvine
AAI Young Investigator Award 2014	**40th La Jolla Immunology Conference** Salk Institute, San Diego
3rd Place Poster Award 2013	**XI Immunology Fair** University of California, Irvine

JOURNAL PUBLICATIONS

Dong, T. X., Greenberg, M. L., Leverrier, S., Yu, Y., Parker, I., Dynes, J. L., Cahalan, M. D. Cell-intrinsic activation of Orai1 regulates human T cell motility. (Manuscript under review in *eLife*).

Tang, B., Chow, J. Y., **Dong, T. X.**, Yang, S. M., Lu, D. S., Carethers, J. M., & Dong, H. (2016). Calcium sensing receptor suppresses human pancreatic tumorigenesis through a novel NCX1/Ca^{2+}/beta-catenin signaling pathway. *Cancer Lett*. 377(1), 44-54.

Matheu, M. P., Othy, S., Greenberg, M. L., **Dong, T. X.**, Schuijs, M., Deswarte, K., Hammad, H., Lambrecht, B. N., Parker, I., Cahalan, M. D. (2015). Imaging regulatory T cell dynamics and CTLA4-mediated suppression of T cell priming*. Nat Commun*. 6: 6219.

Xie, R., **Dong, X.**, Wong, C., Vallon, V., Tang, B., Sun, J., Yang, S., Dong, H. (2014). Molecular Mechanisms of CaSR-mediated Calcium Signaling in Modulation of Epithelial Ion Transport and Bicarbonate Secretion. *J Biol Chem*. 289(50):34642-53.

Tuo, B., Wen, G., Wei, J., Liu, X., Wang, X., Zhang, Y., Wu, H., **Dong, X.**, Chow, J. Y., Vallon, V., Dong, H. (2011). Estrogen regulation of duodenal bicarbonate secretion and sex-specific protection of human duodenum. *Gastroenterology* 141(3), 854-863.

Chow, J. Y., Estrema, C., Orneles, T., **Dong, X.**, Barrett, K. E., & Dong, H. (2011). Calcium-sensing receptor modulates extracellular Ca^{2+} entry via TRPC-encoded receptor-operated channels in human aortic smooth muscle cells. *Am J Physiol Cell Physiol*. 301(2), C461-468.

Dong, X., Ko, K. H., Chow, J., Tuo, B., Barrett, K. E., & Dong, H. (2011). Expression of acid-sensing ion channels in intestinal epithelial cells and their role in the regulation of duodenal mucosal bicarbonate secretion. *Acta Physiol (Oxf).* 201(1), 97-107.

Dong, X., Smoll, E. J., Ko, K. H., Lee, J., Chow, J. Y., Kim, H. D., Insel, P. A., Dong, H. (2009). P2Y receptors mediate Ca^{2+} signaling in duodenocytes and contribute to duodenal mucosal bicarbonate secretion. *Am J Physiol Gastrointest Liver Physiol*. 296(2), G424-432.

Smith, A., Contreras, C., Ko, K. H., Chow, J., **Dong, X.**, Tuo, B., Zhang, H. H., Chen, D. B., Dong, H. (2008). Gender-specific protection of estrogen against gastric acid-induced duodenal injury: stimulation of duodenal mucosal bicarbonate secretion. *Endocrinology*. 149(9), 4554-4566.

CONFERENCE PUBLICATIONS

Dong, T. X., Greenberg, M. L., Leverrier, S., Yu, Y., Parker, I., Cahalan, M. D. *Orai1 modulates steady-state human T cell scanning behavior during amoeboid motility.* Poster session

presented at the 2016 West Regional Meeting of the American Physician Scientists Association, Los Angeles, CA, December 2016.

Dong, T. X, Greenberg, M. L., Leverrier, S., Yu, Y., Parker, I., Cahalan, M. D. *Orai1 modulates intrinsic human T cell scanning behavior during amoeboid motility.* Oral presentation at the 2016 UC Irvine Immunology Fair, Irvine, CA, December 2016.

Dong, T. X., Greenberg, M. L., Leverrier, S., Yu, Y., Parker, I., Cahalan, M. D. *Orai1 modulates steady-state human T cell scanning behavior during amoeboid motility.* Poster session presented at the 2016 UC Irvine Immunology Fair, Irvine, CA, December 2016.

Dong, T. X., Greenberg, M. L., Leverrier, S., Yu, Y., Parker, I., Cahalan, M. D. *Orai1 modulates steady-state human T cell scanning behavior during amoeboid motility.* Poster session presented at the 2016 La Jolla Immunology Conference, La Jolla, CA, October 2016.

Dong, T. X., Greenberg, M. L., Dynes, J. L., Cahalan, M. D. *A Toolkit for Ca^{2+} Imaging of T Cell Activation and Suppression*. Poster session presented at the 2015 UC Irvine Immunology Fair, Irvine, CA, December 2015.

Dong, X., Greenberg, M. L., Dynes, J. L., Cahalan, M. D. *A Toolkit for Ca^{2+} Imaging of T Cell Activation and Suppression*. Poster session presented at the 2014 UC Irvine Immunology Fair, Irvine, CA, November 2014.

Dong, X., Greenberg, M. L., Dynes, J. L., Cahalan, M. D. *A Toolkit for Ca^{2+} Imaging of T Cell Activation and Suppression*. Poster session presented at the 2014 La Jolla Immunology Conference, La Jolla, CA, September 2014.

Dong, X., Greenberg, M. L., Cahalan, M. D. *A Novel* In Vivo *Model for Ca^{2+} Imaging in T Cells.* Poster session presented at the 2013 UC Irvine Immunology Fair, Irvine, CA, November 2013.

Dong, X., Wong, C., Estrema, C., Tuo, B., Dong, H. *Ca-Sensing Receptor Regulates Ca^{2+}-Mediated Duodenal Bicarbonate Secretion via SOC and I_{KCa} Channels*. Oral presentation at Digestive Diseases Week 2012, New Orleans, LA, May 2012.

Dong, X., Ko, K.H., Jones, R., Chow, J., Barrett, K. E., Dong H. *Expression and function of acid-sensing ion channels in intestinal epithelial cells.* Poster session presented at Digestive Diseases Week 2008, San Diego, CA, May 2008.

ABSTRACT OF THE DISSERTATION

Visualizing Calcium Dynamics in the Regulation of T Lymphocyte Motility and Activation

By

Tobias Xiao Dong

Doctor of Philosophy in Biomedical Sciences

University of California, Irvine, 2017

Professor Michael D. Cahalan, Chair

Calcium is a ubiquitous cellular messenger that is essential in regulating a wide variety of functions in living organisms. Our understanding of Ca^{2+} signaling was first made possible by the use of synthetic small-molecule Ca^{2+} indicators to visualize Ca^{2+} dynamics within live cells. The subsequent development of genetically encoded Ca^{2+} indicators opened up new possibilities for *in vivo* monitoring of Ca^{2+} signaling, but until recently, the performance of these genetic indicators has always fallen behind those of small-molecule indicators. With the goal of developing new and improved options for Ca^{2+} imaging studies, we have created a transgenic reporter mouse expressing a novel ratiometric genetically encoded Ca^{+} indicator, and applied it to the study of T lymphocyte motility and activation.

First, I describe the development of a novel ratiometric genetically encoded Ca^{2+} indicator, named "Salsa6f", and demonstrate its use to monitor either cytosolic or near-membrane local Ca^{2+} signaling. Two-photon imaging is utilized to ensure functionality of Salsa6f in future *in vivo* studies. Salsa6f and a dominant-negative Orai1 mutant are then

used to investigate the mechanism of Orai1-regulated stop-and-go T cell motility. Microfabricated channels are used in an *in vitro* assay that replicates the confined environmental conditions experienced by T cells *in vivo* in densely packed lymph nodes. I then describe the development of a transgenic mouse to express Salsa6f in a tissue-specific manner for *in vivo* studies of Ca^{2+} signaling in the immune and nervous systems. Lastly, I present two-photon imaging of cellular dynamics within mouse intact lymph node to study unperturbed, endogenous Tregs interacting with conventional T cells and dendritic cells. We demonstrate the crucial involvement of CTLA-4 in determining cellular dynamics among Tregs, conventional T cells, and dendritic cells *in vivo*. I also lay the groundwork for future *in vivo* studies utilizing transgenic reporter mice expressing genetically encoded Ca^{2+} indicators to study the Treg-mediated suppression of Ca^{2+} signaling in activating conventional T cells.

CHAPTER 1: Introduction

1.1 Calcium signaling

1.1.1 Evolution of calcium as a signaling molecule

Cellular signaling is crucial for survival, as cells must signal in response to constant changes in their environment. Such signaling relies on molecular messengers whose concentration and localization can be precisely varied with time. In cells of living organisms, the role of cellular signaling is dominated by calcium ions (Ca^{2+}) and phosphate ions. As universal tools of signal transduction, Ca^{2+} binding to or phosphorylation of target proteins confers changes in charge and shape, altering protein function and interactions.

As a divalent cation in water, Ca^{2+} is coordinated by oxygen atoms from surrounding water molecules, which rapidly exchange as Ca^{2+} is the fastest binding agent of any available divalent ion, reacting 1000-fold faster than Mg^{2+} (Williams 2006). However, Ca^{2+} readily forms precipitates with organic anions, such as phosphate, and in order to prevent this undesired outcome, cells initially evolved to actively remove Ca^{2+} from the cytosol. This continuous extrusion of Ca^{2+} resulted in a huge electrochemical gradient across the plasma membrane (PM), providing a driving force for Ca^{2+} entry that cells then evolved to utilize as a signaling mechanism. The fast kinetics of Ca^{2+} entry combined with its unique binding properties allowed Ca^{2+} to become an essential second messenger in coordinating intracellular events.

In eukaryotic cells, Ca^{2+} plays a universal role in regulating numerous cellular functions. Ca^{2+} signaling triggers vastly different responses in a wide variety of cell types, from neurotransmitter release in synaptic terminals, to contraction in skeletal muscle cells, to fertilization in mammalian zygotes, to differentiation of cell types in the developing embryo, to gene transcription in activating immune cells, and even to the opposing cell fates of proliferation and apoptosis (Berridge et al. 2000). This versatility arises from an array of molecular components – transporters, pumps, ion channels, buffers, Ca^{2+}-binding effectors – used by different cell types to create a wide variability in the spatial and temporal profiles of individual Ca^{2+} signals (Berridge et al. 2003). Unlike complex molecules, Ca^{2+} cannot be chemically altered, so in order to control its spatial and temporal dynamics, nature has evolved many methods to chelate, compartmentalize, or direct the flow of Ca^{2+} within cells (Clapham 2007).

1.1.2 Ca^{2+} buffers and binding proteins

Cytosolic Ca^{2+} concentration is usually maintained at ~100 nM, but up to 99% of the total Ca^{2+} load is captured by a variety of Ca^{2+} binding proteins (CBPs), which act as physiological buffers as well as chaperones for Ca^{2+} delivery and signal transduction (Neher and Augustine 1992; Belan et al. 1993). The classic protein Ca^{2+} chelator is the EF hand domain, named after the E and F regions of parvalbumin, a helix-turn-helix motif present in hundreds of CBPs (Nakayama and Kretsinger 1994; Lewit-Bentley and Rety 2000). Each EF hand holds a single Ca^{2+} ion using negatively charged oxygen atoms of carbonyl and carboxyl groups from a 12-13 amino acid loop flanked by two perpendicular

α helices (Kretsinger and Nockolds 1973). The wide variety of CBPs have Ca^{2+} affinities that vary over ~100,000-fold due to differences in critical amino acids in the EF hand and in side-chain packing of the protein core.

Some of the most important cytosolic Ca^{2+} buffer proteins are CBPs with EF hand domains, including parvalbumin, calmodulin, calcineurin, and S100 proteins. Calmodulin is perhaps the most famous of these, as much of what is known today about EF hand Ca^{2+} sensors is based on the extensive characterization and structural analysis of calmodulin. Composed of 148 amino acids, calmodulin is shaped like a dumbbell, containing two pairs of EF hands with distinct Ca^{2+} affinities joined by a flexible α helical linker. Ca^{2+} binding causes a conformational change in calmodulin that exposes hydrophobic surfaces, allowing interaction with amphipathic regions of target proteins and triggering calmodulin's Ca^{2+} sensor activity (Clapham 2007). There are over a hundred known protein targets of calmodulin, including myosin light chain kinase (MLCK), calmodulin dependent kinase II (CaMKII), several Ca^{2+}-activated ion channels, and a number of cytoskeletal proteins (Yanez et al. 2012). Thus, calmodulin functions not only as a Ca^{2+} buffer to modulate the diffusion of free Ca^{2+} in the cytosol, but also as a key mediator in amplifying changes in Ca^{2+} concentrations to changes in protein function, prolonging the effects of even brief Ca^{2+} signaling events.

There are also several important intracellular Ca^{2+} buffers that do not contain EF hand domains, including calreticulin, calsequestrin, and calnexin, which are important CBPs responsible for binding large reservoirs of Ca^{2+} within intracellular stores in the endoplasmic reticulum (ER) and the sarcoplasmic reticulum (SR), to be further discussed in

1.1.3. Calreticulin is of particular importance for maintaining ER Ca^{2+} homeostasis, although it also serves as a protein chaperone for misfolded proteins. The chaperone domain of calreticulin is formed by the N-terminal region that binds heavy metals, and the P-domain that binds Ca^{2+} with high-affinity (k_d = 1 μM) and low-capacity (1 mol Ca^{2+}/mol of protein) (Baksh and Michalak 1991). The C-terminal region of calreticulin is a Ca^{2+} binding domain of low-affinity ((k_d = 2 mM) and high-capacity (~20 mol Ca^{2+}/mol of protein), which accounts for the high capacity of ER Ca^{2+} stores, and lack of calreticulin has been shown to reduce ER Ca^{2+} capacity (Nakamura et al. 2001).

Another common Ca^{2+} binding motif is the C2 domain, consisting of ~120 amino acids that make up a common fold, eight-stranded antiparallel β sandwich connected by variable loops (Cho and Stahelin 2005). Most C2 domains bind two or three Ca^{2+} ions within three variable loops, resulting in a substantial change in electrostatic potential of the original protein. A resulting net positive charge would increase a protein's association with anionic membrane leaflets, such as the PM cytosolic surface, while a resulting net neutral charge may allow a protein to penetrate into the phospholipid bilayer. C2 domains are commonly found in signal transduction proteins that require PM association, such as protein kinase C (PKC) and phosphoinositide 3-kinase (PI3K).

1.1.3 Intracellular compartmentalization of Ca^{2+}

Ca^{2+} is actively removed from the cytosol by plasma membrane Ca^{2+}-ATPase (PMCA) pumps and Na^{+}/Ca^{2+} exchangers (NCX) that transport Ca^{2+} across the PM, while sarco-endoplasmic reticulum ATPase (SERCA) pumps move Ca^{2+} into the ER to refill internal Ca^{2+}

stores, usually kept in the hundreds of micromolar range. PMCA and SERCA pumps are high-affinity, low-capacity Ca^{2+} transporters that are effective at maintaining low cytosolic Ca^{2+} levels over long durations. Within intracellular stores, high-capacity and low-affinity CBPs such as calreticulin and calsequestrin hold a large reservoir of Ca^{2+} that can be rapidly released when needed. The ER serves as one of the principal sources of Ca^{2+} for signaling, and release of Ca^{2+} from internal stores is regulated by inositol-1,4,5-trisphosphate receptor (IP_3R) or ryanodine receptor (RYR) Ca^{2+} channels on the ER membrane.

Stimulation of G protein-coupled receptors (GPCRs) leading to phospholipase Cβ (PLCβ) activation, or stimulation of tyrosin-kinase receptors (TKRs) leading to phospholipase Cγ (PLCγ) activation, both lead to cleavage of phosphatidylinositol-4,5-bisphosphate (PIP_2) into inositol-1,4,5-trisphosphate (IP_3) and diacylglycerol (DAG). The cleaved IP_3 then binds to IP_3Rs on the ER membrane to trigger release of Ca^{2+} from internal stores, transiently elevating cytosolic Ca^{2+} levels to concentrations of up to ~1 μM. Although IP_3Rs are commonly known as Ca^{2+} channels, they are actually nonselective cation channels formed from homotetramers of ~3000 amino acids. Similar to IP_3Rs, RYRs are Ca^{2+} permeable channels formed form large 2.2 mDa tetramers on the ER or SR membrane. RYRs are activated by Ca^{2+} in the low μM range, while higher Ca^{2+} levels at the mouth of the channel inhibits gating and prevents Ca^{2+} overload. Both IP_3Rs and RYRs have multiple cytosolic binding sites allowing for interaction with protein regulators, such as calmodulin and CaMKII.

Another important intracellular compartment for controlling Ca^{2+} dynamics is the mitochondria, which acts as an additional Ca^{2+} buffer and contributes to regulation of both

Ca^{2+} release from the ER and extracellular Ca^{2+} entry. Mitochondria were the first intracellular organelles to be associated with Ca^{2+} accumulation, after Ca^{2+} uptake was directly measured in isolated energized mitochondria over half a century ago (Deluca and Engstrom 1961; Vasington and Murphy 1962). It is now appreciated that mitochondria are high capacity buffers of cytosolic Ca^{2+}, as elevations in mitochondrial Ca^{2+} levels closely follow elevations in the cytosol during Ca^{2+} signaling events, and peak Ca^{2+} levels within mitochondria can exceed 100 μM (Montero et al. 2000). Ca^{2+} readily permeates the outer mitochondrial membrane through abundantly expressed voltage-dependent anion channels (VDACs), then passes the inner mitochondrial membrane through the mitochondrial Ca^{2+} uniporter (MCU), a ruthenium red sensitive, highly selective, low conductance Ca^{2+} channel (Kirichok et al. 2004). Close proximity of mitochondria to sites of Ca^{2+} elevations allow for rapid mitochondrial uptake of Ca^{2+} despite the low Ca^{2+} affinity of the MCU. The intracellular positioning of mitochondria plays an important role in regulating Ca^{2+} signaling dynamics, as a large cluster of mitochondria in defined domains of polarized cells can form a fixed buffer to oppose diffusion of Ca^{2+} waves (De Stefani et al. 2016).

Specifically, ER-mitochondria junctions exist in regions of close apposition where Ca^{2+} release from the ER is immediately and preferentially taken up by mitochondria (Rizzuto et al. 1998). The mitochondrial protein mitofusin 2 (MFN2) has been associated with formation of ER-mitochondria junctions, as fibroblasts lacking MFN2 show increased distance between the ER and mitochondria, abnormally altered shape of both organelles, and reduced efficiency of mitochondrial Ca^{2+} uptake (de Brito and Scorrano 2008).

Furthermore, chaperone proteins such as the 75 kDa glucose-regulated protein (GRP75, also known as HSPA9) have been shown to functionally couple VDAC on the outer mitochondrial membrane with IP_3Rs on the ER surface (Szabadkai et al. 2006). Beyond regulating intracellular Ca^{2+} release, mitochondria have also been shown to regulate extracellular Ca^{2+} entry through the PM. In activating T lymphocytes, mitochondria accumulate next to active PM Ca^{2+} channels at the immunological synapse, buffering bulk cytosolic Ca^{2+} elevation (Hoth et al. 1997; Quintana et al. 2011). In both intracellular Ca^{2+} release and extracellular Ca^{2+} entry, mitochondrial Ca^{2+} uptake from the localized microdomain around the mouth of active Ca^{2+} channels prevent inactivation by high cytosolic Ca^{2+} levels, allowing for sustained Ca^{2+} signaling through open channels (Rizzuto et al. 2012).

The existence of various cytosolic Ca^{2+} buffers combined with the distributed nature of Ca^{2+} compartments restrict free Ca^{2+} ions from a Ca^{2+} signal to a localized microdomain around the entry site with a steep outward Ca^{2+} gradient. Any unbound Ca^{2+} ion is only free briefly before encountering an extrusion (PMCA), uptake (SERCA/MCU), or buffering mechanism (calmodulin). The time scale of intracellular Ca^{2+} signals ranges from microsecond transients for release of neurotransmitters, to integrated oscillations over hours and days for gene expression and cell proliferation. The speed at which Ca^{2+} pumps and transporters can clear elevated Ca^{2+} from the cytosol limits the duration of Ca^{2+} signals, while sustained Ca^{2+} entry allows for extended Ca^{2+} signals. On the other hand, spatial distribution of intracellular Ca^{2+} signals can range from “blips” and “puffs” that localize to nanodomains around individual ion channels or clusters of channels (Parker et al. 1996), to

global Ca^{2+} waves that sweep throughout the entire cytoplasm of the cell (Miyazaki et al. 1993). The ability of individual cells to assemble distinctive molecular pathways for Ca^{2+} mobilization and respond to Ca^{2+} signals based on variable spatiotemporal properties is, in part, what allows for coordinated cellular responses that constitute the life of multicellular organisms.

1.2 Tools for calcium imaging

Our current understanding of Ca^{2+} signaling in cellular function has been made possible by the use of Ca^{2+}-sensitive indicators to visualize the spatial and temporal dynamics of Ca^{2+} signals. The bioluminescent protein aequorin was the first Ca^{2+} indicator to be used in imaging experiments (**Figure 1.1**), where it was directly injected into single muscle fibers to follow the time course of intracellular Ca^{2+} release and reabsorption during muscle contraction (Ridgway and Ashley 1967). In squid giant synapse, aequorin was microinjected into the presynaptic terminal to demonstrate that Ca^{2+} entry into the presynaptic terminal triggers neurotransmitter release (Llinas et al. 1972; Llinas and Nicholson 1975). Isolated from the jellyfish *Aequorea*, aequorin produced bioluminescence in the presence of Ca^{2+} and required a chemical cofactor, coelenterazine, that was consumed in the process (Shimomura et al. 1962), which was not feasible for repeated measurements or long term experiments.

1.2.1 Synthetic small-molecule indicators

A breakthrough in the field of Ca^{2+} imaging came with the development of synthetic small-molecule fluorescent indicators, such as quin-2, fura-2, and indo-1 (Tsien et al. 1982; Grynkiewicz et al. 1985). These new Ca^{2+} indicators offered brighter fluorescence, improved Ca^{2+} sensitivity, and higher dynamic range for conditions where signal-to-noise ratio was a limiting factor. Small-molecule indicators also exhibited fast response kinetics, allowing for measurements of brief Ca^{2+} transients over very short time spans. Certain indicators, such as fura-2 and indo-1, demonstrated a shift in their excitation or emission spectra upon Ca^{2+} binding, allowing for ratiometric measurements that can be calibrated to provide absolute Ca^{2+} concentration. Ratiometric indicators provided an intrinsic normalization that accounts for variations in indicator concentration, cell thickness, photobleaching, and detector settings. Furthermore, acetoxymethylated (AM) ester forms of small-molecule indicators were membrane permeable and allowed for non-invasive cell loading (Tsien 1981), whereas newer analogs such as fura-PE3 resisted the rapid leakage and compartmentalization seen in previous small-molecule indicators (Vorndran et al. 1995). All these advantages contributed to their broad use, and even decades after they were first introduced, small molecule-indicators such as fura-2 are still routinely used in Ca^{2+} imaging studies.

The fast kinetics, sensitivity, and brightness of small-molecule Ca^{2+} indicators, when combined with high speed image acquisition, has enabled the detection of localized Ca^{2+} signals from small clusters of ion channels or even single channel activity (Parker et al. 1996; Demuro and Parker 2006). These experiments were performed with newer long-

wavelength fluorescent indicators, such as fluo-3 and fluo-4, which provided a greater change in fluorescence upon Ca^{2+} binding but lack ratiometric capability (Minta et al. 1989; Gee et al. 2000). Further improvements came with subsequent indicators such as Calcium Green and Oregon Green BAPTA-1 (OGB-1), which provided increased brightness, lower phototoxicity, and higher Ca^{2+} affinity for detecting small changes in Ca^{2+} near resting levels (Paredes et al. 2008). These advantages, combined with the compatibility of Calcium Green and OGB-1 for two-photon microscopy, made them ideal choices for imaging neuronal activity *in vivo* (Svoboda et al. 1997). Lastly, Calcium Green and OGB-1 remained uniformly distributed in the cytosol when incubated at 37°C, whereas under the same loading conditions fluo-3 and fluo-4 showed significant compartmentalization within the ER and mitochondria (Thomas et al. 2000). Dye compartmentalization is purposely relied upon when using Mag-fura-2 for specifically measuring Ca^{2+} levels within subcellular organelles, and remained the only method for studying mitochondrial Ca^{2+} dynamics until the later development of genetically targetable indicators.

1.2.2 Genetically encoded Ca^{2+} indicators

The next great advance in Ca^{2+} imaging studies was the realization that endogenously expressed fluorescent proteins such as variants of green fluorescent protein (GFP), could be made Ca^{2+}-sensitive by fusion with calmodulin and a target M13 peptide from myosin light chain kinase (Porumb et al. 1994). This led to the first genetically encoded Ca^{2+} indicators (GECIs), FIP-CB_{SM} and cameleon (**Figure 1.1**), which were Förster resonance energy transfer (FRET)-based fusion probes containing two fluorescent proteins, linked

together by calmodulin and M13 peptide (Miyawaki et al. 1997; Romoser et al. 1997). Binding to Ca^{2+} caused the calmodulin domain to interact with the M13 peptide, resulting in a conformational change and a measurable increase in FRET efficiency between the two flanking fluorescent proteins. There were several key advantages to GECIs that allowed for novel experimental approaches, as their genetically encoded nature enabled inclusion of additional elements into the peptide sequence, or for the entire indicator to be fused to other proteins (Perez Koldenkova and Nagai 2013).

Before the development of GECIs, the only method of measuring Ca^{2+} levels in subcellular organelles was by loading cells with small-molecule indicators, followed by incubation at 37°C to induce compartmentalization. This loading protocol for small-molecule indicators was often unreliable, resulting in variability of dye retention and undesirable background signal, as significant fluorescence remained in the cytosol, (Thomas et al. 2000). GECIs could be directly and selectively targeted to specific subcellular compartments with a signal sequence, such as the nuclear localization sequence PKKKRKVEDA at the C-terminus, four repeats of the cytochrome c oxidase signal sequence at the N-terminus (for mitochondrial localization), or both the calreticulin signal sequence at the N-terminus and the KDEL ER-retention tag at the C-terminus for ER localization (Demaurex 2005; McCombs and Palmer 2008). Soon after their introduction, yellow cameleon family members were the first GECIs to be targeted to the mitochondria, demonstrating that mitochondria prevent Ca^{2+} depletion of the ER and buffer subplasmalemmal Ca^{2+} elevations during agonist stimulation (Arnaudeau et al. 2001; Malli et al. 2003).

For even greater specificity, GECIs could be directly tagged onto a protein of interest to measure local Ca^{2+} levels in the immediate vicinity of the target protein. This would be particularly useful for the study of Ca^{2+} channels, where a low affinity GECI would be activated only by the extremely high local Ca^{2+} levels during channel opening but not by slow rises in global Ca^{2+} elevations in the cytosol (Dynes et al. 2016). Stably integrated GECIs would be continuously expressed by cells over time, allowing for long-term tracking of cell fates even after cell differentiation and proliferation. In a transgenic model, GECIs could allow for endogenous labeling of specific cell populations without the need for invasive cell labeling. Furthermore, their expression level could be controlled by an inducible promoter, such as the tetracycline-responsive promoter, to turn on or off expression of the indicator at specific time points (Gossen and Bujard 1992).

Despite the inherent advantages of GECIs, the initial FRET-based probes were not widely used as their performance, particularly in Ca^{2+} sensitivity, brightness, and dynamic range, fell far behind available small-molecule indicators. The discovery of a circularly permuted variant of GFP (cpGFP) led to its immediate incorporation into GECI design (Baird et al. 1999), and resulted in a new generation of GECIs with higher signal-to-noise ratio, starting with the single fluorescent protein-based GCaMP (**Figure 1.1**) (Nakai et al. 2001). Successive rounds of design based on GCaMP and contributions from numerous researchers led to color and high dynamic range variants of single fluorescent protein-based GECIs with dramatically improved performance (Tian et al. 2009; Zhao et al. 2011; Akerboom et al. 2012; Akerboom et al. 2013; Chen et al. 2013). FRET-based GECIs continued to evolve as well, with various improvements including incorporation of

circularly permuted yellow fluorescent proteins (cpYFPs) to improve dynamic range in the yellow cameleon (YC) family (Nagai et al. 2004), use of troponin C as the Ca^{2+} sensing element in the TN indicator family (**Figure 1.1**) (Heim and Griesbeck 2004), computational redesign of the calmodulin-M13 interface to increase the range of Ca^{2+} sensitivity and reduce perturbation by native calmodulin in the DcpV family (Palmer et al. 2006), and complete redesign of the troponin C domain to increase response kinetics and reduce buffering of cytosolic Ca^{2+} in the TN-XXL family (Mank et al. 2006; Mank et al. 2008). Lastly, there is a special class of grafted sensors (**Figure 1.1**), in which a Ca^{2+}-binding motif was directly inserted into the EGFP barrel, resulting in the smallest possible GECIs available (Zou et al. 2007; Tang et al. 2011).

The latest generation of GECIs have now crossed key performance thresholds previously set by small-molecule indicators, enabling the advantages of GECIs to be widely applied in diverse Ca^{2+} imaging studies without making sacrifices in performance. Members of the GCaMP6 family are capable of tracking cytosolic Ca^{2+} changes from single neuronal action potentials, with higher sensitivity than small-molecule indicators such as OGB-1 (Chen et al. 2013). The availability of multicolored variants in the GECO family and the RCaMP series allowed for simultaneous measurement of Ca^{2+} dynamics in different cell populations in the same preparation, or in different subcellular compartments within the same cell (Zhao et al. 2011; Akerboom et al. 2013). These variants can be integrated with optogenetics to simultaneously evoke channelrhodopsin activity while monitoring localized Ca^{2+} responses in independent spectral channels (Akerboom et al. 2013). Moreover, individual GECIs can be tagged onto membrane Ca^{2+} channels to directly

measure Ca^{2+} influx through the target channel of interest, enabling optical recording of single channel activity without the need for technique-intensive patch clamping (Dynes et al. 2016).

Genetically encoded Ca^{2+} indicators hold the potential to vastly expand the field of Ca^{2+} imaging, with a wide variety of available probes that offer diverse options for increased specificity to accurately measure Ca^{2+} dynamics under unperturbed physiological conditions. The greatest interest in use of GECIs has long been held by neuroscientists, to detect changes in intracellular Ca^{2+} levels as a readout of neuronal activity. Thus, the majority of GECI applications so far has been focused on neuronal studies, while a few have been in the cardiovascular system (Ji et al. 2004; Tallini et al. 2006; Mohamed et al. 2013). Only recently have attempts been made to expand the use of GECIs into other tissue systems, such as in the digestive tract (Hennig et al. 2015) or within immune cells (Mues et al. 2013; Thestrup et al. 2014).

1.3 Calcium signaling in immune cells

T lymphocytes are crucial for the adaptive immune response, and Ca^{2+} signaling is essential for their function. In T cells, Ca^{2+} entry is required for short term processes such as antigen recognition and immune synapse formation, as well as longer term processes including cell activation, gene transcription, differentiation, and proliferation (Feske 2007; Oh-hora and Rao 2008; Rao and Hogan 2009). To maintain immune surveillance, T cells continuously migrate between lymphoid organs and the vasculature, and crawl throughout lymph nodes and peripheral tissues in the search for specific antigen (von Andrian and Mackay 2000;

Cahalan and Parker 2008; Germain et al. 2012). Within lymph nodes, T cells must move rapidly and continuously to sample as many antigen presenting cells (APCs) as possible, while balancing this rapid motility with the need to carefully scan their surroundings to allow for T cell receptor (TCR) association with peptide-bound MHC molecules on the surface of APCs.

A functional network of ion channels in T cells sustains Ca^{2+} signaling following antigen recognition (**Figure 1.2**). Upon TCR engagement with cognate antigen, TCR signaling through PLCγ and IP_3 triggers release of Ca^{2+} from intracellular stores in the ER (Taylor et al. 2009). Depletion of intracellular Ca^{2+} stores results in translocation of the ER-resident Ca^{2+} sensor STIM1 to specialized ER-PM junctions to activate Orai1, the pore forming subunit of the plasmalemmal Ca^{2+} release-activated Ca^{2+} (CRAC) channel (Liou et al. 2005; Roos et al. 2005; Zhang et al. 2005; Luik et al. 2006; Vig et al. 2006; Zhang SL 2006; Calloway et al. 2009; Wu et al. 2014). Also known as store-operated Ca^{2+} entry (SOCE), this Ca^{2+} influx in T cells acts as a "STOP" signal that anchors the T cell to the site of antigen recognition (Donnadieu et al. 1994; Negulescu et al. 1996; Dustin et al. 1997; Bhakta et al. 2005; Moreau et al. 2015). Sustained TCR signaling and elevated cytosolic Ca^{2+} levels then activate calmodulin and calcineurin to trigger the translocation of transcription factor NF-AT (Nuclear Factor of Activated T cells) into the nucleus to initiate gene expression, cytokine production, and cell proliferation (Negulescu et al. 1994; Hogan et al. 2003). Orai1 is the primary mechanism for Ca^{2+} entry in T cells (Lewis 2001; Oh-hora and Rao 2008), and this Ca^{2+} signaling pathway is crucial for T cell function, as several mutations in Orai1 and STIM1 have been identified to cause lethal channelopathies in

patients with severe combined immune deficiency (SCID) (Feske et al. 2006). Thus, it will be crucial to gain a deeper understanding of Orai1 and STIM1, and how they mediate vital immune functions.

Within the entire immune repertoire, only a tiny fraction of T cells can recognize a single given epitope. T cells must constantly circulate the body and scan countless APCs in the search of this rare recognition event. Optimizing T cell motility to balance search sensitivity and speed is crucial for efficient antigen search and proper immune surveillance (Cahalan and Parker 2005; Krummel et al. 2016). Regulation of T cell motility is a Ca^{2+}-dependent process, and in many contexts Ca^{2+} signaling has been shown not only to accompany, but to cause, cell arrest and loss of cell polarity in motile T cells (Negulescu et al. 1996; Dustin et al. 1997; Wei et al. 2007). This Ca^{2+}-dependent "STOP" signal anchors a T cell to the site of antigen recognition, allowing for sustained TCR signaling, formation of a stable immune synapse, and activation of gene transcription. However, in the presence of high affinity antigen recognition, TCR engagement alone can trigger T cell arrest independent of Ca^{2+} signaling (Dustin et al. 1997; Waite et al. 2013; Moreau et al. 2015). It is likely that the "STOP" signal induced by Ca^{2+} signaling reduces T cell motility to facilitate scanning for cognate antigen in the absence of high affinity TCR engagement. However, it is still unclear how Ca^{2+}-dependent modulation of T motility acts to fine-tune the search for cognate antigen, and where such Ca^{2+} signals originate from within the T cell.

1.4 Cellular dynamics and immunoregulation

So far, I have made the case that Ca^{2+} signaling is vital for immune function and that new tools are needed to enhance the "Calcium Toolkit". At another level, T cells need to recirculate and migrate within lymphoid organs in order to respond to antigen and initiate an immune response. Two-photon microscopy has revolutionized the understanding of the cellular dynamics in lymph nodes and other tissues where T cells and other cells of the immune system migrate. The Cahalan and Parker labs pioneered the field of immunoimaging that has illuminated the cellular dynamics of antigen detection and T cell activation (Cahalan et al. 2002; Cahalan and Parker 2008; Germain et al. 2012). T cells are robustly motile in their native environment and migrate in a random walk as they scan the lymph node for the presence of antigen. As they migrate, T cells make contact with dendritic cells and, if antigen is present, Ca^{2+} signaling is initiated causing motility arrest. These key findings set the stage for further studies as I joined the lab.

Regulatory T cells (Tregs) are a small subset of T cells that constitute only 5-10% of the total $CD4^+$ T cell population, but play an indispensable role in the maintenance of immune homeostasis and peripheral tolerance (Sakaguchi et al. 2008). Functional defects in Tregs are associated with several human autoimmune and inflammatory diseases, and selective depletion of Tregs in experimental animals leads to severe systemic autoimmunity and lymphoproliferative disease (Wildin and Freitas 2005; van der Vliet and Nieuwenhuis 2007; Huter et al. 2008). Treg development and function are driven by specific expression of the transcription factor Foxp3, first identified from the mutant gene in a mouse model exhibiting T cell hyperactivation and cytokine overproduction (Brunkow et

al. 2001). Expression of the cytotoxic T cell-associated antigen-4 (CTLA-4) is crucial for Treg function, as treatment with blocking antibodies to CTLA-4 leads to spontaneous development of autoimmune disease (Takahashi et al. 2000). Multiple mechanisms have been identified for how Tregs exert their immune suppressive effects, including soluble factors such as IL-10 and TGFβ (Sakaguchi et al. 2009; Campbell and Koch 2011), or contact-dependent mechanisms such as direct trans-endocytosis of costimulatory ligands from APCs and suppression of Ca^{2+} signaling in activating T cells (Qureshi et al. 2011; Schmidt et al. 2011; Schwarz et al. 2013).

While it is clear that Tregs exert a range of mechanisms for suppression, it is still not fully understood how different mechanisms interact to maintain proper immune homeostasis. All Tregs seem to possess core suppressive mechanisms, but are also able to adapt to stimuli in their surroundings to exert additional suppressive effects (Wing and Sakaguchi 2012). There is an increased need for assays that can preserve Tregs in their physiological environment, allowing for the study of cellular behavior and *in vivo* mechanisms that underlie immunoregulation.

1.5 Overview

In Chapter 2 of my dissertation, I describe the development of a novel ratiometric genetically encoded Ca^{2+} indicator, named "Salsa6f", and describe its use to monitor either cytosolic or near-membrane local Ca^{2+} signaling. In Chapter 3, Salsa6f and a dominant-negative Orai1 mutant are used to investigate the mechanism of Orai1-regulated stop-and-go T cell motility. Chapter 4 describes development of a transgenic mouse to express

Salsa6f in a tissue specific manner for *in vivo* studies of Ca^{2+} signaling in the immune and nervous systems. In Chapter 5, I present two-photon imaging of cellular dynamics within mouse intact lymph node to study unperturbed, endogenous Tregs interacting with conventional T cells and dendritic cells. We demonstrate the crucial involvement of CTLA-4 in determining cellular dynamics among Tregs, conventional T cells, and dendritic cells *in vivo*. I also lay the groundwork for future *in vivo* studies utilizing a transgenic Ca^{2+} reporter mouse to study the suppression of Ca^{2+} signaling in activating conventional T cells by Tregs.

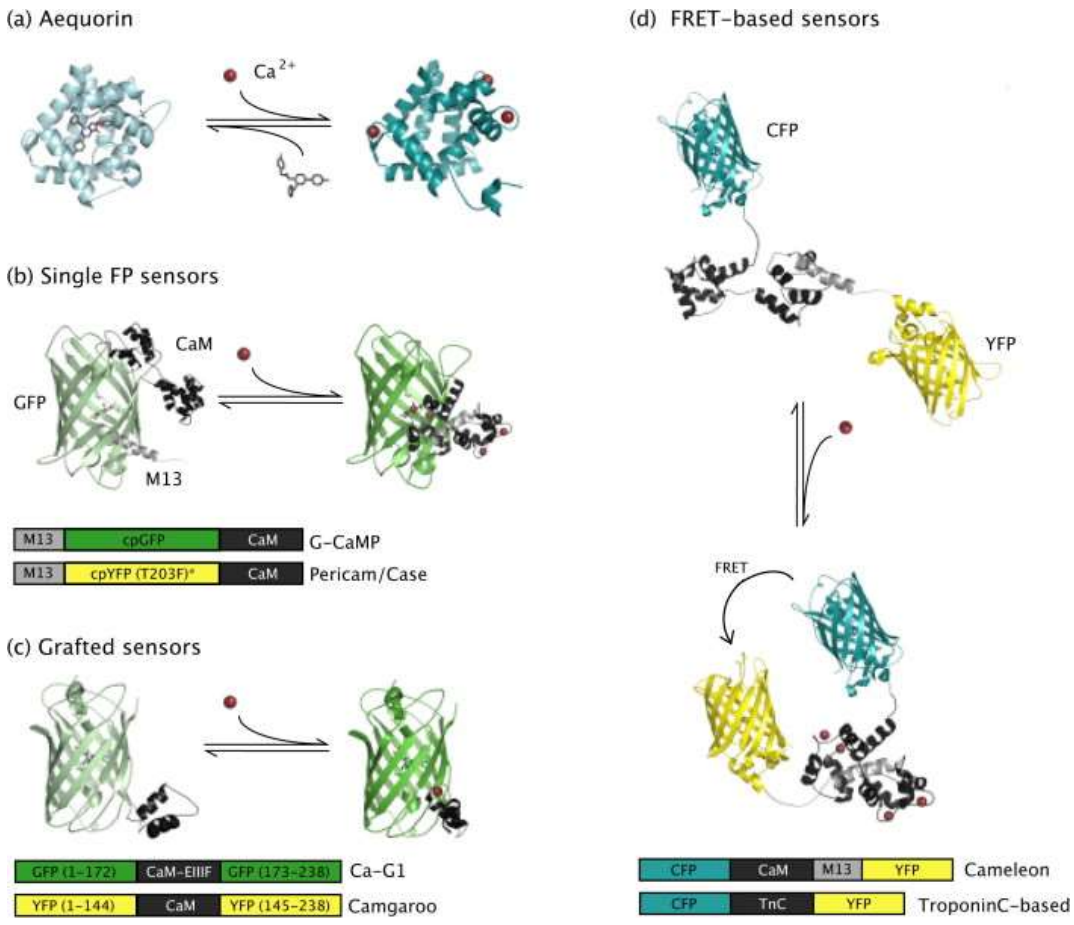

Figure 1.1. Models of the three classes of GECIs.

(**a**) The aequorin photoprotein is shown in complex with coelenterazine. Upon binding of Ca^{2+}, the aequorin undergoes a conformational change, releasing coelenteramide and emitting blue light. (**b**) Single FP sensors employing the Ca^{2+}-responsive element CaM and a CaM binding peptide attached to a circularly permutated FP. On binding Ca^{2+}, CaM executes a conformational change, interacting with the peptide and altering the protonation state of the chromophore, thus changing the fluorescence intensity of the protein. Note the Case sensors are built from a cpYFP with T203F and a few other mutations. (**c**) Grafted sensors utilizing EF-hands or portions of CaM inserted into a fluorescent protein. Binding of Ca^{2+}

causes a change in protein conformation and a shift in the protonation state of the chromophore. (**d**) FRET-based sensors having a Ca^{2+} binding domain located between two flurophorescent proteins. As Ca^{2+} binds, the Ca^{2+} binding domain undergoes a conformational change, interacting with its binding peptide. This brings the two FPs closer together, increasing the efficiency of FRET. Below each model are maps for the various available families of GECIs. (McCombs and Palmer 2008).

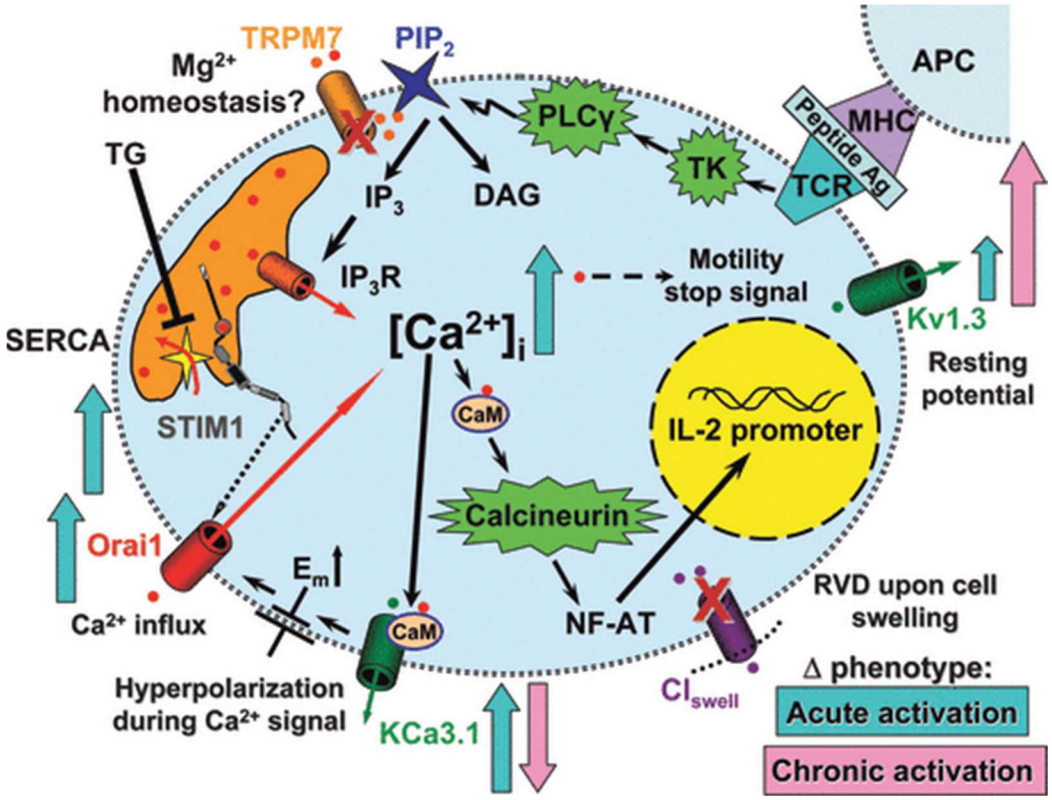

Figure 1.2. Ion channels and Ca^{2+} signaling in T cells.

Signaling pathway from TCR engagement to gene expression in nucleus. Major ion channel types are color coordinated according to ion selectivity, Orai1 (red), Kv1.3 and KCa3.1 (green), cation non-selective TRPM7 and IP_3R channels (orange), and Cl_{swell} (violet). Dots and arrows correspond to ions and fluxes with the same color code. STIM1 is shown (gray) with a Ca^{2+} ion bound to its EF-hand within the ER lumen under basal conditions with the ER Ca^{2+} store filled. Ion channels and functions include (clockwise from right): Kv1.3 maintains the resting membrane potential and participates in RVD; Cl_{swell} triggers RVD by opening in response to cell swelling; KCa3.1 hyperpolarizes the membrane potential when cytosolic Ca^{2+} rises; Orai1 embodies the pore-forming subunit of the CRAC channel and is

activated by STIM1 following ER Ca^{2+} store depletion (dotted line); TRPM7, activated by PIP_2 and inhibited by Mg^{2+} inside, may regulate Mg^{2+} homeostasis in the cell. Proximal signaling events inside the cell following presentation of antigen include the following (counterclockwise from top right): TCR engagement of peptide–MHC, activation of tyrosine kinases (TK: Lck, Fyn, and ZAP-70), and phospholipase-C-γ (PLCγ), resulting in the cleavage of PIP_2 to generate the second messengers IP_3 and DAG; IP_3-induced Ca^{2+} release; depletion-induced mobilization of STIM1 and activation of Ca^{2+}influx through Orai1 subunits. Post-Ca^{2+} events include activation of KCa3.1 via prebound CaM, activation of calcineurin via CaM, accumulation of dephosphorylated NFAT subunits in the nucleus, binding to DNA promoter regions, and altered gene expression. Functionally significant changes in ion channel expression and Ca^{2+} signaling are indicated by arrows corresponding to changes during acute and chronic activation. TCR, T-cell receptor; STIM, stromal interacting molecule; RVD, regulatory volume decrease; Cl_{swell}, swelling-activated Cl^-current; PIP, phosphatidylinositol 4,5-bisphosphate; MHC, major histocompatibility complex; DAG, diacylglycerol; CaM, calmodulin. (Cahalan and Chandy 2009).

CHAPTER 2: A novel ratiometric genetically encoded Ca^{2+} indicator, Salsa6f

In this chapter, I wrote all the sections, performed all the experiments, and made all of the figures.

2.1 Introduction

Our understanding of the diverse Ca^{2+} signaling events that underlie cellular processes has been furthered by imaging studies using synthetic small-molecule Ca^{2+} indicators such as fura-2 and indo-1 (Cobbold and Rink 1987; Tsien 1989). These small-molecule Ca^{2+} indicators are derived from Ca^{2+} chelators bound to fluorescent organic chemical moieties, allowing for clear temporal resolution of cytosolic Ca^{2+} signals with fast kinetics and high dynamic range. However, small-molecule Ca^{2+} indicators cannot be reliably targeted to subcellular organelles or specific cell populations, and their slow leakage out of cells over time means they are unsuitable for long term imaging studies. Furthermore, small-molecule Ca^{2+} indicators must be invasively loaded into isolated cell populations, which is often difficult or impossible in whole tissue preparations.

To overcome the limitations of small-molecule Ca^{2+} indicators, genetically encoded Ca^{2+} indicators (GECIs) were developed to allow endogenous and continuous expression of a fluorescent protein-based Ca^{2+} indicator from a nucleic-acid sequence. Successive rounds of improvement have resulted in the currently available GECIs with performance comparable to small-molecule Ca^{2+} indicators; the latest GCaMP6 series is sufficiently

bright and fast enough to track cytosolic Ca^{2+} changes from single neuronal action potentials (Chen et al. 2013). Despite this achievement, an important consideration with single fluorescent protein-based GECIs is their low fluorescence intensity in the absence of Ca^{2+} binding, resulting in difficulties identifying labeled cells at resting cytosolic Ca^{2+} concentrations. Furthermore, single fluorescent protein-based GECIs lack the ratiometric capability to determine absolute Ca^{2+} concentration, and are unsuitable for use in motile cells, since fluorescence changes due to movement would be undistinguishable from changes in Ca^{2+} levels. While these limitations are overcome by FRET-based indicators such as the recently developed Twitch indicators from the TN-XXL family of GECIs (Thestrup et al. 2014), FRET-based indicators still fall behind GCaMP variants in terms of response kinetics and signal-to-noise ratio.

One of the main driving forces behind the steady improvements to GECIs has been specifically for their use in imaging neuronal activity. Since neurons are immobile, motility artifacts have not been a concern for neuronal imaging. However, the need to track and monitor signaling simultaneously becomes a greater concern in rapidly moving lymphocytes of the immune system, or in actively contracting cardiomyocytes of the heart. Furthermore, the ability to distinguish cell morphology and location remains an important consideration for neuronal imaging, particularly when detection of sporadic events is required, so that cells of interest can be clearly identified in the absence of signaling. Ultimately, the current GECIs that could potentially address these issues are ratiometric probes which are limited by slow response kinetics and lower dynamic range compared to single fluorescent protein-based GCaMP variants. Here we show the design and

characterization in living cells of a novel ratiometric genetically encoded Ca^{2+} indicator that combines the performance of the latest GCaMP6 single fluorescent protein-based Ca^{2+} indicator, with the stable and consistent fluorescence of tdTomato for tracking motile cells.

2.2 Results

2.2.1 Screening of current GECIs *in vitro*

A variety of the latest single fluorescent protein-based GECIs were screened in HEK 293A cells. Each probe was cotransfected along with Orai1 and STIM1 in order to measure responses during store-operated Ca^{2+} entry using epifluorescence microscopy (**Figure 2.1A**). Store-operated Ca^{2+} influx was induced by thapsigargin (TG) followed by readdition of extracellular Ca^{2+} and changes in single cell fluorescence intensity were monitored. GCaMP6f was selected for further evaluation from the candidates tested based on superior brightness and dynamic range, the key requirements for use in *in vivo* imaging (**Figure 2.1B**). Another consideration is Ca^{2+} affinity: the resting cytosolic Ca^{2+} concentration in lymphocytes is around 50-100 nM, but with activation of CRAC channels after store depletion, Ca^{2+} levels can rise to the low micromolar range. The ideal probe would have an affinity that would allow for detection of Ca^{2+} changes within 0.1 – 1 μM without saturation, while being relatively unaffected by noise from basal Ca^{2+} levels. Thus, GCaMP6f, with a reported k_d of 373 nM, is a more suitable candidate over GCaMP6s and GCaMP6m, which each have a k_d around 150 nM. These new-generation GECIs represent a potential breakthrough for *in vivo* imaging of any cell type where brightness and dynamic range are

crucial. A further consideration is response kinetics, for which GCaMP6f (named 6f for fast kinetics) exhibits the shortest decay time of any currently available GECI, and is able to resolve individual action potentials with minimal inter-spike interval of 50-75 ms (Chen et al. 2013). Lastly, GCaMP6f was tested by nucleofection into Jurkat E6-1 cells and primary human T cells, to ensure functionality in hematopoietic cells (**Figure 2.1C,D**).

2.2.2 Optimizing RFP-GCaMP fusion probes for *in vivo* imaging

To allow for cell tracking even in the absence of Ca^{2+} signaling and to enable ratiometric measurement of Ca^{2+} concentration, the next step was to create a fusion probe that would preserve the performance of GCaMP6f. We began with a commonly used monomeric red fluorescent protein (mRFP), mCherry, and fused it to the N-terminus of GCaMP6f with a V5 epitope linker, for biochemical detection (Lobbestael et al. 2010). The same mRFP-V5-GCaMP6f template was also used to create fusions with mApple and TagRFP-T, an improved variant of the highly photostable TagRFP (Shaner et al. 2008) (**Figure 2.2A**). While these mRFP-V5-GCaMP6f fusions were readily expressed in HEK 293A cells and retained Ca^{2+} sensitivity, fluorescence intensity of the RFP component was poor when imaged with two-photon microscopy using femtosecond excitation at 900 nm (**Figure 2.2B,C**).

Based on reports of two-photon excitation spectra for RFPs (Drobizhev et al. 2011), there is minimal excitation of mRFPs at 900 nm, the wavelength used for optimal two-photon excitation of GCaMP probes (Akerboom et al. 2012). Instead, the optimal two-photon excitation range for mRFPs is between 1000 nm and 1100 nm, at which point

GCaMP6f would no longer be excited. However, the tandem dimer tdTomato and the obligate tetramer DsRed both possessed increased two-photon excitation at 900 nm (Drobizhev et al. 2011), which would allow for simultaneous excitation and imaging of both the RFP component and GCaMP6f in a fusion probe. To evaluate these new choices, we individually expressed tdTomato and DsRed-Express2, an improved version of DsRed with accelerated maturation and reduced cytotoxicity (Strack et al. 2008), in HEK 293A cells and imaged them at 900 nm femtosecond excitation on two-photon microscopy. Both tdTomato and DsRed-Express2 exhibited greatly increased fluorescence compared to mCherry and TagRFP-T (**Figure 2.3B**), so fusions to GCaMP6f were produced using the tandem dimer of tdTomato and the monomer for DsRed-Express2 (**Figure 2.3A**).

The new tdTomato-V5-GCaMP6f and DsRed-Express2-V5-GCaMP6f fusions were then expressed in HEK 293A cells and imaged using two-photon microscopy. Both probes showed robust responses to ionomycin-induced cytosolic Ca^{2+} elevation (**Figure 2.3C,D**). However, we noted that the DsRed-Express2-V5-GCaMP6f fusion sometimes exhibited only red fluorescence or only Ca^{2+}-sensitive green fluorescence in individual cells, possibly due to folding defects caused by obligate tetramerization of DsRed-Express2 (**Figure 2.3C**, arrowheads). Thus, if DsRed-Express2-V5-GCaMP6f was to be tagged to another target protein for monitoring local Ca^{2+} levels, the tetramerization of DsRed-Express2 could undesirably disturb function of the target protein. Furthermore, DsRed variants are reported to exhibit an immature green form, and multiphoton excitation results in selective photobleaching of the mature red form to enhance emission of the immature green form (Marchant et al. 2001). Since the tdTomato-V5-GCaMP6f fusion did not have these issues,

we chose it as the ideal probe and named it "Salsa6f" for the mixture of red and green fluorescence seen during Ca^{2+} signaling. When imaged by two-photon microscopy, Salsa6f expression in HEK 293A cells was localized to the cytosol, and both the tdTomato and the GCaMP6f components were clearly visualized by excitation at 900 nm (**Figure 2.3D**). The tdTomato component provided a stable red fluorescence to label Salsa6f expressing cells, while the GCaMP6f component maintained a dim baseline in the absence of Ca^{2+} signaling and produced a bright green fluorescence upon elevations in cytosolic Ca^{2+}, such as when induced by ionomycin (**Figure 2.3D**).

The TagRFP-T-V5-GCaMP6f fusion, which was named "RedGCaMP6f", remains a capable alternative for single molecule microscopy, particularly for tagging onto other target proteins to monitor localized Ca^{2+} fluctuations. As a proof of concept, we fused RedGCaMP6f to the C-terminus of the plasma membrane Orai1 Ca^{2+} channel (**Figure 2.4A**), and co-transfected the resulting Orai1-RedGCaMP6f fusion construct with STIM1 into HEK 293A cells for imaging with two-photon microscopy. In resting cells, red fluorescence from Orai1-RedGCaMP6f was localized to the plasma membrane without detectable green fluorescence, demonstrating the spatial distribution of inactive Orai1 channels. Upon TG-induced store depletion, green fluorescence was still undetectable (**Figure 2.4B**), suggesting Orai1-RedGCaMP6f localized to the plasma membrane is insensitive to transient elevations in cytosolic Ca^{2+} concentration. Subsequent readdition of extracellular Ca^{2+} resulted in a dramatic jump in green fluorescence with Ca^{2+} influx from open Orai1 channels (**Figure 2.4C**), demonstrating the specificity of Orai1-RedGCaMP6f in detecting localized Ca^{2+} entry through active Orai1 channels.

2.2.3 Characterizing Salsa6f performance in live cells

To ensure that the performance of GCaMP6f was preserved in the Salsa6f fusion construct, we co-transfected Salsa6f into HEK 293A cells with Orai1 and STIM1, then monitored fluorescence of the GCaMP6f component using arc lamp excitation with conventional epifluorescence microscopy. Upon TG-induced store depletion and subsequent Ca^{2+} influx through activated plasma membrane Orai1 channels, Salsa6f exhibited a ten-fold dynamic range in green fluorescence and comparable brightness to control cells co-transfected with GCaMP6f alone (**Figure 2.5A-C**). This demonstrates that fusion of GCaMP6f to tdTomato with a V5 epitope linker did not significantly affect the function of GCaMP6f.

The tdTomato component of Salsa6f provides a stable red fluorescence to facilitate cell tracking, but also allows for ratiometric measurement of Ca^{2+} concentration when combined with green fluorescence from the GCaMP6f component. To compare Salsa6f to the currently available GECIs with ratiometric capability, we obtained the recently released Twitch1 and Twitch2B, members of the TN-XXL family of FRET-based indicators containing troponin C for the Ca^{2+}-sensing element (Mues et al. 2013; Thestrup et al. 2014). Either Salsa6f, Twitch1, or Twitch2B was individually co-transfected with Orai1 and STIM1 into HEK 293A cells, then imaged by two-photon microscopy. Comparing ratios for Salsa6f, calculated using the green fluorescence over the red fluorescence, with ratios for the Twitch probes, calculated using YFP fluorescence over CFP fluorescence, Salsa6f exhibited almost twice the dynamic range from TG-induced store-operated Ca^{2+} entry compared to Twitch1 and Twitch2B (**Figure 2.5D**). Our results agree with published reports for

dynamic range of TN-XXL indicators, as well as the general consensus that FRET-based GECIs are still inferior in dynamic range to the latest single fluorescent protein-based GCaMP indicators (Mues et al. 2013). Furthermore, GCaMP6f boasts the fastest response kinetics of any currently available GECI, another advantage of Salsa6f over FRET-based indicators (Chen et al. 2013).

Lastly, we evaluated the performance of Salsa6f expressed by nucleofection in primary human T cells, and saw similar performance of Salsa6f in measuring TG-induced Ca^{2+} entry (**Figure 2.5E**). Furthermore, Salsa6f could detect physiological Ca^{2+} signals in human T cells with high signal-to-noise ratio and time resolution, such as Ca^{2+} oscillations induced by activation with immobilized anti-CD3/28 antibodies (**Figure 2.5F,G**). Thus, Salsa6f is a novel genetically encoded fusion probe that combines the high performance of single fluorescent protein-based GCaMP6f with the stable fluorescence of tdTomato to facilitate cell tracking, identification, and ratiometric measurement of cytosolic Ca^{2+} signals.

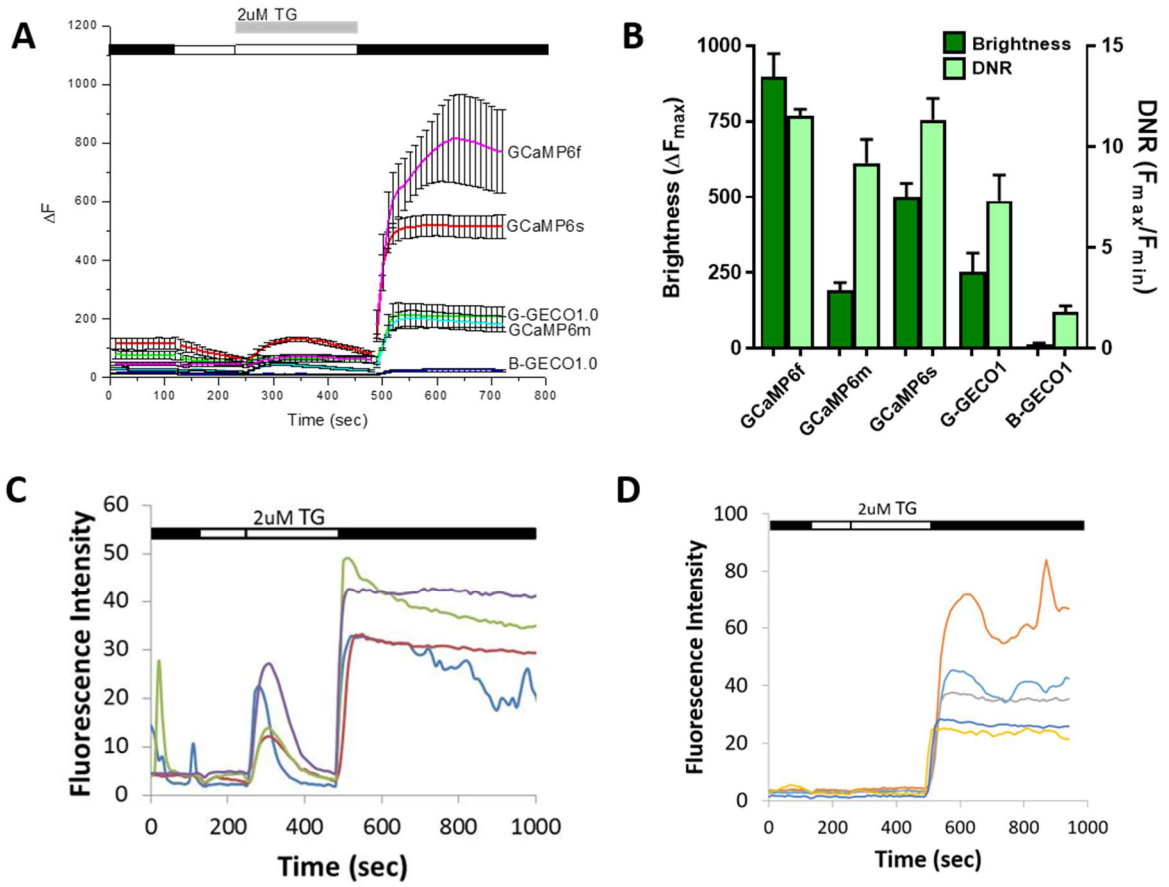

Figure 2.1. Screening of single fluorescent protein-based GECIs for *in vivo* imaging.

A. Averaged thapsigargin-induced Ca^{2+} entry, measured by change in fluorescence intensity, of various GECI probes co-transfected with Orai1/STIM1 in HEK 293A cells; error bars indicate SEM. **B**. Maximal brightness and dynamic range of screened GECIs, calculated from data shown in (**A**). **C,D**. Representative cell traces of GCaMP6f fluorescence responses to thapsigargin-induced Ca^{2+} entry when transfected in Jurkat E6-1 cells (**C**) or primary human T cells (**D**).

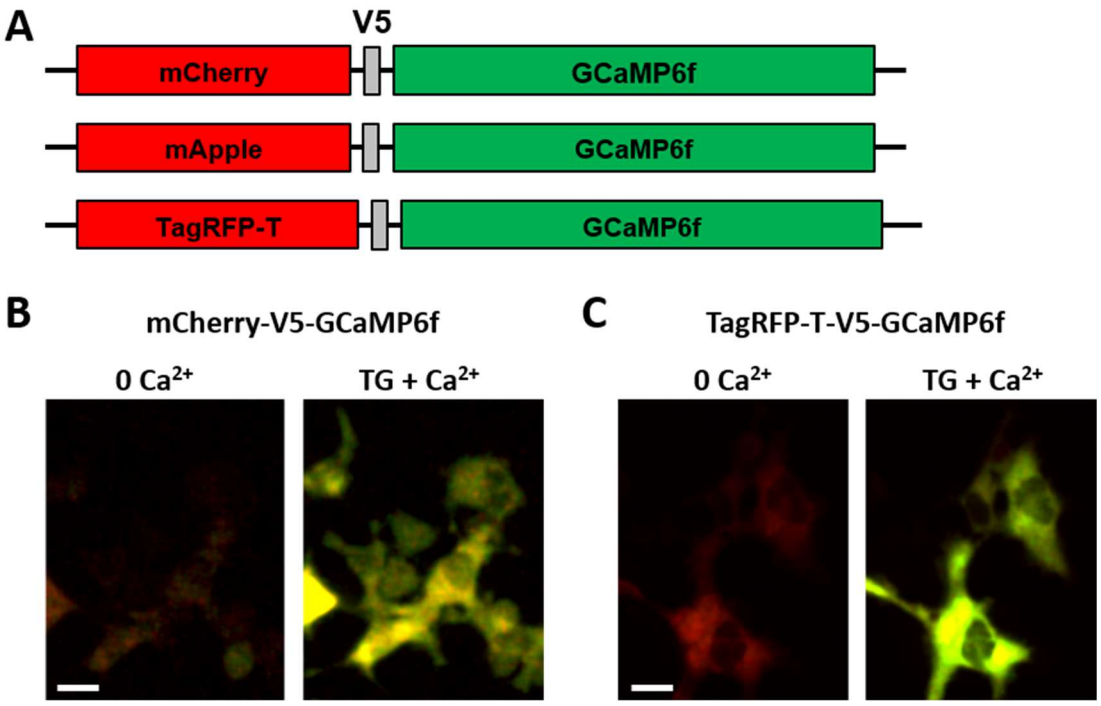

Figure 2.2. GCaMP6f fusion probes with monomeric RFPs for ratiometric imaging.

A. Diagram of initial mRFP-V5-GCaMP6f fusion constructs. **B,C**. Two-photon images of mCherry-V5-GCaMP6f (**B**) or TagRFP-T-V5-GCaMP6f (**C**, RedGCaMP6f) co-transfected into HEK cells with Orai1/STIM1, showing merged red and green channels, at baseline in 0 mM extracellular Ca^{2+} and after stimulation with 2 μM thapsigargin (TG) in 2 mM extracellular Ca^{2+}; scale bar = 20 μm.

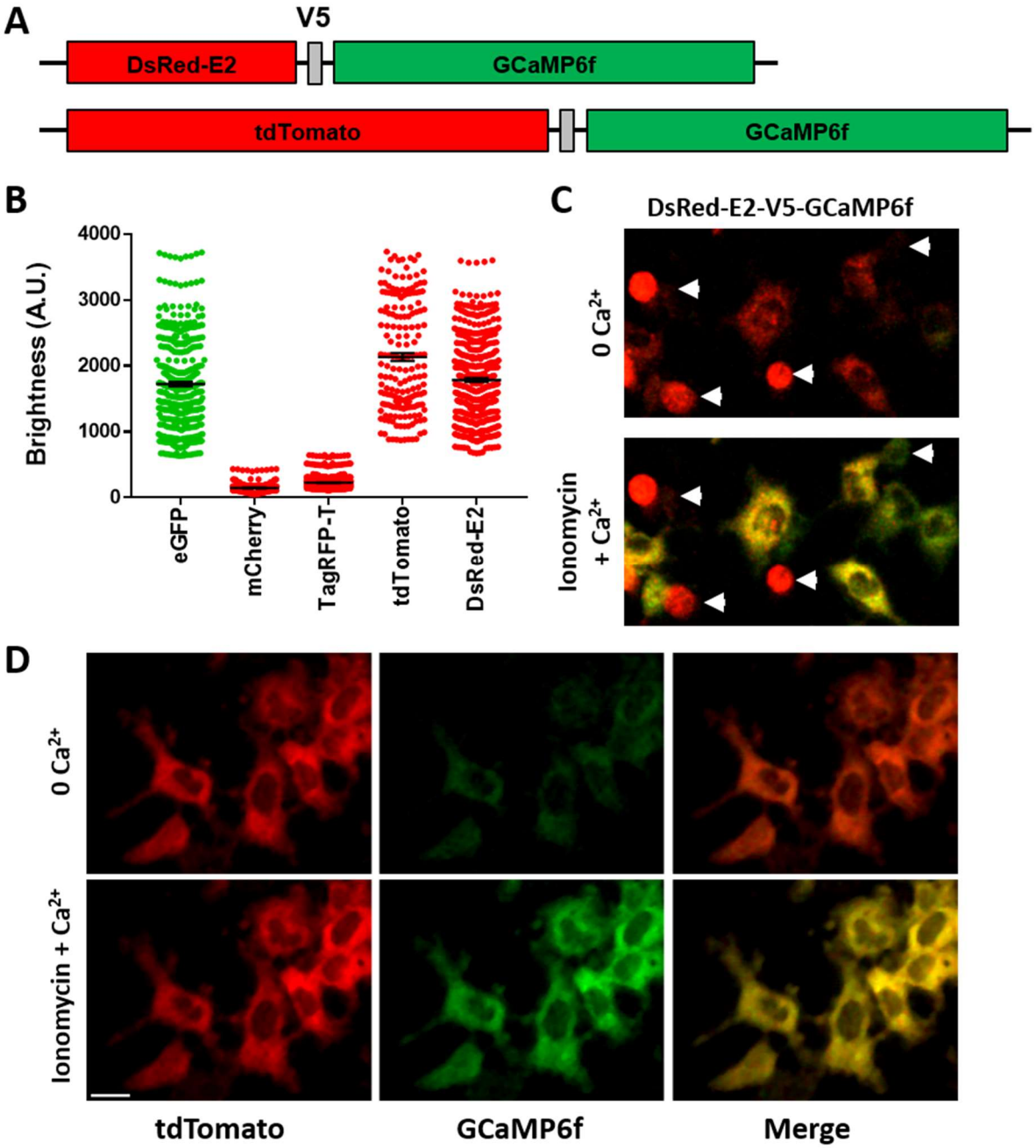

Figure 2.3. Optimizing RFP-V5-GCaMP6f fusions for two-photon capability.

A. Diagram of new RFP-V5-GCaMP6f fusion constructs for two-photon imaging. **B**. Fluorescence intensity of eGFP and various RFPs expressed in HEK cells and imaged on two-photon microscopy, at 900 nm excitation with identical PMT and laser power settings;

bars represent mean ± SEM. Although eGFP and RFP were collected in different PMTs, the standard experimental PMT settings for eGFP were used as a comparison to evaluate the performance of RFPs. **C**. Two-photon images of DsRed-Express2-V5-GCaMP6f fusion co-transfected in HEK cells with Orai1/STIM1, showing merged red and green channels, at baseline in 0 mM extracellular Ca^{2+} (top) and after maximum stimulation with 2 μM ionomycin in 2 mM extracellular Ca^{2+} (bottom); arrowheads point to cells with incomplete responses. **D**. Two-photon images of tdTomato-V5-GCaMP6f (Salsa6f) co-transfected in HEK cells with Orai1/STIM1, showing red (tdTomato), green (GCaMP6f), and merged channels, at baseline in 0 mM extracellular Ca^{2+} and after maximum stimulation with 2 μM ionomycin in 2 mM extracellular Ca^{2+}; scale bar = 20 μm.

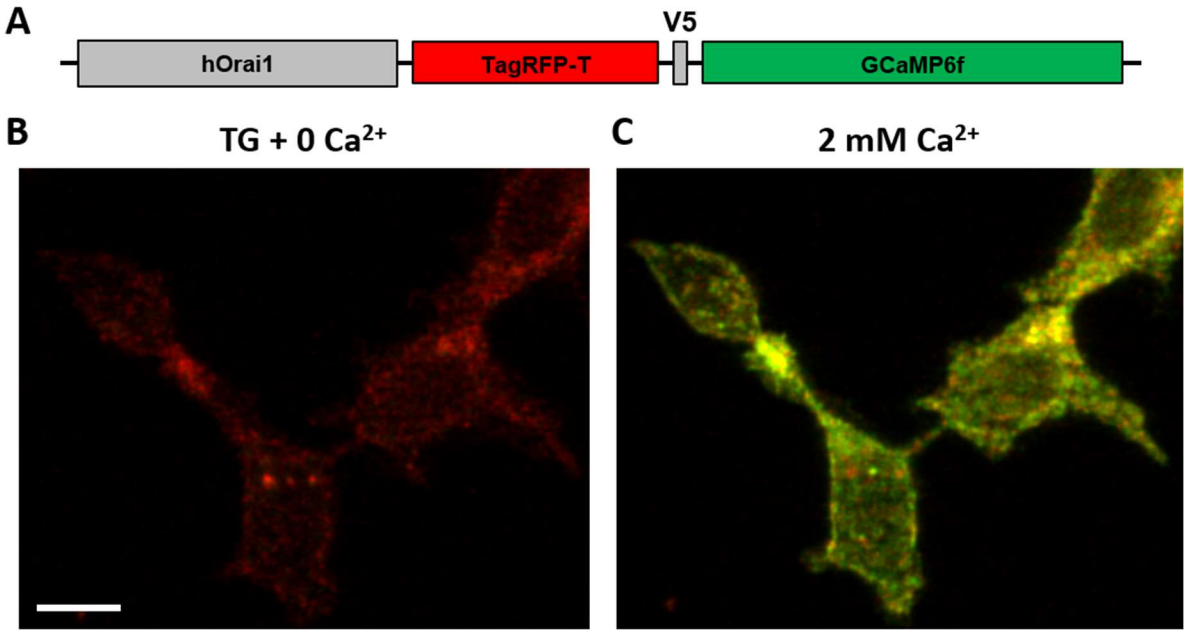

Figure 2.4. RedGCaMP6f as a fusion tag to Orai1 for measuring localized Ca^{2+} signaling.

Two-photon imaging of Orai1-RedGCaMP6f co-transfected with STIM1 into HEK cells, showing merged red and green channels. **A**. Diagram of C-terminus tagged Orai1-RFP-V5-GCaMP6f fusion construct. **B**. Intracellular Ca^{2+} stores were first depleted by treatment with thapsigargin (TG) in the absence of extracellular Ca^{2+}; scale bar = 20 μm. **C**. Same cells following by addback of 2 mM extracellular Ca^{2+} to allow store-operated Ca^{2+} entry through open Orai1 channels.

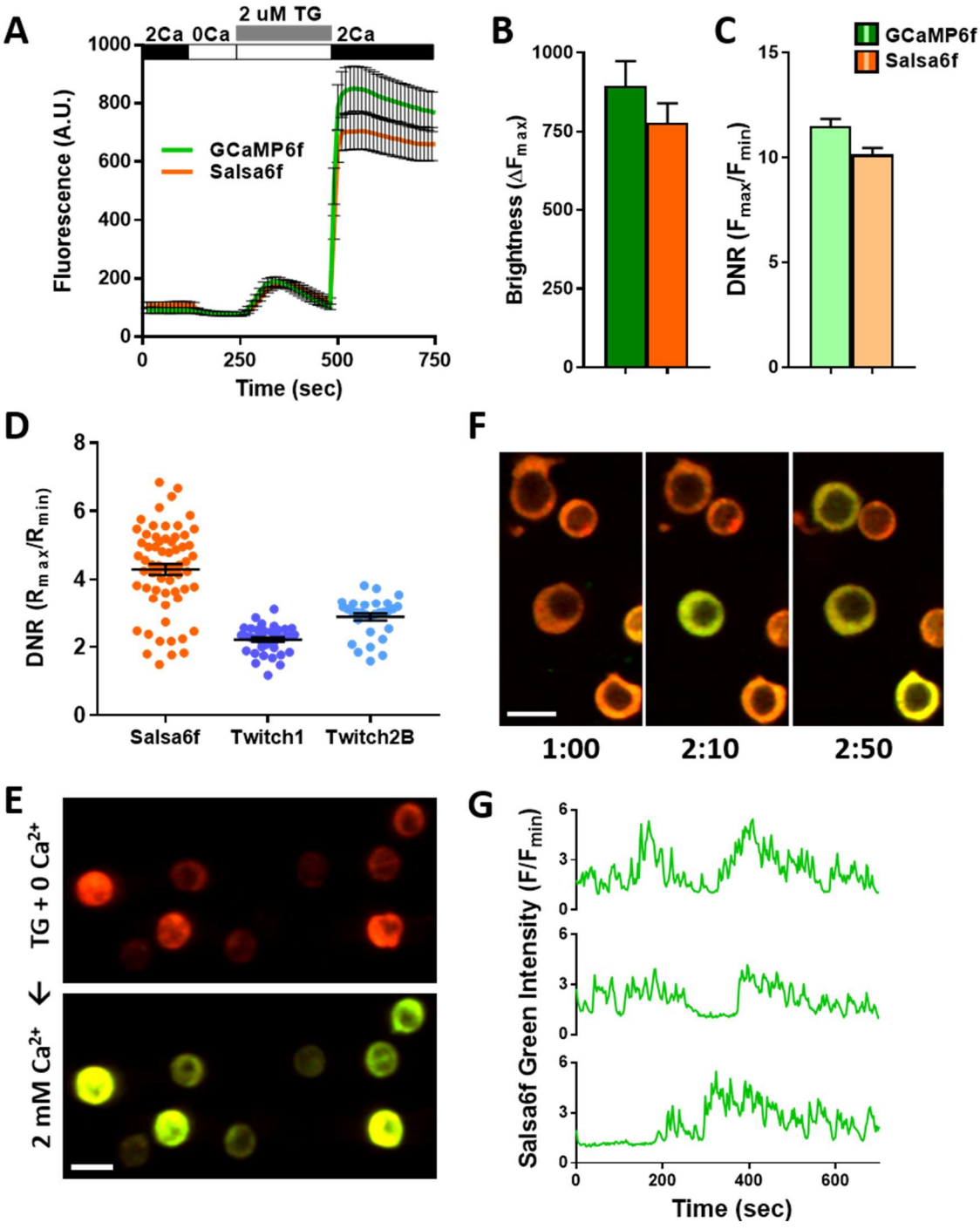

Figure 2.5. Characterizing Salsa6f performance in live cells.

A. Averaged thapsigargin-induced Ca^{2+} entry, measured by green fluorescence, in GCaMP6f (green) or Salsa6f (orange) co-transfected with Orai1/STIM1 in HEK cells; error bars indicate SEM. **B,C**. Mean brightness (**B**) and dynamic range (**C**) based on green fluorescence of GCaMP6f (green) and Salsa6f (orange), calculated from data shown in (**A**); bars indicate SEM. **D**. Ratiometric dynamic range of Salsa6f, Twitch1, or Twitch2B. Each probe was co-transfected with Orai1/STIM in HEK cells, then imaged by two-photon microscopy. Minimum and maximum fluorescence values were obtained by treating cells with thapsigargin in free extracellular Ca^{2+} to deplete ER stores, followed by addback of extracellular Ca^{2+}. Ratios were then calculated using GCaMP6f/tdTomato fluorescence for Salsa6f, or YFP/CFP fluorescence for Twitch probes. Bars represent mean ± SEM. **E**. Two-photon imaging of Salsa6f expressed in resting primary human T cells, then imaged by two-photon microscopy at 900 nm excitation. Intracellular Ca^{2+} was depleted by thapsigargin treatment in free Ca^{2+}, followed by addback of extracellular Ca^{2+} to allow for store-operated Ca^{2+} entry. Scale bar = 10 μm. **F**. Confocal time lapse microscopy of human T cells transfected with Salsa6f, then activated for two days on platebound anti-CD3/28 antibodies; time = min:sec, scale bar = 10 μm. **G**. Representative cell traces of activated Salsa6f transfected human T cells from (**F**), tracking green fluorescence intensity.

2.3 Discussion

Here we show the design and characterization of novel RFP-V5-GCaMP6f fusion probes with ratiometric capability and high performance in live cells. Of these fusions, the most notable are RedGCaMP6f containing the monomeric TagRFP-T, and Salsa6f containing the tandem dimer tdTomato. Both fusion probes can be expressed in cell lines and primary human hematopoietic cells, while preserving the functionality of GCaMP6f in detecting cytosolic Ca^{2+} fluctuations with high dynamic range. Salsa6f is the optimal choice for two-photon microscopy, allowing for simultaneous excitation and imaging of both fluorescent components. The increased brightness of tdTomato over TagRFP-T is also an advantage for *in vivo* imaging, when detection of fluorescent cells within deep tissue preparations can be challenging. The ratiometric capability of Salsa6f exceeds the dynamic range of the most recently released FRET-based Twitch probes (Mues et al. 2013). Furthermore, the fast response kinetics of GCaMP6f crosses key performance thresholds compared to synthetic small-molecule Ca^{2+} indicators, as the GCaMP6 series has been reported to have higher sensitivity and reliability in detecting individual action potentials than OGB-1 (Chen et al. 2013).

Genetically encoded Ca^{2+} indicators were first introduced almost two decades ago, but the initial designs were severely limited in performance compared to synthetic small-molecule Ca^{2+} indicators (Miyawaki et al. 1997). The discovery of a circularly permuted variant of eGFP (cpGFP) (Baird et al. 1999), when combined with calmodulin and M13 peptide, led to the development of the first single fluorescent protein-based GECI with high signal-to-noise ratio, GCaMP (Nakai et al. 2001). Subsequent protein structure-guided

mutagenesis and semi-rational library screening eventually resulted in the widely used GCaMP3 (Tian et al. 2009; Zariwala et al. 2012). The development of GCaMP3 was a crucial point in GECI design, as a genetically encoded indicator that was brighter and more stable, with Ca^{2+} sensitivity and response kinetics that began to approach the standards set by synthetic small-molecules indicators. Combined with the inherent advantages of its genetically encoded nature, GCaMP3 became a viable alternative to standard Ca^{2+} imaging assays relying on small-molecule indicators. Due to its success, GCaMP3 was used as a basis for continued improvements by numerous researchers, resulting in the currently available GECO series and the GCaMP6 series that can now exceed the performance of small-molecule indicators in some aspects (Zhao et al. 2011; Chen et al. 2013).

The main driving force for these improvements has primarily been for use of GECIs in neuronal imaging, to measure changes in cytosolic Ca^{2+} as a means to assess action potential firing and synaptic inputs. Although attempts have been made designing new FRET-based indicators for use in other cell types, such as the new Twitch probes which were designed specifically for expression in immune cells, no such attempt has been made using the powerful single fluorescent protein-based GCaMP variants. Due to the importance of Ca^{2+} signaling in T lymphocytes to modulate a variety of immune functions (Feske 2007), we sought to apply the capabilities of the latest available GCaMP6 to studying immune cell function. Both RedGCaMP6f and Salsa6f could be expressed in Jurkat E6-1 cells and primary human T cells, while maintaining a ten-fold dynamic range to pharmacologically-induced Ca^{2+} signaling. Furthermore, Salsa6f could detect physiological Ca^{2+} signals during T cell activation with a five-fold dynamic range. Thus, using GCaMP6f with a k_d of 373 nM is

an ideal choice for imaging Ca^{2+} signals in T cells, as physiological responses can be reliably detected without fear of saturation. The fast response kinetics of GCaMP6f allows for clear temporal resolution of transient Ca^{2+} signals, limited only by the acquisition speed of the experimental system.

We also demonstrate, by fusing RedGCaMP6f to the C-terminus of Orai1, that our fusion probes will be an excellent choice as a function tag to measure local Ca^{2+} signaling in the cytosolic nanodomain adjacent to the channel protein. In future work it will be worthwhile to compare signals with other function tags varying in Ca^{2+} affinity and proximity to the channel, such as G-GECO1.2-Orai1 (Dynes et al. 2016).

Most importantly for the subsequent development of a transgenic Ca^{2+} reporter mouse described in Chapter 4, we introduce Salsa6f, a novel genetically encoded Ca^{2+} indicator that combines the performance of the latest single fluorescent protein-based GCaMP6f with ratiometric capability surpassing the latest FRET-based Twitch probes. Salsa6f is universally applicable to multiple cell types, and is ideal for single-photon or two-photon microscopy, with potential in both *in vitro* or *in vivo* based assays.

2.4 Materials and Methods

2.4.1. GECI screening

Plasmids encoding GECIs (GECOs and GCaMPs) were obtained from Addgene for screening in whole cells. Each probe was cotransfected with Orai1 and STIM1 into HEK 293A cells using Lipofectamine 2000 (Invitrogen, Carlsbad, CA) for 24 hr, then plated on to poly-L-

lysine coated coverslip chambers overnight before imaging the next day, at 48 hr post-transfection. Before imaging, each coverslip was washed with Ca^{2+} free Ringer's solution before mounting onto an epifluorescence microscope with a perfusion system enabling rapid solution exchange. GECIs were imaged using xenon arc lamp excitation and a 495 nm single-edge dichroic beamsplitter with a 460/40 excitation filter and a 525/50 emission filter. Images were acquired every 10 seconds and analyzed using MetaFluor software (Molecular Devices, Sunnyvale, CA).

2.4.2. Human T cell purification and nucleofection

Human peripheral blood mononuclear cells (PBMCs) were isolated from blood of voluntary healthy donors by Histopaque-1077 (1.077 g/mL; Sigma, St. Louis, MO) density gradient centrifugation. Human $CD3^+$ T cells were isolated using the EasySep Human T Cell Isolation Kit (StemCell Technologies, Vancouver, Canada) according to manufacturer's instructions. The purity of isolated cells was confirmed to be >95% by flow cytometry. Purified cells were rested overnight in complete RPMI, then transfected by nucleofection (Lonza, Walkersville, MD), using the Cell Line Nucleofector Kit V with the high-viability "X-001" protocol for Jurkats E6-1, and the Human T Cell Nucleofector Kit with high-viability "U-014" protocol for primary human T cells. GCaMP6f or Salsa6f (tdTomato-V5-GCaMP6f construct) were transfected as indicated. Human T cells were used for experiments 24-48 hr after transfection. For experiments using activated T cells, transfected T cells were rested for 3-4 hr in complete RPMI as indicated in the manufacturer's instructions, then washed and activated on plate-bound αCD3 and αCD28 (Tonbo Biosciences, San Diego, CA)

in 2.5 ng/mL recombinant human IL-2 (BioLegend, San Diego, CA), and imaged 24-48 hr after transfection.

2.4.3 Two-photon imaging and analysis

Multi-dimensional (x, y, z, time, emission wavelength) two-photon microscopy using a custom-built system (Nguyen et al. 2001) was employed to image transfected HEK, Jurkat, or human T cells plated onto poly-L-lysine coated coverslip chambers, using a 900 nm femtosecond pulsed laser. Fluorescence emission was split by 510 nm & 560 nm dichroic mirrors into three detector channels, but only two were acquired to visualize fluorescence from GCaMP6f (green) and the various RFPs (red). For imaging, a custom perfusion system allowed for rapid solution exchange. Data was acquired using MetaMorph software (Molecular Devices, Sunnyvale, CA), then processed and analyzed using Imaris software (Bitplane USA, Concord, MA). Volume analysis was used to determine the total fluorescence intensity in the green and red channels, which was then used to calculate the ratio for Salsa6f. Photobleaching of tdTomato fluorescence intensity (20-30% decline) was corrected in ratio calculations, as a linear function of time.

2.4.4 RFP-V5-GCaMP6f plasmid generation

For construction of fusion probes to GCaMP6f, plasmids encoding various RFPs were obtained from Addgene (TagRFP-T, mApple, tdTomato, DsRed-Express2), and the pEGFP-N1 vector (Clontech, Mountain View, CA) was used as a backbone. GCaMP6f was amplified via PCR with N- and C-terminal primers (5’ CACAACCGGTCGCCACCATGGTCGACTCATCACG-

TC 3’ and 5’ AGTCGCGGCCGCTTTAAAGCTTCGCTGTCATCATTTGTAC 3’) and ligated into pEGFP-N1 at the AgeI/NotI sites to replace the eGFP gene, while all RFPs were amplified via PCR with common N- and C-terminal primers (5’ ATCCGCTAGCGCTACCGGTCGCC 3’ and 5’ TAACGAGATCTGCTTGTACAGCTCGTCCATGCC 3’) and ligated into the backbone at the NheI/BglII sites. An oligo containing the V5 epitope tag was synthesized with sense and antisense strands (5’ GATCTCGGGTAAGCCTATCCCTAACCCTCTCCTCGGTCTCGATTCTACG 3’ and 5’ GATCCGTAGAATCGAGACCGAGGAGAGGGTTAGGGATAGGCTTACCCGA 3’) and ligated into the backbone at the BglII/BamHI sites, linking the RFP to GCaMP6f. The amplified regions of each construct were verified by sequencing (Eton Bioscience Inc., San Diego, CA). The resulting plasmids, driven by the CMV immediate early gene promoter, were used for transient transfections in HEK 293A cells with Lipofectamine 2000, and in Jurkat cells and primary human T cells with Amaxa Nucleofection.

CHAPTER 3: Cell-intrinsic activation of Orai1 regulates human T cell motility

(Dong et al., manuscript under review)

In this chapter, I wrote all of the sections with guidance and contributions from J.L.D. and M.D.C., performed all of the experiments except for **3.1B,C,D**, **3.S1**, **3.2**, and made all of the figures.

3.1 Introduction

To initiate the adaptive immune response, T cells must make direct contact with antigen-presenting cells (APCs) in the lymph node, enabling T cell receptors (TCRs) to engage peptide-bound MHC molecules presented on the APC surface. Because cognate antigens are rare for any given TCR, many APCs must be scanned to identify those bearing cognate antigens. Thus, optimizing T cell motility to balance search sensitivity and speed is crucial for efficient antigen search and proper immune function (Cahalan and Parker 2005; Krummel et al. 2016). Both cell-intrinsic and environmental factors have been proposed to regulate T cell motility within lymph nodes and peripheral tissues (Miller et al. 2002; Bousso and Robey 2003; Mempel et al. 2004; Mrass et al. 2010). T cell motility in lymph nodes, sometimes referred to as "basal motility", has been likened to diffusive Brownian motion, resembling a "stop-and-go" random walk with an overall exploratory spread that results in a linear mean squared displacement over time (Miller et al. 2002). Subsequent studies defined a role of cellular cues in guiding T cell migration, such as contact with the

lymph node stromal cell network or short-term encounters with resident dendritic cells (Miller et al. 2004; Bajenoff et al. 2006; Khan et al. 2011). Whereas the basic signaling mechanisms for cell-intrinsic induction of random motility have been previously explored in several cell types (Petrie et al. 2009), it remains unclear if such mechanisms apply in T cells.

Upon T cell recognition of cognate antigen, TCR engagement results in an elevated cytosolic Ca^{2+} concentration that acts as a "STOP" signal to halt motility and anchor the T cell to the site of antigen presentation (Donnadieu et al. 1994; Negulescu et al. 1996; Dustin et al. 1997; Bhakta et al. 2005; Moreau et al. 2015). The predominant mechanism for increasing cytosolic Ca^{2+} in T cells is through store-operated Ca^{2+} entry (SOCE), which is mediated by the molecular components STIM1 and Orai1. TCR stimulation triggers depletion of intracellular Ca^{2+} stores in the endoplasmic reticulum (ER), resulting in translocation of the ER-resident Ca^{2+} sensor STIM1 to specialized ER-plasma membrane (PM) junctions where Orai1 channels aggregate into puncta and activate to allow sustained Ca^{2+} influx (Liou et al. 2005; Roos et al. 2005; Zhang et al. 2005; Luik et al. 2006; Vig et al. 2006; Zhang SL 2006; Calloway et al. 2009; Wu et al. 2014). Orai1 channel activity is crucial for immune function, as human mutations in Orai1 result in severe combined immunodeficiency (SCID) (Feske et al. 2006). Additional roles of Orai1 have been defined in chemotaxis to certain chemokines and T cell homing to lymph nodes (Greenberg et al. 2013); actin cytoskeleton rearrangement (Schaff et al. 2010; Dixit et al. 2011; Babich and Burkhardt 2013); migration during shear flow (Schaff et al. 2010; Dixit et al. 2011); lipid metabolism (Maus et al. 2017); and dendritic spine maturation in neurons (Korkotian et al.

2017). However, despite their contributions to other aspects of T cell function, no role has been identified for Orai1 channels in T cell motility patterns underlying scanning behavior.

Ca^{2+} imaging studies commonly rely on small synthetic Ca^{2+} indicators such as the ratiometric probe fura-2. However, synthetic indicators must be loaded into cells and cannot be targeted to subcellular compartments or specific cell populations. Furthermore, synthetic indicators slowly leak out of cells over time, and thus are unsuitable for long-term studies. To overcome these limitations, genetically encoded Ca^{2+} indicators (GECIs) were first developed two decades ago as probes based on Förster Resonance Energy Transfer (FRET) (Miyawaki et al. 1997; Romoser et al. 1997; Perez Koldenkova and Nagai 2013). Since then, GECIs have undergone remarkable improvements in variety and functionality, including the optimization of single fluorescent protein-based indicators such as the GCaMP and the GECO series (Nakai et al. 2001; Zhao et al. 2011), as well as the new FRET-based TN indicators utilizing troponin C instead of calmodulin for the Ca^{2+} sensing element (Heim and Griesbeck 2004; Thestrup et al. 2014). Whereas single fluorescent protein-based indicators have high brightness and fast response kinetics, as non-ratiometric probes they are problematic for Ca^{2+} imaging in motile cells because fluorescence changes resulting from movement are indistinguishable from actual changes in Ca^{2+} levels. Here, we introduce a novel genetically encoded Ca^{2+} indicator, Salsa6f, consisting of GCaMP6f fused to tdTomato, providing high dynamic range and ratiometric capabilities.

In this study, we use human T cells to assess the role of Orai1 in cell motility. Expression of a dominant-negative Orai1-E106A construct was used to block Orai1 channel activity both *in vivo* within immunodeficient mouse lymph nodes (Greenberg et al. 2013),

and *in vitro* within microfabricated polydimethylsiloxane (PDMS) chambers (Jacobelli et al. 2010). We then utilize our genetically encoded Salsa6f probe to monitor spontaneous Ca^{2+} signaling in confined microchannels *in vitro*. Our results indicate that Ca^{2+} influx through Orai1 channels, activated intermittently in a cell-intrinsic manner, triggers spontaneous pauses during T cell motility that fine-tunes the search for cognate antigens.

3.2 Results

3.2.1 Validating a dominant-negative construct to inhibit Orai1 in human T cells

To study the role of Orai1 channel activity in T cell motility, we took a molecular genetic approach using the dominant-negative mutant Orai1-E106A to selectively eliminate ion conduction through the Orai1 pore. The glutamate residue at position 106 in human Orai1 forms the selectivity filter of the Orai1 pore (Prakriya et al. 2006; Vig et al. 2006; Yeromin et al. 2006), and because the Orai1 channel is a functional hexamer (Hou et al. 2012), mutation of E106 to neutrally charged alanine completely inhibits Ca^{2+} permeation in a potent dominant-negative manner (Greenberg et al. 2013). We confirmed Orai1 channel block by E106A by fura-2 Ca^{2+} imaging in activated human T cells transfected with either eGFP-tagged Orai1-E106A or empty vector for control. Following thapsigargin treatment to deplete the ER Ca^{2+} store, Ca^{2+} entry was greatly diminished in cells expressing eGFP-Orai1-E106A identified by fluorescence, referred to here as eGFP-E106^{hi} T cells, compared to empty vector-transfected control cells (**Figure 3.1A**). Ca^{2+} entry was also partially inhibited in some transfected T cells even though their eGFP fluorescence was too low to

detect. We refer to this mixed population as eGFP-E106A^{lo} cells. To further confirm that eGFP-E106A inhibits T cell activation, we challenged transfected human T cells with autologous dendritic cells pulsed with the superantigen Staphylococcal enterotoxin B (Lioudyno et al. 2008). T cell proliferation was markedly suppressed in eGFP-E106A^{hi} CD4^{+} and CD8^{+} T cells, but not in eGFP-E106A^{lo} T cells (**Figure 3.S1A**). This shows that reduced Orai1 channel activity present in eGFP-E106A^{lo} T cells is sufficient for T cell activation and proliferation. Taken together, these experiments show that eGFP-tagged Orai1-E106A expression can serve as a robust tool to assess cellular roles of Orai1 channel activity, and that transfected cells without detectable eGFP fluorescence can be used as an internal control.

Orai1 function in human T cell motility was evaluated *in vivo* using a human xenograft model in which immunodeficient NOD.SCID.β2 mice were reconstituted with human peripheral blood lymphocytes, followed by imaging of excised lymph nodes using two-photon microscopy (Greenberg et al. 2013). Reconstitution has been shown to produce a high density of human immune cells within the lymph nodes of immunodeficient mice (Mosier et al. 1988), simulating the crowded migratory environment experienced by T cells under normal physiological conditions. Three weeks after reconstitution, human T cells were purified from the same donor, transfected, and adoptively transferred into the reconstituted NOD.SCID.β2 mice (**Figure 3.S1B**). Whereas control T cells transfected with eGFP showed robust expression and successfully homed to lymph nodes following adoptive transfer 24 hr post-transfection (**Figure 3.1B**), eGFP-E106A transfected T cells did not home to lymph nodes when adoptively transferred 24 hr post-transfection (**Figure 3.1C**).

This result confirms our previous study indicating that functional Orai1 channel activity is required for T cell homing to lymph nodes (Greenberg et al. 2013). To circumvent the homing defect, we injected eGFP-E106A transfected T cells only 3 hr post-transfection, before the expression level of eGFP-E106A had become sufficiently high to block lymph node entry (**Figure 3.1D**).

3.2.2 Orai1 block increases human T cell motility within intact lymph node

To evaluate Orai1 function in T cell motility, we imaged human T cells within intact lymph nodes of reconstituted NOD.SCID.β2 mice by two-photon microscopy (**Figure 3.2A**). We found that eGFP-E106A^{hi} T cells migrated with higher average velocities than co-transferred, mock-transfected CMTMR-labeled T cells (12.8 ± 0.5 μm/min vs. 11.1 ± 0.5 μm/min, p = 0.0268; **Figure 3.2B**). Although both populations had similar maximum (Hodges-Lehmann median difference of -0.21 μm/min, -2.82 to 2.16 μm/min 95%CI) and minimum (Hodges-Lehmann median difference of -0.36 μm/min, -1.02 to 0.36 μm/min 95%CI) instantaneous cell velocities (**Figure 3.2C**), the arrest coefficient, defined by the fraction of time that cell velocity was < 2 μm/min, was six-fold lower for eGFP-E106A^{hi} T cells than for control T cells (0.02 ± 0.01 vs. 0.12 ± 0.03, p = 0.0406; **Figure 3.2D**). These differences in motility suggest that the increase in average cell velocity caused by Orai1 block is not due to eGFP-E106A^{hi} T cells moving faster than control T cells, but rather due to a reduced frequency of pausing. Consistent with this interpretation, no eGFP-E106A^{hi} T cells with average velocities < 7 μm/min were observed, unlike control T cells in which 23% of average velocities were < 7 μm/min (**Figure 3.2E**).

To replicate our findings in a different immunodeficient mouse model, we repeated our human T cell adoptive transfer protocol using NOD.SCID mice depleted of NK cells. Lymph nodes in these mice are small and contain reticular structures but are completely devoid of lymphocytes (Shultz et al. 1995). Similar to experiments on reconstituted NOD.SCID.β2 mice, eGFP-E106A^{hi} human T cells in NOD.SCID lymph nodes migrated with elevated average velocities compared to control T cells (11.0 ± 0.5 μm/min vs. 8.8 ± 0.3 μm/min, p = 0.0004; **Figure 3.2F**), and exhibited lower arrest coefficients (0.10 ± 0.02 vs. 0.16 ± 0.01, p = 0.0516; **Figure 3.2G**). Both eGFP-E106A^{hi} and control T cells migrated at lower speeds in the NK-depleted NOD.SCID model compared to the reconstituted NOD.SCID.β2 model. Because control human T cells in reconstituted NOD.SCID.β2 lymph nodes migrated at similar speeds to what we have previously seen for wildtype mouse T cells *in vivo* (Miller et al. 2002), reconstitution results in a lymph node environment that more closely mimics normal physiological conditions. Furthermore, the greater effect of Orai1 block on T cell arrest coefficients in crowded reconstituted lymph nodes suggests that Orai1's role in motility is more pronounced in crowded cell environments.

3.2.3 Orai1 channel activity triggers pauses during human T cell motility *in vitro* in the absence of extrinsic cell contact

To evaluate whether the pronounced effect of Orai1 channel block on the arrest coefficient in reconstituted lymph nodes was a result of environmental factors such as increased cellular contacts or increased confinement, we tracked human T cells in microfabricated PDMS chambers with cell-sized microchannels 7 μm high x 8 μm wide. These ICAM-1

coated microchannels simulate the confined environment of densely packed lymph nodes (Jacobelli et al. 2010), while eliminating possible cell-extrinsic factors. Transfected human T cells were activated with plate-bound anti-CD3/28 antibodies and soluble IL-2, then dropped into chambers and monitored by time-lapse confocal microscopy, using phase contrast to visualize eGFP-E106A^{lo} T cells (**Figure 3.3A,B**). Upon entry into microchannels, eGFP-E106A^{hi} T cells migrated with higher average cell velocities than eGFP-E106A^{lo} T cells (14.2 ± 0.6 μm/min vs. 10.9 ± 0.5 μm/min, $p < 0.0001$; **Figure 3.3C**), similar to our *in vivo* findings from intact lymph node (*c.f.*, **Figures 3.3C, 3.2B**). To ensure that the observed difference in cell velocity was due to suppressed Orai1 channel function and not overexpression of Orai1 protein, we also tracked T cells transfected with eGFP-tagged wildtype Orai1. Both eGFP-Orai1^{hi} and eGFP-Orai1^{lo} T cells migrated at the same average cell velocity (10.7 ± 0.8 μm/min vs. 10.5 ± 0.8 μm/min; Hodges-Lehmann median difference of -0.84 μm/min, -2.96 to 1.28 μm/min 95%CI; **Figure 3.3C**), demonstrating that Orai1 channel overexpression, in itself, does not perturb T cell motility in microchannels. Since eGFP-E106A^{lo} T cells have reduced Orai1 channel activity but still retain the same cell velocity as eGFP-Orai1 transfected T cells (*c.f.*, **Figures 3.1A, 3.3C**), this suggests that partial Orai1 function is sufficient to generate normal pausing frequency in confined environments. The frequency distribution of cell velocities *in vitro* is comparable to our *in vivo* data: fewer GFP-E106A^{hi} T cells migrated with average cell velocities < 7 μm/min as compared to eGFP-E106A^{lo} T cells (11% vs 29%; *c.f.*, **Figures 3.3D, 3.2E**). Furthermore, eGFP-E106A^{hi} T cells exhibited lower arrest coefficients (0.05 ± 0.01 vs. 0.08 ± 0.01, $p = 0.0015$; **Figure 3.3E**) and less variation in velocity than eGFP-E106A^{lo} T cells (39.5 ± 1.9 %

vs. 45.1 ± 1.6 %, p = 0.0138; **Figure 3.3F**). Although eGFP-E106A^{hi} T cells had lower arrest coefficients, the durations of their pauses were not significantly different than in eGFP-E106A^{lo} T cells (Hodges-Lehmann median difference of 0 seconds, -8.43 to 4.71 seconds 95%CI; **Figure 3.3G**). Taken together, the reduced arrest coefficients in eGFP-E106A^{hi} T cells without any change in the durations of pauses indicate that inhibition of Orai1 channel activity results in reduced frequency of pauses during T cell motility. These *in vitro* results confirm our *in vivo* findings and support the hypothesis that Orai1 activity intermittently triggers cell arrest, resulting in an overall decrease in motility within confined environments. Moreover, since our *in vitro* microchannel assay eliminates extrinsic cell-cell interactions, this indicates that Orai1 is activated in a cell-intrinsic manner when modulating T cell motility.

3.2.4 A novel ratiometric genetically encoded Ca^{2+} indicator, Salsa6f

In order to develop a better tool to monitor Ca^{2+} signaling in T cells both *in vivo* and *in vitro*, we took advantage of the latest generation of genetically encoded Ca^{2+} indicators (GECIs) (Zhao et al. 2011; Chen et al. 2013). A variety of single fluorescent protein-based GECIs were transiently expressed and screened in HEK 293A cells (**Figure 3.4A**), and GCaMP6f was selected based on fluorescence intensity, dynamic range, and Ca^{2+} affinity (k_d = 373 nM) suitable for detecting a variety of cytosolic Ca^{2+} signals. To enable cells to be tracked even when their basal Ca^{2+} level evokes little GCaMP6f fluorescence, we fused GCaMP6f to the Ca^{2+}-insensitive red fluorescent protein tdTomato, chosen for its photostability and efficient two-photon excitation (Drobizhev et al. 2011). A V5 epitope tag (Lobbestael et al.

2010) serves to link tdTomato to GCaMP6f (**Figure 3.4C**). The resultant ratiometric fusion indicator, coined "Salsa6f" for the combination of red tdTomato with the green GCaMP6f, was readily expressed by transfection into HEK 293A cells or human T cells. Salsa6f exhibited a ten-fold dynamic range, with a brightness comparable to GCaMP6f alone (**Figure 3.4A,B**). For two-photon microscopy, both components of Salsa6f can be visualized by femtosecond excitation at 900 nm (**Figure 3.4D**). GCaMP6f produces increased green fluorescence during elevations in cytosolic Ca^{2+}, while tdTomato provides a stable red fluorescence that facilitates cell tracking and allows for ratiometric Ca^{2+} imaging (**Figure 3.4D**). Salsa6f is excluded from the nucleus, ensuring accurate measurement of cytosolic Ca^{2+} fluctuations (**Figure 3.4D**). When expressed in human T cells, Salsa6f reported Ca^{2+} oscillations induced by immobilized anti-CD3/28 antibodies with a high signal to noise ratio and time resolution (**Figure 3.4E,F**).

3.2.5 Spontaneous Ca^{2+} signals during confined motility *in vitro* are correlated with reduced T cell velocity

Human $CD4^+$ T cells were transfected with Salsa6f, activated for two days with plate-bound anti-CD3/28 antibodies, then dropped into ICAM-1 coated microchambers. As previously shown (**Figure 3.4E**), Salsa6f is localized to the cytosol, with red fluorescence from tdTomato that reflects fluctuations in cell movement and very low baseline green fluorescence from GCaMP6f that rises sharply during Ca^{2+} signals (**Figure 3.5A-D**). Salsa6f-transfected human T cells were tracked in both confined microchannels (**Figure 3.5A**) and the open space adjacent to entry into microchannels (**Figure 3.5C**), to evaluate T cell

motility under varying degrees of confinement. Intracellular Ca^{2+} levels were monitored using the ratio of total GCaMP6f fluorescence intensity over total tdTomato fluorescence intensity, enabling detection of a notably stable baseline ratio unaffected by motility artifacts in moving T cells while reporting spontaneous Ca^{2+} signals that could be compared to changes in motility (**Figure 3.5B,D**, orange and black traces, respectively).

Human T cells expressing Salsa6f migrating in confined microchannels exhibited stable baseline cytosolic Ca^{2+} levels (**Figure 3.6A**), although sporadic Ca^{2+} signals were apparent as brief peaks unrelated to changes in motility (**Figure 3.6B**, arrowheads), or as more sustained periods of Ca^{2+} elevation associated with reduced cell velocity (**Figure 3.6B**, gray highlights). To evaluate the correspondence between T cell velocity and Ca^{2+} signals, we compared average T cell velocities during periods of sustained Ca^{2+} elevations to average velocities at baseline Ca^{2+} levels. T cell velocity decreased significantly when cytosolic Ca^{2+} was elevated above baseline (5.9 ± 0.1 μm/min vs. 10.0 ± 0.1 μm/min, $p < 0.0001$; **Figure 3.6C**). Ca^{2+} signaling episodes that last for 30 seconds or longer accompany and appear to closely track the duration of pauses in cell movement. Comparison of instantaneous velocities with corresponding cytosolic Ca^{2+} signals by scatter plot revealed a strong inverse relationship: highly motile T cells always exhibited baseline Ca^{2+} levels, while elevated Ca^{2+} levels were only found in slower or arrested T cells (**Figure 3.6D**). It is important to note that these Ca^{2+} signals and reductions in velocity occurred in the absence of any extrinsic cell contact or antigen recognition, indicating that Ca^{2+} elevations, like pausing and Orai1 activation, are triggered in a cell-intrinsic manner.

To compare the effects of Orai1 activity on the motility of T cells in different *in vitro* environments, we also monitored T cell migration within the open space in PDMS chambers adjacent to entry into microchannels (*c.f.*, **Figure 3.5A,C**). We reasoned that in this two-dimensional space with reduced confinement, T cells may not gain sufficient traction for rapid motility, and instead may favor integrin-dependent sliding due to increased exposure to the ICAM-1 coated surface (Krummel et al. 2014). In addition, the same population of T cells could be tracked as they migrated into and along the confined microchannels, providing a valuable internal control. We found that eGFP-E106A^{hi} T cells migrated with similar velocities to eGFP-E106A^{lo} T cells in the open space (12.0 ± 1.0 μm/min vs. 12.2 ± 0.7 μm/min; Hodges-Lehmann median difference of 0.15 μm/min, -2.46 to 2.40 μm/min 95%CI; **Figure 3.6E**), but these eGFP-E106A^{hi} T cells still exhibited higher motility in the microchannels than eGFP-E106A^{lo} T cells (15.4 ± 1.2 μm/min vs. 11.3 ± 1.0 μm/min; p = 0.0099; **Figure 3.6E**). Furthermore, Salsa6f transfected T cells within the open space rarely produced Ca^{2+} transients that coincided with reduced instantaneous velocity (*c.f.*, **Figure 3.6D,F**, top left quadrants, 13% of the time in microchannels vs 2% in open space), implying that Ca^{2+} elevations, and by extension, Orai1 channel activity, do not generate pauses when T cells are reliant on integrin binding for motility. Taken together, these experiments establish a role for the cell-intrinsic activation of Orai1 channels in modulating T cell motility within confined environments.

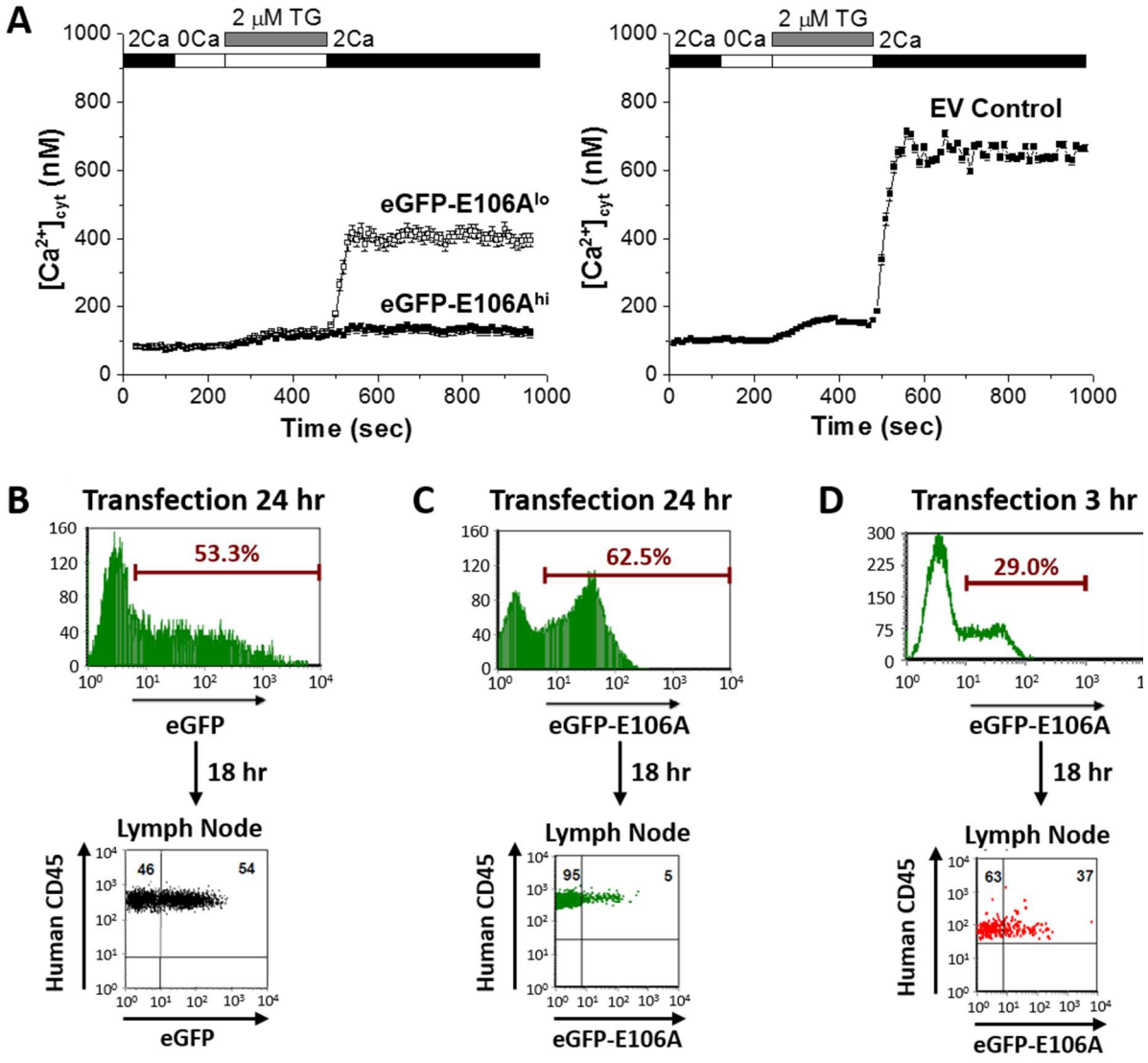

Figure 3.1. Effects of expressing Orai1-E106A on human T cell function.

(**A**) Averaged thapsigargin-induced Ca^{2+} entry, measured by fura-2, in activated human $CD4^+$ T cells transfected with eGFP-Orai1-E106A (left) or empty vector control (EV, right, n = 133 cells); eGFP-E106A transfected cells were grouped into two populations, either eGFP-E106A^{hi} with high eGFP fluorescence (solid squares, n = 43 cells) or eGFP-E106A^{lo} with no detectable eGFP fluorescence (empty squares, n = 115 cells); bars represent SEM,

data representative of at least three different experiments. (**B**) Human $CD3^+$ T cells transfected with eGFP for control and expression level was measured at 24 hr post-transfection before adoptive transfer into reconstituted NOD.SCI.β2 mice; cells were recovered from lymph nodes 18 hr later and eGFP fluorescence was used to measure homing to lymph nodes. (**C,D**) Human $CD3^+$ T cells were transfected with eGFP-E106A and expression level was measured before adoptive transfer into reconstituted NOD.SCI.β2 mice either 24 hr (**C**) or 3 hr (**D**) post-transfection; cells were recovered from lymph nodes 18 hr later and eGFP fluorescence was used to measure homing to lymph nodes; data representative of independent experiments from 12 different donors.

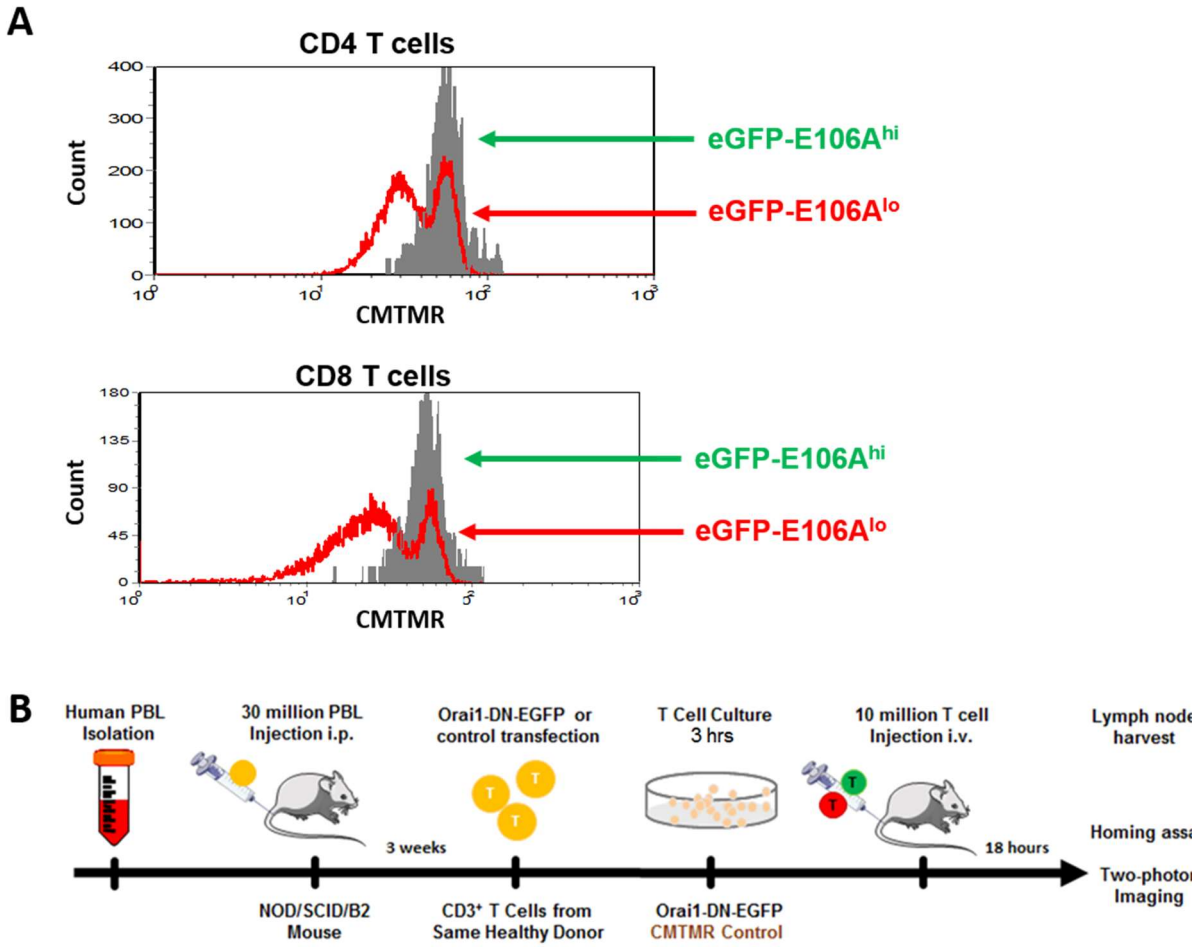

Figure 3.S1. Validation of dominant-negative eGFP-Orai1-E106A to assess activation, homing, and motility of human T cells.

(**A**) Primary human $CD4^+$ and $CD8^+$ T cells were transfected with eGFP-E106A, then uniformly labeled with the fluorescent cell tracker dye CMTMR and co-cultured with SEB-pulsed primary human dendritic cells from the same donor; proliferation was assessed after 72 hr by CMTMR dilution as measured by flow cytometry. (**B**) Protocol for homing and two-photon imaging of transfected human $CD3^+$ T cells in reconstituted NOD.SCID.β2 mouse lymph node.

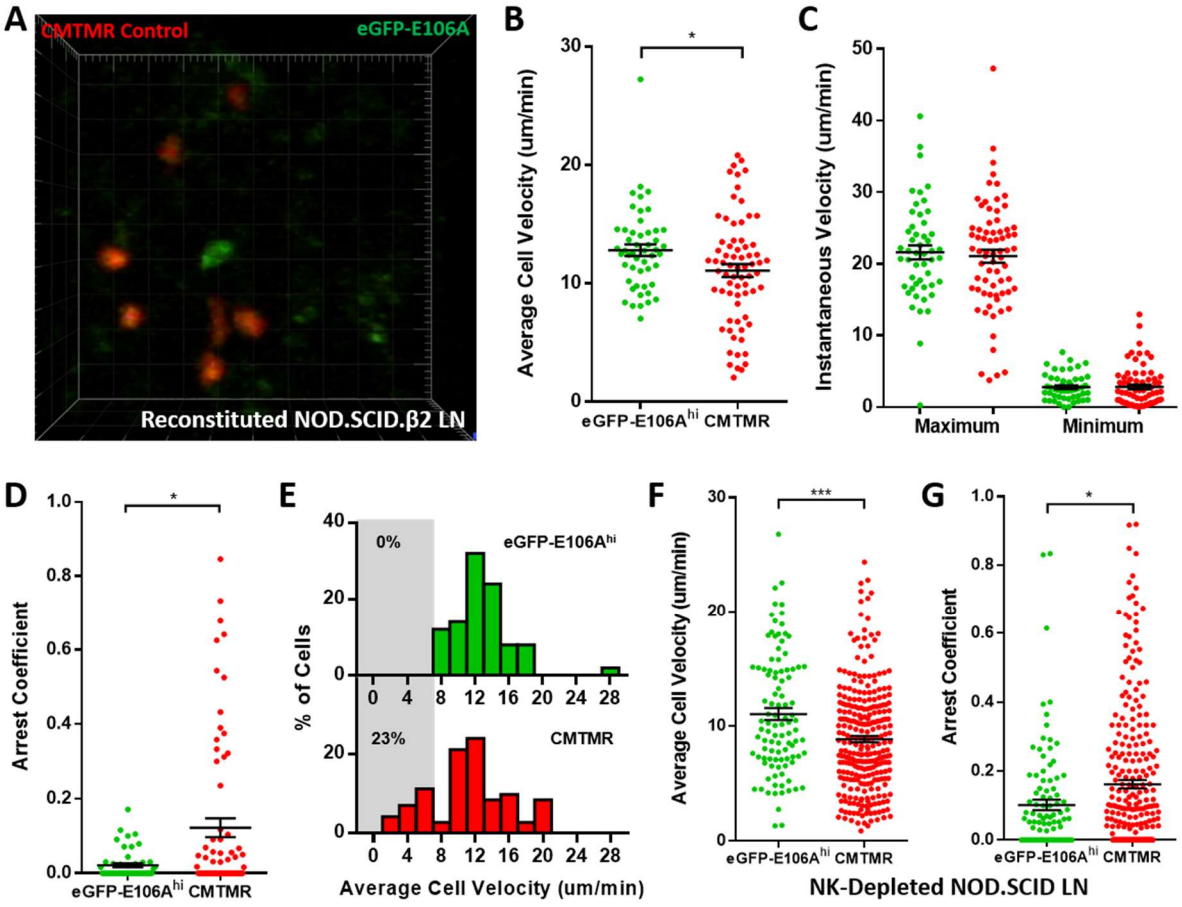

Figure 3.2. Orai1 block increases human T cell motility within reconstituted NOD.SCID.β2 lymph nodes.

(**A**) Two-photon microscopy of migrating human T cells, showing eGFP-E106A transfected cells in green and CMTMR-labeled mock transfected cells in red, within intact mouse lymph node 18 hours after adoptive co-transfer of $5x10^6$ of each cell type. (**B**) Average cell velocities of eGFP-E106A^{hi} (n = 50) versus CMTMR-labeled control (n = 71) T cells; bars represent mean ± SEM, data from independent experiments using 4 different donors. (**C**) Maximum and minimum cellular instantaneous velocities of eGFP-E106A^{hi} (green) versus CMTMR-labeled (red) control T cells. (**D**) Arrest coefficients of eGFP-E106A^{hi} compared

with CMTMR-labeled control T cells, defined as fraction of time with instantaneous velocity < 2 μm/min. (**E**) Frequency distribution of average cell velocities for eGFP-E106A^{hi} (top) and CMTMR-labeled control T cells (bottom), cells with average velocity < 7 μm/min are highlighted in gray; tick marks denote the center of every other bin. (**F,G**) Average cell velocities (**F**) and arrest coefficients (**G**) of eGFP-E106A^{hi} (green, n = 102) versus CMTMR-labeled control (red, n = 278) human T cells in NK cell depleted immunodeficient mouse lymph nodes; bars represent mean ± SEM, data from independent experiments using 8 different donors, *** = $p < 0.005$.

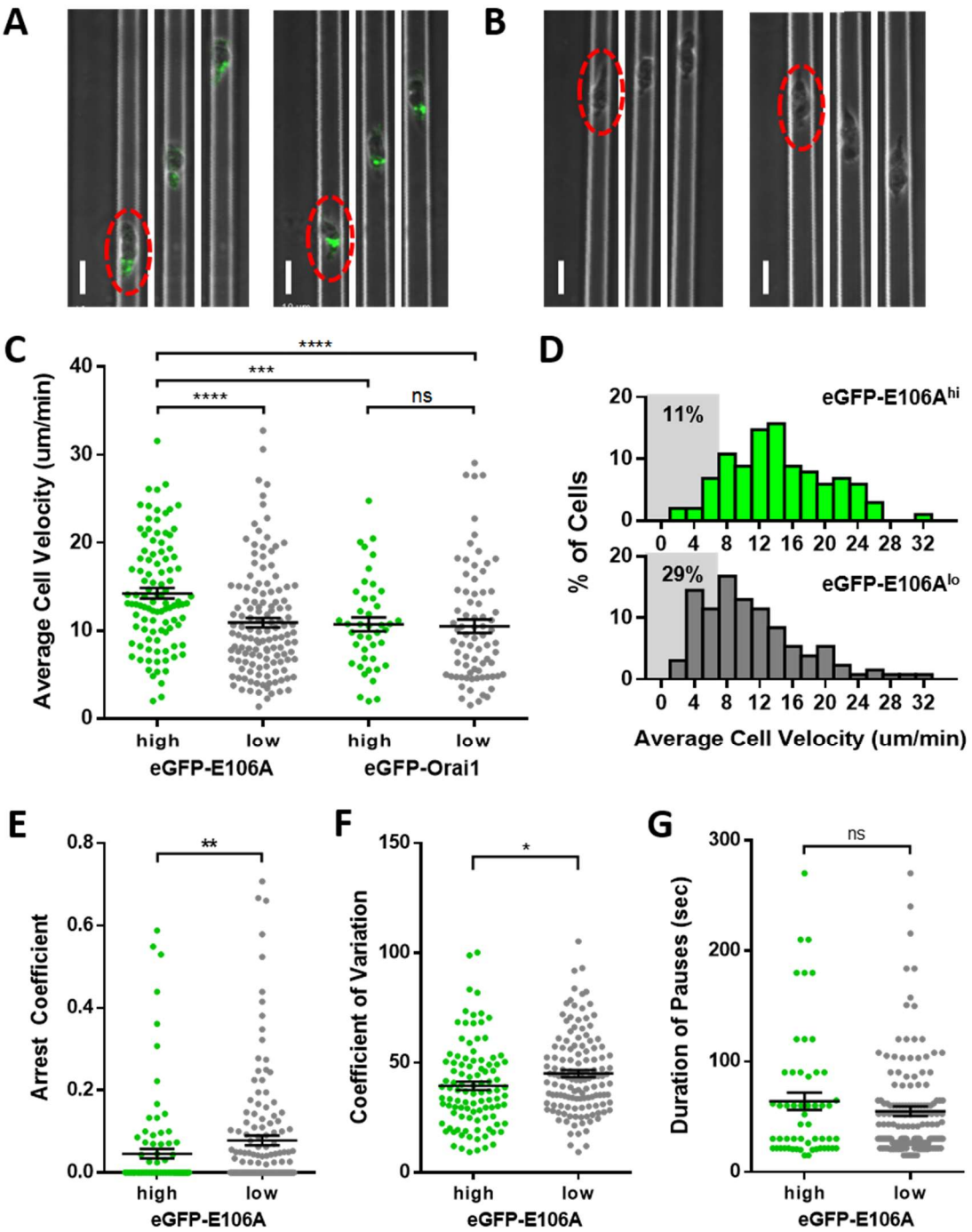

Figure 3.3. Orai1 block reduces frequency of pausing during human T cell motility *in vitro*.

(**A,B**) Confocal microscopy of eGFP-E106A transfected human $CD4^+$ T cells in microfabricated channels 7 μm high by 8 μm wide, showing two individual eGFP-$E106A^{hi}$ T cells (**A**) and two eGFP-$E106A^{lo}$ T cells (**B**), each circled in red in the first frame; individual images taken 1 min apart, scale bar = 10 μm. (**C**) Comparison of average cell velocities of eGFP-E106A transfected T cells (eGFP-$E106A^{hi}$ cells in green, n = 102; eGFP-$E106A^{lo}$ cells in gray, n =131) vs eGFP-Orai1 transfected control T cells (eGFP-$Orai1^{hi}$ cells in green, n = 43; eGFP-$Orai1^{lo}$ cells in gray, n = 76); bars represent mean ± SEM, data from independent experiments using 5 different donors. (**D**) Frequency distribution of average cell velocities of eGFP-$E106A^{hi}$ (top) and eGFP-$E106A^{lo}$ (bottom) human T cells, cells with average velocity < 7 μm/min are highlighted in gray; tick marks denote the center of every other bin. (**E**) Arrest coefficients of eGFP-$E106A^{hi}$ vs eGFP-$E106A^{lo}$ human T cells, defined as fraction of time each individual cell had an instantaneous velocity < 2 μm/min. (**F**) Variance in velocity of eGFP-$E106A^{hi}$ vs eGFP-$E106A^{lo}$ human T cells, coefficient of variation is calculated by standard deviation divided by the mean of instantaneous velocity for each individual cell. (**G**) Duration of pauses for eGFP-$E106A^{hi}$ vs eGFP-$E106A^{lo}$ human T cells; bars represent mean ± SEM, * = $p < 0.05$, ** = $p < 0.01$, *** = $p < 0.005$, **** = $p < 0.001$.

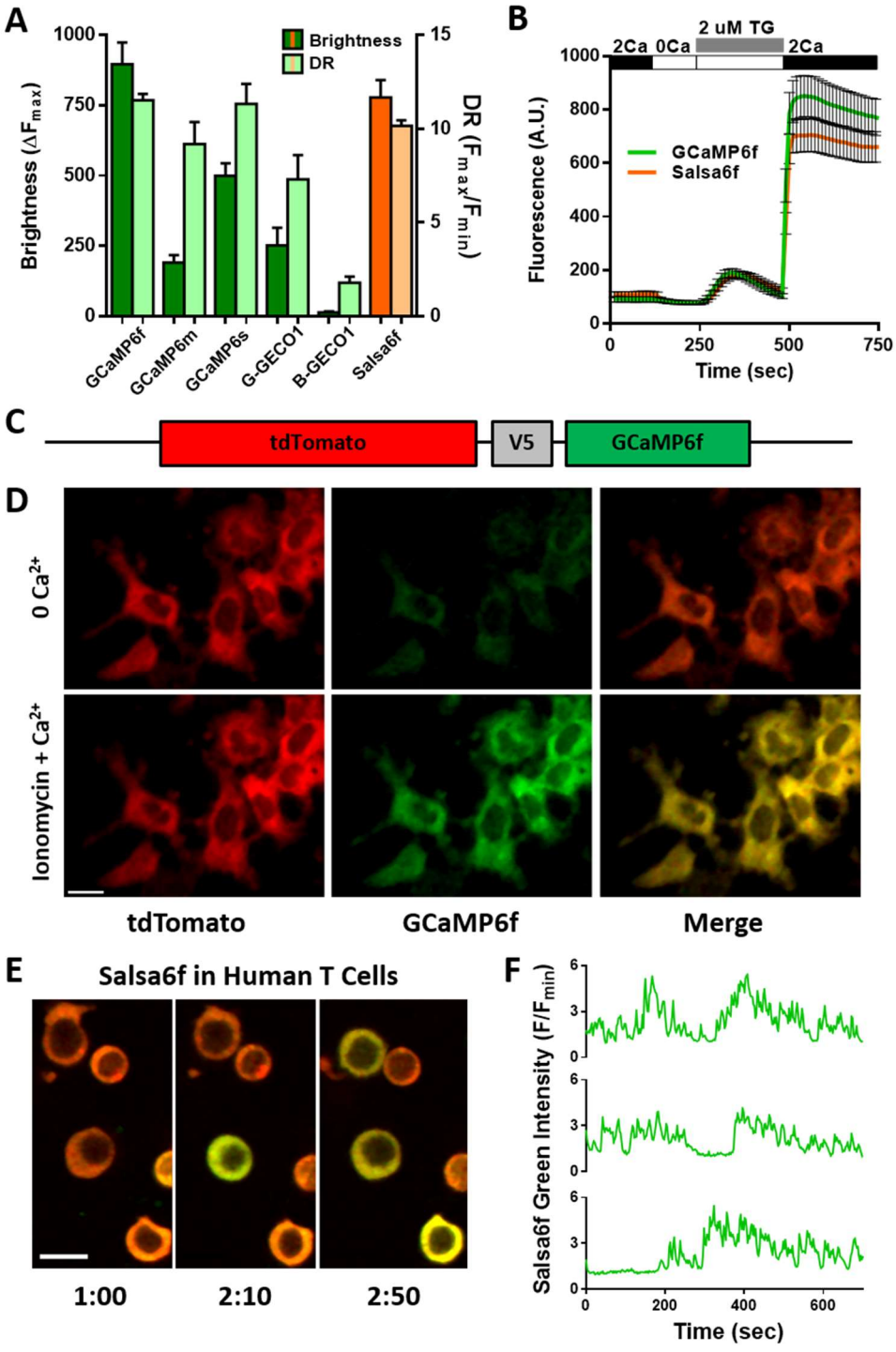

Figure 3.4. Design of novel tdTomato-V5-GCaMP6f fusion probe "Salsa6f" and characterization in living cells.

(**A**) Several genetically encoded Ca^{2+} indicators were screened *in vitro* in HEK 293A cells, by co-transfecting with Orai1/STIM1 and measuring Ca^{2+} influx after thapsigargin-induced store depletion, showing maximum change in fluorescence intensity in dark green bars and dynamic range (DR) in light green bars, with Salsa6f shown in orange bars on right; n > 30 cells per probe, from two different transfections, error bars indicate SEM. (**B**) Averaged thapsigargin-induced Ca^{2+} entry, measured by change in GFP fluorescence, in GCaMP6f (green, 11.52 ± 0.34, n = 63) or Salsa6f (orange, 10.16 ± 0.31, n = 78) transfected HEK cells; data from two different transfections, error bars indicate SEM. (**C**) Diagram of Salsa6f construct used in transfection. (**D**) Two-photon images of Salsa6f co-transfected in HEK cells with Orai1/STIM1, showing red (tdTomato), green (GCaMP6f), and merged channels, at baseline in 0 mM extracellular Ca^{2+} and after maximum stimulation with 2 μM ionomycin in 2 mM extracellular Ca^{2+}; scale bar = 20 μm; data representative of at least three different experiments. (**E**) Confocal time lapse microscopy of human $CD4^+$ T cells transfected with Salsa6f, then activated for two days on platebound anti-CD3/28 antibodies; time = min:sec, scale bar = 10 μm. (**F**) Representative cell traces of activated Salsa6f transfected human T cells, tracking green fluorescence intensity; data representative of at least three different experiments.

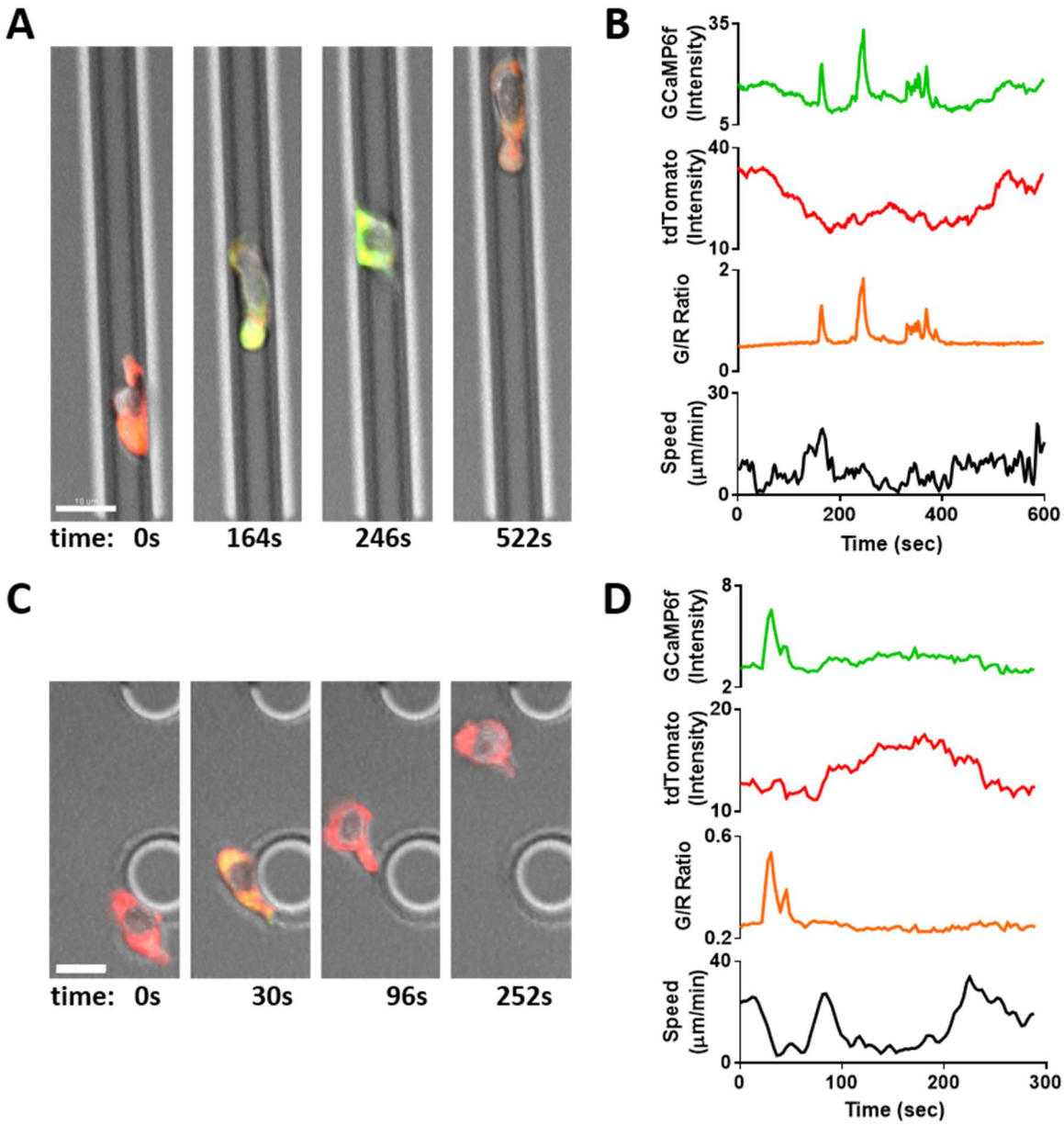

Figure 3.5. Tracking Ca^{2+} signals in human T cells *in vitro* with Salsa6f.

(**A,C**) Confocal microscopy of Salsa6f transfected human $CD4^+$ T cells in ICAM-1 coated microchannels 7 µm high by 8 µm wide (**A**) and open space (**C**), showing merged red (tdTomato), green (GCaMP6f), and DIC channels; circular structures shown in (**C**) are

support pillars part of the PDMS chamber; scale bar = 10 μm, time = sec. (**B,D**) Total intensity tracings of GCaMP6f (green) and tdTomato (red) fluorescence, GCaMP6f/tdTomato ratio (orange), and speed (black), for corresponding T cells shown in (**A**) and (**C**); data representative of independent experiments from three different donors.

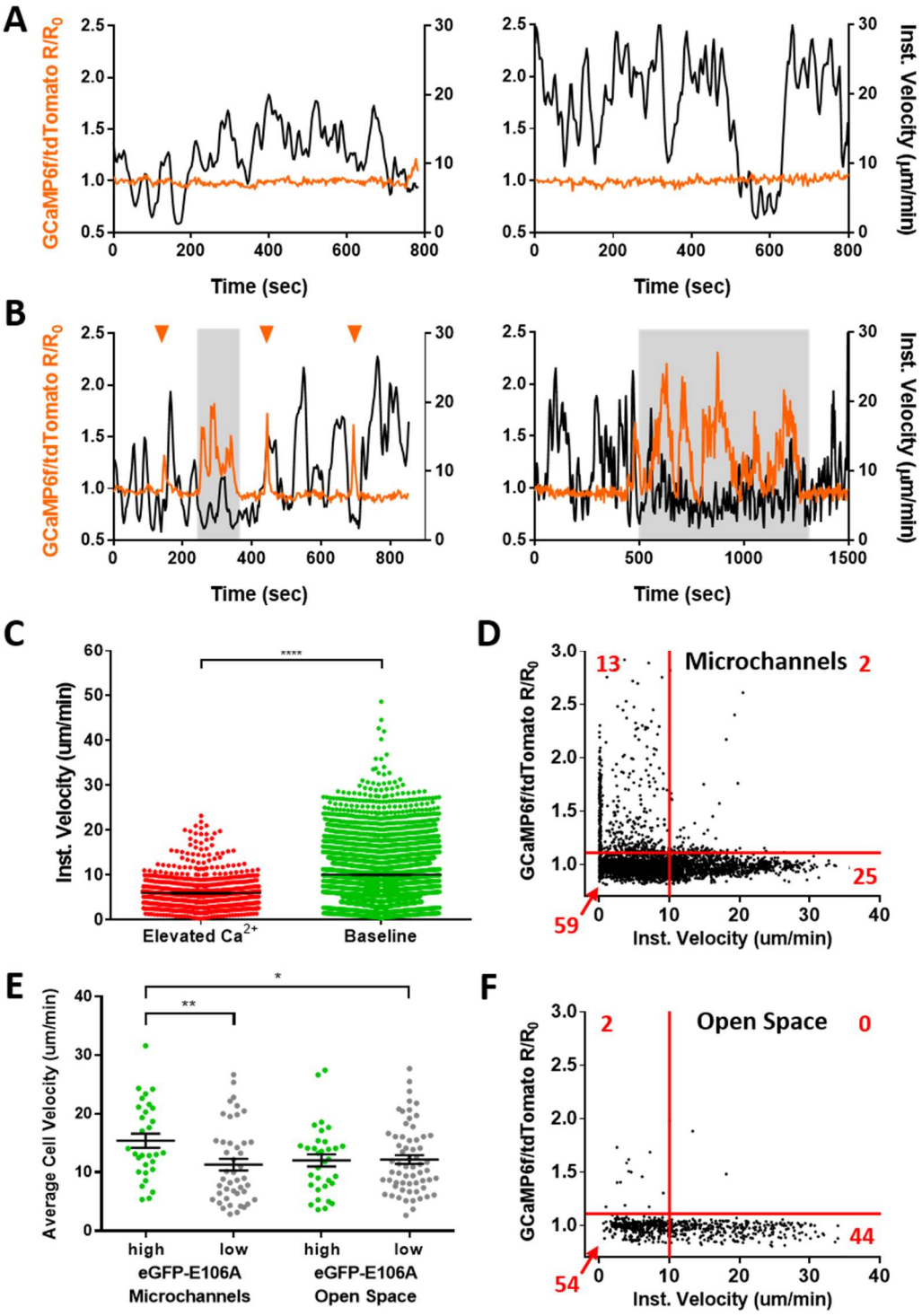

Figure 3.6. Spontaneous Ca2+ signals during human T cell motility in vitro are correlated with reduced velocity.

Sample tracks from Salsa6f transfected human T cells in microchannels, with intracellular Ca^{2+} levels measured by R/R_0 of GCaMP6f over tdTomato fluorescence intensity (orange), overlaid with instantaneous cell velocity (black), cells in (**A**) have stable Ca^{2+} levels, cells in (**B**) show brief Ca^{2+} transients (arrowheads) or sustained Ca^{2+} signaling (gray highlights). (**C**) Instantaneous velocity of Salsa6f transfected human T cells in microchannels during elevated cytosolic Ca^{2+} levels (red) and during basal Ca^{2+} levels (green); n = 22 cells, data from independent experiments using three different donors; **** = $p < 0.001$. (**D**) Scatter plot of Salsa transfected human T cells in microchannels, instantaneous cell velocity versus GCaMP6f/tdTomato R/R_0 for each individual time point analyzed; red numbers in each quadrant show percent of time points, split by 1.10 R/R_0 and 10 μm/min; n = 4081 points. (**E**) Mean track velocity of eGFP-E106A transfected human T cells, comparing eGFP-E106A^{hi} (green) versus eGFP-E106A^{lo} T cells (gray) in confined microchannels vs open space; n = 30, 44, 33, and 62 cells, respectively; bars represent mean ± SEM, data from independent experiments using two different donors, * = $p < 0.05$, ** = $p < 0.01$. (**F**) Scatter plot of Salsa transfected human T cells in open space, instantaneous cell velocity versus GCaMP6f/tdTomato R/R_0 for each individual time point analyzed; red numbers in each quadrant show percent of cells, split by 1.10 R/R_0 and 10 μm/min; n = 723 points.

3.3 Discussion

In this study, we demonstrate that Orai1 channel activity regulates motility patterns that underlie immune surveillance, specifically within confined environments. Human T cells expressing the dominant-negative Orai1-E106A construct migrated with higher average velocities than controls, both *in vivo* in immunodeficient mouse lymph nodes and *in vitro* in confined microchannels. In particular, we found that the increase in average cell velocity was not due to an increase in maximum cell velocity, but to a reduced frequency of cell arrest. Furthermore, we introduce a novel ratiometric genetically encoded Ca^{2+} indicator, Salsa6f, and show in confined microchannels devoid of cell-extrinsic factors, that human T cells exhibit spontaneous Ca^{2+} signals that coincide with reduced cell velocity. We propose that cell-intrinsic activation of Orai1 channel activity regulates the timing of stop-and-go motility in T cells and tunes the search for cognate antigen in the crowded lymph node.

Salsa6f preserves the exceptional performance of GCaMP6f, with similar brightness and dynamic range, and adds to it the bright fluorescence of tdTomato, allowing cell tracking in the absence or presence of Ca^{2+} signaling. FRET based ratiometric indicators (Heim and Griesbeck 2004; Thestrup et al. 2014) lack the brightness and dynamic range of Salsa6f. Exclusion of Salsa6f from the nucleus enables precise monitoring of cytosolic Ca^{2+} signals. In addition, we observed no overt effects of Salsa6f expression on cell behavior. Ratiometric imaging of Salsa6f eliminates motility artifacts and reveals stable baseline levels of Ca^{2+} in the cytoplasm of rapidly moving human T cells; this finding enables Ca^{2+} signals to be identified clearly and their temporal progression followed precisely. Moreover, both GCaMP6f and tdTomato components of Salsa6f can be visualized in two-

photon microscopy by femtosecond excitation at 900nm. The genetically encoded nature of Salsa6f allows it to be continuously expressed in stably integrated cell lines or transgenic reporter animals, enabling tracking of cell fates and long term studies. Taken together, these considerations indicate that Salsa6f is well suited for assessing links between Ca^{2+} signaling and T cell motility and activation, and demonstrate that Salsa6f could be usefully employed to study Ca^{2+} signaling dynamics in many other cell types.

Our Orai1-E106A construct derives its specificity and potency by targeting the pore residue responsible for the channel selectivity filter. Incorporation of Orai1-E106A likely blocks heterodimers of Orai1 and other channels, such as Orai2 or Orai3, in addition to homomeric Orai1 channels. Very recent evidence demonstrates the existence of heteromeric channels composed of Orai1 and Orai2 in T cells (Vaeth et al. 2017). These heteromers appear to simply reduce the flow of Ca^{2+} through the Orai1 channel without targeting additional signaling pathways. In the absence of contradictory evidence, we conclude that in T cells Orai1-E106A acts to produce an essentially complete functional knockdown of Orai1-mediated store-operated Ca^{2+} entry.

In lymph nodes, T cells experience a dense and crowded environment packed with fibroblastic reticular cells, resident dendritic cells, and numerous other migrating immune cells (Miller et al. 2002; Bajenoff et al. 2006). Over the last decade there has been a developing realization that mechanisms of motility in the lymph node differ in important ways from mechanisms used in less densely packed tissues and in standard, adhesion-rich *in vitro* assays. First, integrins – key determinants of lymphocyte adhesion and key components of *in vitro* motility assays – are dispensable for T cell and dendritic cell motility

in the lymph node, where the absence of shear forces prevent stable integrin adhesiveness (Woolf et al. 2007; Lammermann et al. 2008). Second, theoretical and experimental work suggested the existence of a novel motility mode in which confined cells brace against their neighbors to push through crowded environments (Hawkins et al. 2009). Third, development of an *in vitro* assay using microchannels has enabled cell confinement to be varied *in vitro*, allowing confinement to be studied in isolated cells and mimicking the effects of cell crowding inside intact tissues such as the lymph node (Jacobelli et al. 2010). Under confined conditions that elicit maximal cell velocities, T cells utilize high speed "amoeboid walking" which relies on multiple brief contacts to substrate, independent of integrin function. This motility mode appears to be driven by actin-network expansion and contraction of myosin IIA motors, which facilitates protrusive flowing of the cell's leading edge (Jacobelli et al. 2010; Krummel et al. 2014). Taken together, these studies indicate that amoeboid walking is the predominant mode of T cell motility within lymph nodes.

Alternatively, when abundant extracellular adhesion molecules are available, T cells favor an integrin-dependent motility mode termed "haptokinetic sliding", such as in peripheral tissues, or in open field cell motility assays (Svensson et al. 2010; Krummel et al. 2014). Haptokinetic sliding is generally slower than amoeboid walking and relies upon a single continuous zone of contact to substrate. Integrin-dependent open field *in vitro* assays have been used to highlight the accumulation of $K_{Ca}3.1$ and TRPM7 channels at the uropod where the Ca^{2+} dependent protease calpain-2 may regulate turnover of LFA-1 adhesions (Svensson et al. 2010; Kuras et al. 2012). While these integrin-dependent assays reportedly exclude a role for Orai1 in T cell motility, we argue that they do not reflect the predominant

mode of motility used *in vivo* in the lymph node, and so do not bear directly upon the involvement of Orai1 in T cell motility in the lymph node. However, assessing integrin-dependent motility in parallel with confinement-dependent motility allows identification of motility mode-specific mechanisms and controls for cell health and cytoskeletal integrity.

Many studies demonstrate that Ca^{2+} influx through Orai1 is a signal that selectively activates downstream effectors, including calmodulin, calcineurin, and the transcription factor NFAT (Dolmetsch and Lewis 1994; Negulescu et al. 1994; Dolmetsch et al. 1997; Kar et al. 2014). We observe inhibition of pausing by Orai1 block only under confined conditions both *in vitro* and *in vivo*; this indicates that Orai1 block is not generally deleterious for cell health and movement, but instead acts upon subcellular mechanisms that are selectively employed during confined motility. The maximum cell velocity and mean pause length are unchanged by Orai1 block. Instead, Orai1 block selectively alters the timing of when pauses are triggered during T cell motility. The selective alteration of timing by mutation is a hallmark of cell regulatory pathways and, together with the widespread signaling roles already ascribed to Orai1 in other systems, establishes that Orai1 channel activity acts to regulate T cell motility. This model is supported by our Ca^{2+} imaging data: episodes of Ca^{2+} signaling lasting longer than 30 s coincide with pauses in cell movement. In many contexts, Ca^{2+} signaling has been to shown not only accompany, but also to cause, cell arrest and loss of cell polarity, such as in T cells after activation by antigen (Negulescu et al. 1996; Dustin et al. 1997; Wei et al. 2007). While we do not show that the Ca^{2+} signals we observe emanate directly from Orai1 channels, taken together our

data are consistent with Orai1 actively regulating cell motility by directly inducing subcellular mechanisms that lead to cell arrest.

In previous studies of Orai1 signaling, Orai1 activation has been placed downstream of extracellular ligand binding to cell surface receptors, integrating their input upon use-dependent depletion of Ca^{2+} from the ER (Feske 2007; Cahalan and Chandy 2009). Using *in vitro* microchannel assays, we find that Orai1 block alters motility in the absence of ongoing cell-cell interactions. Therefore, Orai1 is activated in an unknown cell-intrinsic manner; at this point it is unclear which aspects of internal cell state lead to Orai1 channel opening and pauses in motility. Our identification of Orai1 provides a clear new entry into mechanisms that drive T cells motility patterns used for immune surveillance. Of particular interest is determining the step in the signaling cascade from phospholipase C to Orai1 that is targeted by this novel activation pathway.

The apparently random nature of naïve T cell movement in the lymph node has led to the hypothesis that T cells use intrinsic and stochastic motility mechanisms to accomplish immune surveillance (Wei et al. 2003; Mrass et al. 2010; Germain et al. 2012). Because of recent studies, our understanding of the molecular mechanisms that produce intrinsic motility patterns is beginning to take shape (Jacobelli et al. 2010; Gerard et al. 2014). Myosin 1g, like Orai1, is selectively required for cell-intrinsic motility mechanisms under confined conditions (Gerard et al. 2014). Yet differences in phenotype between Orai1 and Myo1g block suggest that these proteins act in different, and in part opposing, ways to control T cell motility. While Orai1 block reduces pausing but does not alter T cell velocity, Myo1g block increases pausing and causes cells to move faster. Our observations support

the assertion that Myo1g and Orai1 act in parallel cell-intrinsic pathways that jointly modulate T cell motility.

Our identification of an intrinsic Orai1-dependent T cell motility program provides further support for the hypothesis that intrinsic and stochastic T cell motility patterns underlie immune surveillance in the lymph node. Immune surveillance requires balancing many factors associated with antigen search, including speed and sensitivity. Myo1g activity biases surveillance toward sensitivity by increasing the duration of individual T cell- dendritic cell contacts. Pauses in motility caused by Orai1 activity could allow similar biases in surveillance by increasing the fraction of time that, collectively, T cells are stationary and available for extended contacts with dendritic cells. Moreover, in the absence of other motility changes, the interval between Orai1-dependent pauses determines the distance T cells travel between pauses. In this way Orai1 channel activity could tailor T cell excursions to match the density and reach of dendritic cells in the lymph node.

3.4 Materials and Methods

3.4.1 Human T cell purification and transfection

Human PBMCs were isolated from blood of voluntary healthy donors by Histopaque-1077 (1.077 g/mL; Sigma, St. Louis, MO) density gradient centrifugation. Human $CD3^+$, $CD4^+$, or $CD8^+$ T cells were isolated using the appropriate EasySep Human T Cell Isolation Kit (StemCell Technologies, Vancouver, Canada) according to manufacturer's instructions. The

purity of isolated cells was confirmed to be >95% by flow cytometry. Purified cells were rested overnight in complete RPMI, then transfected by nucleofection (Lonza, Walkersville, MD), using the high-viability "U-014" protocol. Enhanced green fluorescent protein (eGFP)-tagged wildtype Orai1, eGFP-tagged Orai1-E106A mutant, Salsa6f (tdTomato-V5-GCaMP6f construct), or empty vector control were transfected as indicated. Human T cells were used for experiments 3-48 hr after transfection. For *in vitro* imaging experiments, T cells were rested for 3-4 hr in complete RPMI as indicated in the manufacturer's instructions, then washed and activated on plate-bound αCD3 and αCD28 (Tonbo Biosciences, San Diego, CA) in 2.5 ng/mL recombinant human IL-2 (BioLegend, San Diego, CA), and imaged 24-48 hr after transfection.

3.4.2 Mice

NOD.Cg-*Prkdc*^{scid}*B2m*^{tm1Unc}/J (NOD.SCID.β2) and NOD.CB17-*Prkdc*^{scid}/J (NOD.SCID) mice obtained from Jackson Laboratory (Stock #002570 and #001303) were housed and monitored in a selective pathogen-free environment with sterile food and water in the animal housing facility at the University of California, Irvine. NOD.SCID.β2 mice were reconstituted with human peripheral blood leukocytes (PBLs) as described previously (Mosier et al. 1988). A total of 3×10^7 human PBLs were injected i.p., and experiments were performed three weeks later. To inhibit NK cell activity, NOD.SCID mice were i.p. injected with 20 μL anti-NK cell antibody (rabbit anti-Asialo GM1, Wako Chemicals, Irvine, CA) according to manufacturer's instructions 3-4 days before adoptive transfer of human T cells. Mice used were between 8 and 18 weeks of age. For adoptive transfer experiments,

$5x10^6$ human $CD3^+$ T cells were labeled with 10 μM CellTracker CMTMR dye (Invitrogen, Carlsbad, CA) for 10 min at 37 °C and adoptively transferred into NOD.SCID.β2 or NOD.SCID mice by tail-vein or retro-orbital injection.

3.4.3 Two-photon imaging and analysis

Multi-dimensional (x, y, z, time, emission wavelength) two-photon microscopy was employed to image fluorescently labeled lymphocytes in explanted mouse lymph nodes, using a 780 nm femtosecond pulsed laser as described previously (Matheu et al. 2012). Fluorescence emission was split by 510 nm & 560 nm dichroic mirrors into three detector channels, used to visualize eGFP-Orai1E106A transfected (green) adoptively-transferred cells, CMTMR-labelled control cells (red), and collagen (blue). For imaging, lymph nodes were oriented with the hilum away from the water dipping microscope objective (Olympus 20x, NA 0.9) on an upright microscope (Olympus BX51). The node was maintained at 36-37 °C by perfusion with medium (RPMI) bubbled with carbogen (95% O_2 / 5% CO_2). 3D image stacks of x=200 μm, y=162 μm, and z=50 μm were sequentially acquired at 18-20 second intervals using MetaMorph software (Molecular Devices, Sunnyvale, CA). This volume collection was repeated for up to 40 min to create a 4D data set. Data were processed and analyzed using Imaris software (Bitplane USA, Concord, MA), and the x,y,z coordinates of individual lymphocytes in the intact lymphoid organ were used to create individual cell tracks.

3.4.4 Microchannel fabrication and imaging

Microchannel fluidic devices were fabricated by a soft lithography technique with PDMS (polydimethylsiloxane; Sylgard Elastomer 184 kit; Dow Corning, Auburn, MI) as described (Jacobelli et al. 2010; Gerard et al. 2014). PDMS base and curing agent were mixed 10:1 and poured onto the silicon master, then left overnight in vacuum. Once the PDMS was set, it was baked at 55 °C for 1 hr and cooled at room temperature. The embedded microchambers were then cut from the mold, and a cell well was punched adjacent to entry into the channels. The PDMS cast and a chambered coverglass (Nunc Lab-Tek, ThermoFisher, Grand Island, NY) were activated for two minutes in a plasma cleaner (Harrick Plasma, Ithaca, NY), bonded together, then incubated at 55 °C for 10 min. Prepared chambers were stored for up to 1 month before use. Prior to imaging, microchambers placed in the plasma cleaner for 5 min under vacuum and 1 min of activation, then coated with 5 μg/mL recombinant human ICAM-1/CD54 Fc (R&D Systems, Minneapolis, MN) in PBS for at least 1 hr at 37 °C. The microchambers were then washed three times with PBS, and T cells were loaded into cell wells (3-5x10^5 cells resuspended in 10 μL) and incubated at 37 °C for at least 1 hr before imaging.

3.4.5 Confocal imaging and analysis

Two different Olympus confocal microscopy systems were used to image T cells *in vitro*. For experiments tracking T cell motility in microchambers, we used the self-contained Olympus Fluoview FV10i-LIV, with a 473 nm diode laser for excitation and a 60x phase contrast water immersion objective (NA 1.2). The FV10i-LIV contains a built-in incubator

set to 37 °C, together with a Tokai-Hit stagetop incubator to maintain local temperature and humidity. T cells were imaged in RMPI adjusted to 2 mM Ca^{2+} and 2% FCS, and mounted at least half an hour before imaging to allow for equilibration. Cells were imaged at 20-sec intervals for 20-30 min, and the data analyzed using Imaris software. For Ca^{2+} imaging of Salsa6f transfected T cells, we used a Fluoview FV3000RS confocal laser scanning microscope, equipped with high speed resonance scanner and the IX3-ZDC2 Z-drift compensator. Diode lasers (488 and 561 nm) were used for excitation, and two high sensitivity cooled GaAsP PMTs were used for detection. Cells were imaged using the Olympus 40x silicone oil objective (NA 1.25), by taking 4 slice z-stacks at 1.5 µm/step, at 3 sec intervals, for up to 20 min. Temperature, humidity, and CO_2 were maintained using a Tokai-Hit WSKM-F1 stagetop incubator. Data were processed and analyzed using Imaris software.

3.4.6 GECI Screening and Salsa6f Plasmid Generation

Plasmids encoding GECIs (GECO and GCaMP6) were obtained from Addgene for screening in live cells. Each probe was cotransfected with Orai1 and STIM1 into HEK 293A cells using Lipofectamine 2000 (Invitrogen, Carlsbad, CA) for 48 hr before screening on an epifluorescence microscope. For construction of Salsa6f, tdTomato was obtained from Addgene, and the pEGFP-N1 vector (Clontech, Mountain View, CA) was used as a backbone. GCaMP6f was amplified via PCR with N- and C-terminal primers (5’ CACAACCGGTCGCCACCATGGTCGACTCATCACGTC 3’ and 5’ AGTCGCGGCCGCTTTAAAGCTT-CGCTGTCATCA TTTGTAC 3’) and ligated into pEGFP-N1 at the AgeI/NotI sites to replace

the eGFP gene, while tdTomato was amplified via PCR with N- and C-terminal primers (5' ATCCGCTAGCGCTACCGGTCGCC 3' and 5' TAACGAGATCTGCTTGTACAGCTCGTCCATGCC 3') and ligated into the backbone at the NheI/BglII sites. An oligo containing the V5 epitope tag was synthesized with sense and antisense strands (5' GATCTCGGGTAAGCCTATCCCTAACC-CTCTCCTCGGTCTCGATTCTACG 3' and 5' GATCCGTAGAATCGAGACCGAGGAGAGGGTTAGG-GATAGGCTTACCCGA 3') and ligated into the backbone at the BglII/BamHI sites, linking tdTomato to GCaMP6f and creating Salsa6f. The amplified regions of the construct were verified by sequencing (Eton Bioscience Inc., San Diego, CA). This plasmid, driven by the CMV promoter, was used for transient transfections in HEK 293A cells with Lipofectamine 2000 and in primary human T cells with Amaxa Nucleofection.

3.4.7 Data Analysis and Statistical Testing

Samples sizes were comparable to previous single cell analyses of motility (Jacobelli et al. 2010; Greenberg et al. 2013; Gerard et al. 2014). Each experiment used separate isolations of human T cells from different donors. With the exception of momentary velocities in Figure 6, each measurement corresponds to a different cell. Mean ± standard error of the mean was used as a measure of the central tendency of distributions. Video analysis was performed using Imaris software, Spots analysis was used for tracking of cell velocity and Volumes analysis was used for measuring total fluorescence intensity of GECI probes. To reduce selection bias in our analysis of motility and trajectory, all clearly visible and live cells were tracked from each video segment. The arrest coefficient is defined as fraction of time each cell had an instantaneous velocity < 2 μm/min. The coefficient of variation was

defined for each individual cell as the standard deviation divided by the mean of its instantaneous velocity. For Salsa6f imaging analysis, ratio (R) was calculated by total GCaMP6f intensity divided by total tdTomato intensity, while initial ratio (R_0) was calculated by averaging the ratios of the first five time points in each individual cell trace. Photobleaching of tdTomato fluorescence intensity (20-30% decline) was corrected in ratio calculations, as a linear function of time. Figures were generated using Prism 6 (GraphPad Software, San Diego, CA) and Origin 5 (OriginLabs, Northampton, MA). Due to the expectation that individual cells exhibit multiple motility modes, and to avoid assumptions concerning the shapes of motility distributions, non-parametric statistical testing was performed (Mann-Whitney *U* test, unpaired samples, two-tailed). Differences with a *P* value of ≤ 0.05 were considered significant: **P* ≤ 0.05; ***P* < 0.01; ****P* < 0.005; *****P* < 0.001. Similar distributions were compared using the Hodges-Lehmann median difference value and 95% confidence intervals under the assumption that the starting distributions had similar shapes.

CHAPTER 4: A Cre-dependent Salsa6f reporter mouse for Ca^{2+} imaging

In this chapter, I wrote all the sections, performed all experiments and made all figures except for **4.2B,C** and **4.3A,D**. The targeting of Salsa6f into ES cells, blastocyst injections, and implantations were done by the UCI Transgenic Mouse Facility.

4.1 Introduction

In recent years, a new generation of genetically encoded Ca^{2+} indicators (GECIs) has been produced through numerous rounds of development, with capabilities matching or even exceeding the best small-molecule indicators (Zhao et al. 2011; Akerboom et al. 2012; Chen et al. 2013). Of this new generation, GCaMP6f stands out with the most advantageous combination of brightness, dynamic range, response kinetics, k_d, and pK_a (Chen et al. 2013). We have used GCaMP6f to construct a novel fusion probe, Salsa6f, containing tdTomato to enable ratiometric measurement of Ca^{2+} levels while preserving the high performance of GCaMP6f. The production of this new ratiometric GECI offers new possibilities for imaging Ca^{2+} *in vivo* with increased functionality.

Optical detection of neuronal firing has been a primary driver for the development of new GECIs, and in particular GCaMP6f. Recent experiments demonstrate that GCaMP6f can be used to detect single action potentials and, when virally transduced, allows visual cortex neurons to be classified based upon activity *in vivo* (Chen et al. 2013). However, long-term viral transduction of GCaMP variants into mouse visual cortex has been shown to cause overexpression artifacts and abnormal cell physiology, including brightly labeled

nuclei, attenuated GCaMP responses, and reduced Ca^{2+} changes evoked by neuronal activity (Tian et al. 2009; Akerboom et al. 2012). Due to these limitations, the timeline of experiments has been restricted to short-term studies. Furthermore, viral injection into mouse cranium is an invasive procedure that requires surgery on experimental animals and produces inhomogeneous expression patterns. A transgenic model for GECI expression could potentially solve many of these issues, while allowing for increased specificity in labeling cell populations.

Although several GECI-expressing transgenic mouse lines have already been reported, many of these used older variants of GECIs that are expressed only in selected tissues (Hasan et al. 2004; Ji et al. 2004; Tallini et al. 2006; Heim et al. 2007). The recently characterized Ai38 mouse line overcomes these issues by combining GCaMP3 with a robust and flexible Cre/lox system for selective expression in specific cell populations (Zariwala et al. 2012). Based on a series of Cre-responder lines designed for characterization of the whole mouse brain (Madisen et al. 2010), the Ai38 mouse line has GCaMP3 targeted to the *Rosa26* locus but requires Cre recombinase for expression. By crossing with various Cre mouse lines, the Ai38 mouse line allows for selective expression of GCaMP3 only in specific cell populations. Thus, target cell populations may be endogenously labeled without surgical procedures, avoiding potential off-target side effects reported in GECI transgenic lines with global expression (Direnberger et al. 2012).

Despite the many advantages of the Ai38 mouse line and its universal applicability, the performance of GCaMP3 is still limited compared to small-molecule Ca^{2+} indicators, and GCaMP3-expressing cells are difficult to identify or track in the absence of Ca^{2+} signaling.

The newly released PC::G5-tdT mouse line provides improved functionality by targeting a Cre-dependent GCaMP5G-IRES-tdTomato transgene to the *Polr2a* locus (Gee et al. 2014). In the presence of Cre recombinase, positively labeled cells will express both GCaMP5G and tdTomato. However, in the PC::5G-tdT mouse line, GCaMP5G and tdTomato are expressed individually, and localize to different cell compartments. Since expression of tdTomato is driven by an internal ribosomal entry site, the expression level is highly variable and weaker than GCaMP5G, limiting identification of positive cells and preventing accurate ratiometric measurements. Thus, there is room for improvement in the currently available GECI transgenic mouse lines. Here, we present the design and initial characterization in immune cells of a novel GECI transgenic mouse line, by targeting our Salsa6f ratiometric probe to the *Rosa26* locus with Cre-dependent expression, similar to the Ai38 mouse line. The Salsa6f transgenic mouse line imparts powerful new capabilities for imaging of Ca^{2+} of selected cell types *in vivo*.

4.2 Results

4.2.1 Evaluation of the Ai38 mouse model for immune imaging

Most previously characterized GECI transgenic mouse lines have been targeted to neuronal cell populations, with some targeted to cardiomyocytes (Ji et al. 2004; Tallini et al. 2006), but none has been reported in the immune system. While there have been recent studies using virally transduced TN-XXL and Twitch GECIs in T lymphocytes (Mues et al. 2013; Thestrup et al. 2014), so far no effort has been made to characterize transgenic expression

of a genetic Ca^{2+} indicator in immune cells. Initially, we sought to use the established Ai38 mouse line as a proof of concept to evaluate the effects of a transgenically expressed GCaMP variant in T lymphocytes. Ai38 mice were bred to *CD4-Cre* mice to produce a *CD4-Cre*:Ai38 cross, from which GCaMP3-expressing $CD4^+$ T cells were purified and imaged *in vitro* with two-photon microscopy (**Figure 4.1E**). Upon TG-induced Ca^{2+} influx, GCaMP3 fluorescence reliably reported cytosolic Ca^{2+} elevations in resting mouse T cells with a five-fold dynamic range (**Figure 4.1A,C**). For comparison, we transfected resting human T cells with GCaMP6f, and repeated two-photon imaging under the same experimental conditions. As expected, GCaMP6f showed significantly higher brightness and dynamic range compared to GCaMP3 (**Figure 4.1B,D**). It is possible that this difference in brightness is due to the wide variability in expression level of GCaMP6f from transient transfection, in which case the homogeneity of expression level in T cells from the *CD4-Cre*:Ai38 cross emphasizes another advantage of a transgenic expression sysstem (**Figure 4.1A**).

Lastly, we evaluated potential effects of GCaMP3 expression on T cell motility in the lymph node. GCaMP3-expressing $CD4^+$ T cells from *CD4-Cre*:Ai38 mice were labeled with CellTrace Violet and adoptively co-transferred with CMTMR-labeled control $CD4^+$ T cells from *GCaMP3*$^{-/-}$*CD4-Cre*$^{+/-}$ littermates into wildtype recipients. Intact lymph nodes were excised 24 hr after adoptive co-transfer and imaged with two-photon microscopy. GCaMP3-expressing T cells homed properly to lymph nodes and exhibited similar cell velocities compared to control T cells (10.6 ± 0.2 μm/min vs 10.5 ± 0.2 μm/min, **Figure 4.1G**). Whereas these experiments demonstrate that a GCaMP variant can be transgenically expressed in T lymphocytes and used to measure Ca^{2+} responses *in vitro*, we noted that

GCaMP3-expressing $CD4^+$ T cells were undetectable within the lymph node if relying on GCaMP3 fluorescence alone at 900 nm two-photon excitation (data not shown). Thus, our results validate the use of the Ai38 transgenic mouse model for expression in immune cells and highlight the need for another fluorescent marker to enable cell tracking at basal Ca^{2+} levels.

4.2.2 Generation of Salsa6f transgenic mouse line targeted to the *Rosa26* locus

Based on the transgenic targeting strategy for the Ai38 mouse line, we inserted Salsa6f into a CAG-LSL-Salsa6f-WPRE-bGHpA cassette flanked by *Rosa26* homology arms, then targeted it to the *Rosa26* locus in JM8.N4 mouse embryonic stem (ES) cells (**Figure 4.2A**). Insertion events were selected by neomycin resistance, and correctly targeted clones were screened by Southern blot after HindIII or BglI digest, for the 5' or 3' end, respectively (**Figure 4.2B**). Correctly targeted clones were then checked for euploidy by chromosome counting, before select clones were injected into C57BL/6J blastocysts for implantation. Blastocysts were transferred into the uterus of pseudopregnant foster mothers and resulting chimeric pups carrying the Salsa6f transgene were identified by PCR screening for the *Nnt* gene (**Figure 4.2C**), as the initial JM8.N4 ES cells were $Nnt^{+/+}$ while the C57BL/6J blastocysts were $Nnt^{-/-}$. Finally, positive chimeras were bred to R26ΦC31o mice to remove the neomycin resistance gene flanked by AttB and AttP sites in the original transgenic cassette (**Figure 4.2A**), and to produce F1 founders carrying the allele for Salsa6f at the *Rosa26* locus.

4.2.3 Characterization of Salsa6f reporter mouse in immune cells

Salsa6f F1 founders were bred to CD4-Cre mice to obtain Salsa6f$^{+/-}$CD4-Cre$^{+/-}$ reporter mice that selectively express Salsa6f in all CD4^{+} T cells. We found that >98% of CD4^{+} T cells from this these reporter mice expressed Salsa6f, as detected by tdTomato fluorescence on flow cytometry, and Salsa6f expression was also detected in >98% of CD8^{+} T cells (**Figure 4.3A**). This is due to the double-positive stage of thymocyte development, in which developing thymocytes will express both CD4 and CD8 before undergoing positive and negative selection to become either mature CD4^{+} or CD8^{+} T cells. CD4^{+} T cells were purified from Salsa6f$^{+/-}$CD4-Cre$^{+/-}$ reporter mice and stimulated with platebound αCD3/28 antibodies for two days, then activating T cells were imaged by confocal microscopy while still in contact with immobilized antibodies (**Figure 4.3B**). Activating CD4^{+} T cells expressing Salsa6f exhibited consistent red fluorescence and wide fluctuations in green fluorescence due to Ca^{2+} oscillations resulting from T cell receptor engagement (**Figure 4.3C**). Despite variability in total fluorescence between cells due to individual differences in cell size, the basal and peak Salsa6f ratios (green/red fluorescence) were comparable between cells and showed up to six-fold increases during peaks in Ca^{2+} fluctuations. This level of response matches our previous experiments in activated human T cells transfected with Salsa6f (Chapter 2, **Figure 2.4**), and supports the consistency in making ratiometric measurements with Salsa6f. Flow cytometry analysis of Salsa6f$^{+/-}$-expressing mouse T cells revealed a fifteen-fold increase in green/red ratio, by pretreatment with ionomycin in free Ca^{2+} to deplete cytosolic Ca^{2+} followed by addback of extracellular Ca^{2+}, emphasizing the high dynamic range of Salsa6f (**Figure 4.3D**). Lastly, to test if increasing the genetic dosage can

improve the brightness of Salsa6f, we compared $CD4^+$ T cells from heterozygotic $Salsa6f^{+/-}$ $CD4\text{-}Cre^{+/-}$ mice and homozygotic $Salsa6f^{+/+}CD4\text{-}Cre^{+/-}$ mice. T cells from homozygous mice with two allelic copies of the Salsa6f reporter cassette exhibited almost a two-fold increase in tdTomato fluorescence compared to heterozygous mice (**Figure 4.3E**), allowing for genetic control of Salsa6f expression level when brightness is an issue.

4.2.4 Comparison of GECI expression patterns in CD4 T cells

To compare our Salsa6f reporter mouse with the best of currently available GECI reporter mice, we acquired the recently released PC::G5-tdT reporter mouse, which expresses a Cre-dependent GCaMP5G-IRES-tdTomato (5G-tdT) transgenic cassette. 5G-tdT is very similar to Salsa6f as it also contains both a GCaMP variant and tdTomato, but the key difference is that tdTomato is expressed behind an internal ribosomal entry site (IRES), so the expression level of tdTomato in G5-tdT is variable and lower than that of the upstream GCaMP5G. Furthermore, since GCaMP5G and tdTomato are not directly linked in 5G-tdT, their cellular distributions would not be identical, preventing the use of 5G-tdT in making true ratiometric measurements. Although GCaMP5G is an older variant of GCaMP, it has comparable brightness to GCaMP6f, but GCaMP6f is still superior in terms of Ca^{2+} sensitivity and response kinetics.

Both Salsa6f and 5G-tdT mice were bred to CD4-Cre mice to allow for specific expression in $CD4^+$ T cells. $CD4^+$ T cells were purified from both $Salsa6f^{+/-}CD4\text{-}Cre^{+/-}$ and $5G\text{-}tdT^{+/-}CD4\text{-}Cre^{+/-}$ mice and resting T cells were imaged by confocal microscopy (**Figure 4.4A,B**). When imaged at identical experimental settings, $Salsa6f^{+/-}CD4\text{-}Cre^{+/-}$ cells were

clearly brighter based on tdTomato fluorescence, and Salsa6f expression was localized to the cytosol, unlike tdTomato expression in 5G-tdT$^{+/-}$CD4-Cre$^{+/-}$ cells (**Figure 4.4A,B**). However, since resting T cells contain very limited cytosol and do not exhibit basal Ca^{2+} signals, we stimulated purified CD4^{+} T cells by crosslinking TCR with platebound αCD3/28 antibodies. After 24 hr, activating T cells were imaged on confocal microscopy in the same coverslip chambers they were stimulated in, without any perturbation (**Figure 4.4C,D**). Looking specifically at fluorescence in the green channel, both GCaMP6f and GCaMP5G reliably detected Ca^{2+} oscillations in activating T cells, as expected. However, the red channel clearly shows that for Salsa6f, tdTomato is co-localized with GCaMP6f in the cytosol, but for 5G-tdT, tdTomato is uniformly distributed throughout the cell while GCaMP5G is concentrated in the cytosol. These results show that the Salsa6f mouse can perform better than the PC::G5-tdT mouse in providing a consistent reporter for tracking cells in the absence of Ca^{2+} signaling and make true ratiometric measurements.

4.2.5 Role of Treg-contact in suppression of Ca^{2+} signaling in T cell activation

As we now have a reliable *in vitro* system using endogenously expressed Ca^{2+} indicators to measure T cell activation without perturbation, we decided to apply our methods to study contact-dependent mechanisms of regulatory T cell (Treg) function. Tregs constitute only a small subset of the total T cell population, yet they are crucial in maintaining immune homeostasis and peripheral tolerance (Paust and Cantor 2005; Sakaguchi et al. 2008; Yamaguchi T 2011). While many mechanisms have been identified for Treg function, there is still considerable debate over exactly how Tregs exert their immunosuppressive effects

(Rubtsov et al. 2008; Wing and Sakaguchi 2012). Recent studies have suggested a role for direct contact in the Treg-mediated suppression of Ca^{2+} signaling in T cell activation (Schmidt et al. 2011; Schwarz et al. 2013).

$CD4^+CD25^-$ conventional T cells (Tcons) were purified from 5G-$tdT^{+/-}$CD4-$Cre^{+/-}$ mice, and activated in coverslip chambers coated with αCD3/28 antibodies either alone or in the presence of preactivated Foxp3-EGFP Tregs (Haribhai et al. 2007). 24 hr after activation, the coverslip chambers were directly imaged by confocal microscopy, preserving any cellular contacts and all soluble factors during the activation process (**Figure 4.5A**). When activated in a co-culture with a 2:1 Tcon-to-Treg ratio, Tcons showed reduced Ca^{2+} signaling regardless of whether they were in direct contact with Tregs or not, as compared to control Tcons activated in the absence of Tregs (**Figure 4.5B,C**). Although these results suggest that direct contact with Tregs is not necessary for suppression of T cell activation, it is possible that a 2:1 Tcon-to-Treg ratio is high enough to allow other mechanisms of suppression, such as from soluble factors, to play a dominant role. Since Tregs naturally make up only 10% of the T cell population, we repeated our co-culture experiments using an 8:1 Tcon-to-Treg ratio. After 24 hr activation in the presence of sparse Tregs, we found that all Tcons still showed a reduction in Ca^{2+} signaling compared to control, but Tcons in direct contact with Tregs showed an even further reduction in Ca^{2+} signaling (**Figure 4.5D**). While this data now supports a role for direct contact in Treg-mediated suppression of T cell activation, it is clear that careful replication of physiological conditions is required to dissect the complex nature of Treg function.

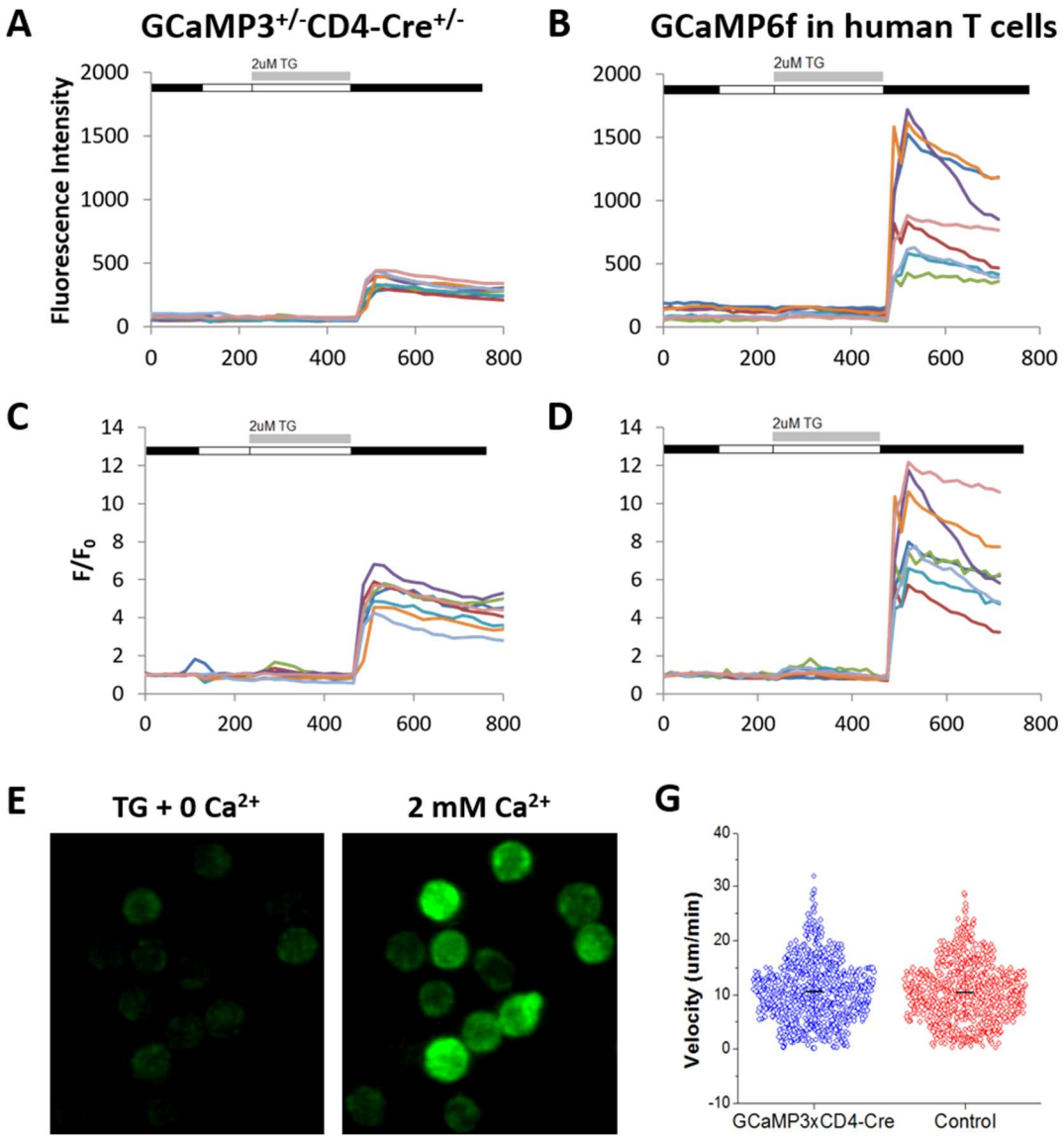

Figure 4.1. Evaluation of the Ai38 transgenic model for immune imaging.

A,C. Representative cell traces of brightness (**A**) and dynamic range (**C**) of GCaMP3 fluorescence response to thapsigargin-induced Ca^{2+} entry in resting mouse T cells purified from a *CD4-Cre*:Ai38 cross, which are GCaMP3$^{+/-}$CD4-Cre$^{+/-}$, imaged with two-photon microscopy at 900 nm excitation. **B,D**. Representative cell traces of brightness (**B**) and

dynamic range (**D**) of GCaMP6f fluorescence response to thapsigargin-induced Ca^{2+} entry in resting human T cells transfected with GCaMP6f, imaged on two-photon microscopy at 900 nm excitation. **E**. Two-photon images of resting mouse $CD4^+$ T cells from a *CD4-Cre*:Ai38 mouse, showing before and after thapsigargin-induced Ca^{2+} entry. **G**. $5x10^6$ CellTrace Violet-labeled $GCaMP3^{+/-}CD4\text{-}Cre^{+/-}$ mouse T cells (blue) were adoptively co-transferred into a wildtype syngeneic mouse with equal numbers of CMTMR-labeled $CD4^+$ T cells (red) from control $GCaMP3^{-/-}CD4\text{-}Cre^{+/-}$ littermates, intact lymph nodes were excited 24 hr later and imaged by two-photon microscopy. Cell homed properly and cell velocity was tracked. Bars represents mean.

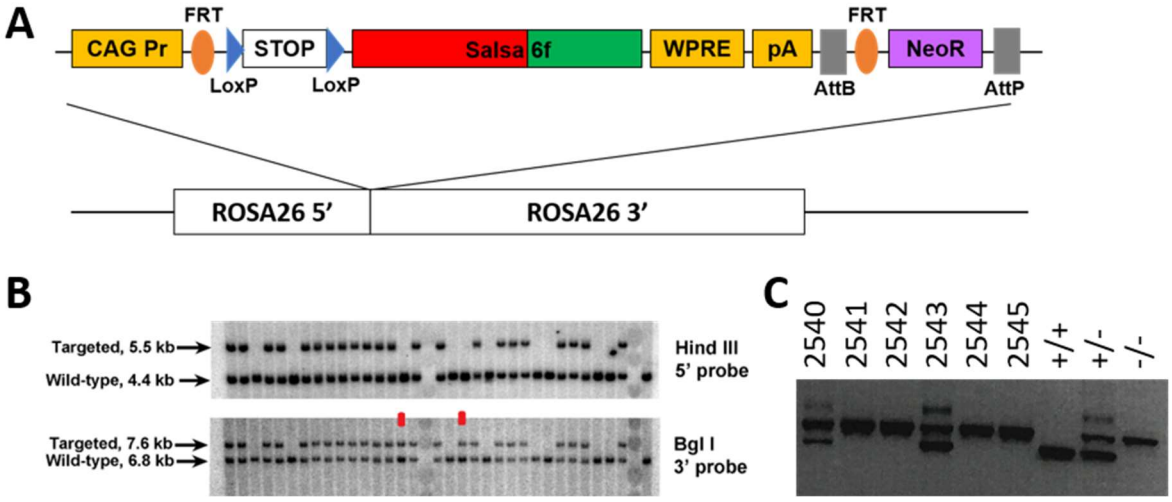

Figure 4.2. Generation of Salsa6f transgenic mouse line targeted to *Rosa26* locus.

A. Transgenic targeting vector for Salsa6f, to be inserted between Rosa26 homology arms and electroporated into embryonic stem cells. CAG Pr: cytomegalovirus early enhancer/chicken β-actin promoter; Salsa6f: tdTomato-V5-GCaMP6f; FRT, LoxP, AttB, AttP: recombinase sites; WPRE: woodchuck hepatitis virus posttranscriptional regulatory element; pA: bovine growth hormone polyadenylation sequence; NeoR: neomycin resistance gene. **B**. Corrected targeted ES cells were screened by Southern blot after HindIII digest for the 5' end (top) or BglI digest for the 3' end (bottom). The two clones marked in red failed to integrate at the 5' end. **C**. PCR screening for chimeras based on presence of the *Nnt* mutation, present only in JM8.N4 ES cells. 2540 and 2543 are chimeras. Control lanes on the right are wildtype ($Nnt^{+/+}$), heterozygous ($Nnt^{+/-}$), or homozygous mutant ($Nnt^{-/-}$).

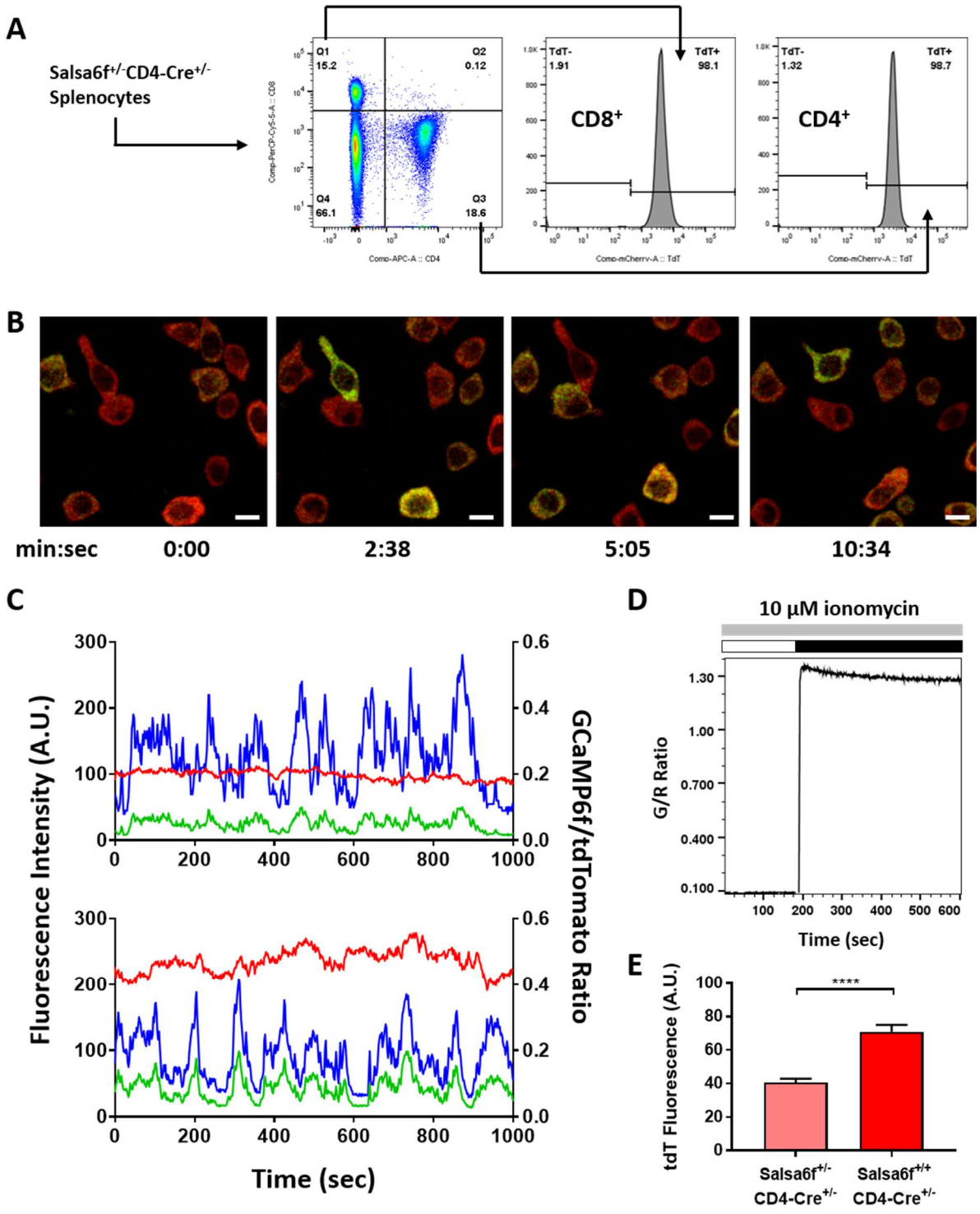

Figure 4.3. Characterization of Salsa6f transgenic expression in mouse T cells.

A. Analysis of Salsa6f expression in $CD4^+$ and $CD8^+$ T cell subsets in the spleen of Salsa6f$^{+/-}$ CD4-Cre$^{+/-}$ mice, based on tdTomato fluorescence measured by flow cytometry. **B**. Confocal imaging of Ca^{2+} signals in activating $CD4^+$ T cells from Salsa6f$^{+/-}$CD4-Cre$^{+/-}$ mice, after two day stimulation on platebound αCD3/28 antibody, showing merged green (GCaMP6f) and red (tdTomato) channels; time = min:sec; scale bar = 10 μm. **C**. Representative traces from cells shown in (**B**), showing total fluorescence intensity from GCaMP6f (green) and tdTomato (red), with green/red ratio (blue). **D**. Dynamic range of resting Salsa6f-expressing T cells, measured by green/red fluorescence from flow cytometry, using FlowJo Kinetics tool. Cells were pre-treated with 10 μM ionomycin in Ca^{2+}-free solution (white bar), followed by addback of 2 mM Ca^{2+} (black bar). **E**. Averaged tdTomato fluorescence intensity in resting T cells from heterozygotic Salsa6f$^{+/-}$CD4-Cre$^{+/-}$ compared to homozygotic Salsa6f$^{+/+}$CD4-Cre$^{+/-}$ mice.

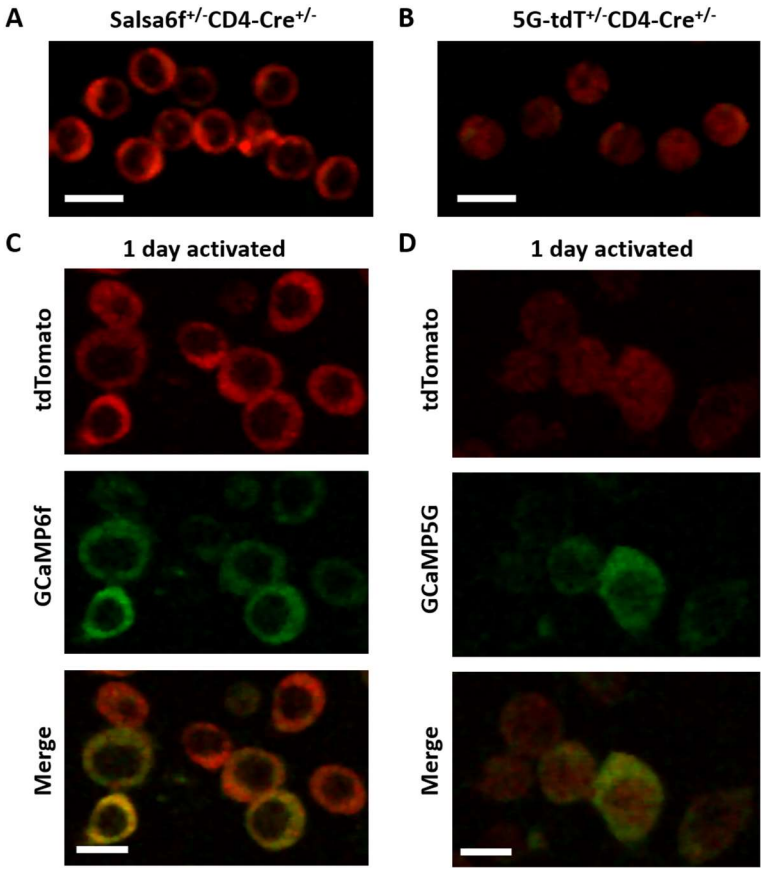

Figure 4.4. Comparison of GECI expression in CD4 T cells of Salsa6f mouse and PC::G5-tdT mouse.

A,B. Confocal images of CD4$^+$ T cells purified from a Salsa6f$^{+/-}$CD4-Cre$^{+/-}$ mouse (**A**) or a 5G-tdT$^{+/-}$CD4-Cre$^{+/-}$ mouse (**B**), showing merged red and green; cells were plated onto poly-L-lysine coated coverslips and imaged at the same laser and PMT settings; scale bar = 10 μm. **C,D**. CD4$^+$ T cells purified from a Salsa6f$^{+/-}$CD4-Cre$^{+/-}$ mouse (**C**) or a 5G-tdT$^{+/-}$CD4-Cre$^{+/-}$ mouse (**D**), then activated for 24 hr on platebound αCD3/28 antibodies, and imaged with confocal microscopy, showing red (tdTomato), green (GCaMP6f or GCaMP5G), and merged channels; scale bar = 10 μm.

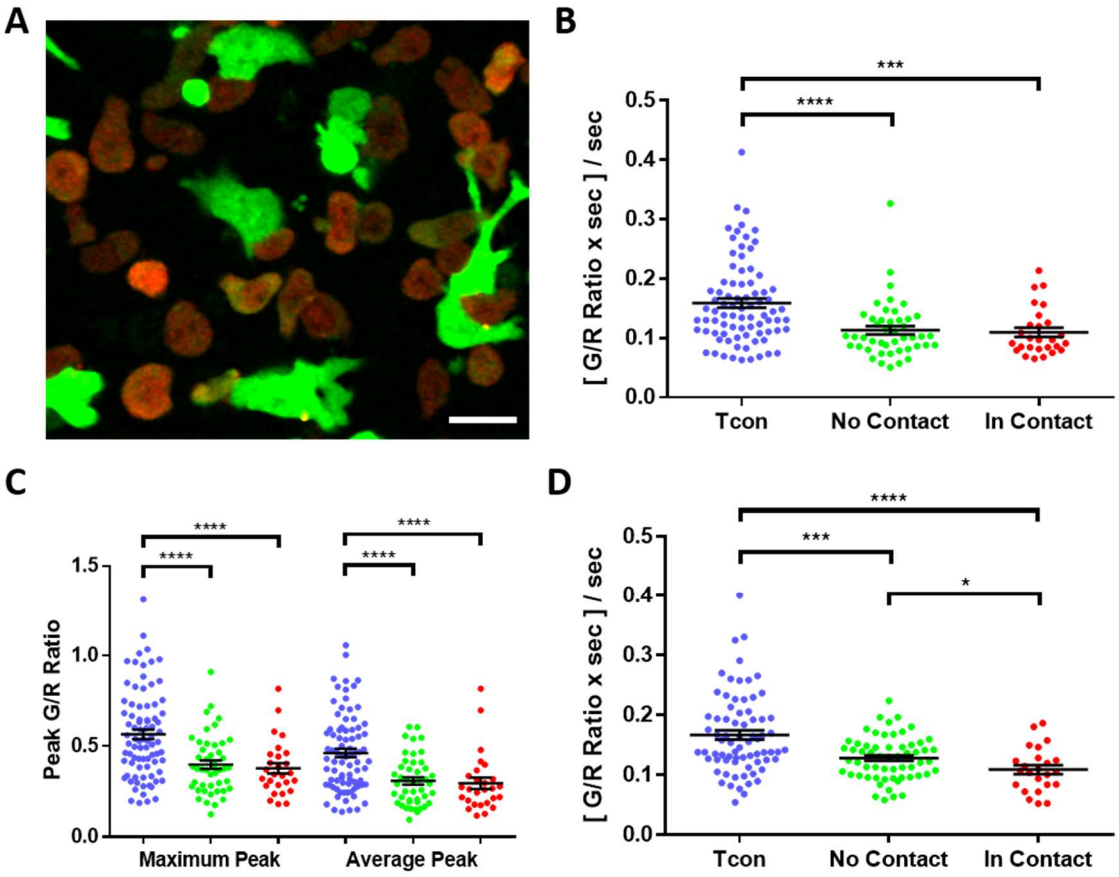

Figure 4.5. Role of Treg-contact in suppression of Ca^{2+} signaling in T cell activation.

A. Confocal imaging of 5G-tdT-expressing Tcons (red with green flashes) after 24 hr activation on platebound αCD3/28 antibodies in the presence of preactivated Foxp3-EGFP Tregs (green only), showing merged green (EGFP or GCaMP5G) and red (tdTomato) channels, scale bar = 20 μm. **B**. Normalized area under the curve (AUC) of Ca^{2+} signals in 5G-tdT-expressing Tcons after 24 hr activation, either activated alone (blue), or activated in co-culture with preactivated FoxP3-EGFP Tregs at a 2:1 Tcon-to-Treg ratio, and without direct contact to Tregs (green) or in direct contact with Tregs (red); bars represent mean ± SEM. **C**. Maximum and average peaks in Ca^{2+} signals of data shown in (**B**); bars represent

mean ± SEM. **D**. Normalized AUC of Ca^{2+} signals in 5G-tdT-expressing Tcons after 24 hr activation, either activated alone (blue), or activated in co-culture with preactivated FoxP3-EGFP Tregs at a 8:1 Tcon-to-Treg ratio, and without direct contact to Tregs (green) or in direct contact with Tregs (red); bars represent mean ± SEM.

4.3. Discussion

We present the design and initial characterization of the Salsa6f reporter mouse, a novel transgenic mouse line expressing a high performance GECI with ratiometric capability. Following the successful transgenic targeting strategy of the GCaMP3-expressing Ai38 reporter mouse (Zariwala et al. 2012), we targeted Salsa6f to the *Rosa26* locus under Cre-dependent expression. Breeding with the wide variety of Cre driver mice currently available allows for selective expression of Salsa6f in specific tissue and cell populations, enabling Ca^{2+} imaging studies to be performed without the need for invasive cell labeling. We used a CD4-Cre mouse to express Salsa6f in T cells and showed the reliable measurement of physiological Ca^{2+} fluctuations during T cell activation. Salsa6f signals exhibited a wide dynamic range and its ratiometric capability allows for comparison of Ca^{2+} levels despite differences in expression level.

The performance of our Salsa6f reporter mouse was compared to another currently available GECI reporter mouse, the PC::G5-tdT line expressing GCaMP5G and tdTomato (Gee et al. 2014). When transgenically expressed in $CD4^+$ T cells, Salsa6f offers the clear advantage of cytosolic co-localization of both tdTomato and GCaMP6f components, allowing for true ratiometric measurements. Fluorescence intensity of tdTomato was also brighter in Salsa6f mice, a key advantage for *in vivo* imaging. The Salsa6f reporter mouse imparts powerful new capabilities for imaging of Ca^{2+} of selected cell types *in vivo*.

Due to the earlier availability of the PC::G5-tdT reporter mouse, we used 5G-tdT-expressing T cells in an unperturbed cell activation assay to study the involvement of direct contact in Treg-mediated suppression of T cell activation. Two recent studies have

suggested a potential contact-dependent mechanism of Tregs to suppress Ca^{2+} signaling in T cell activation (Schmidt et al. 2011; Schwarz et al. 2013). A limitation of previous studies is the use of small-molecule Ca^{2+} indicators that slowly leak out of cells, so the time course of experiments is restricted to a few hours. Endogenously expressed GECIs allow for imaging to be done days to weeks after initial activation and culture of cells, so that cell fates and differentiation can also be evaluated. In our *in vitro* co-culture assay, Tcons and Tregs are left unperturbed during stimulation, so that any cell contacts are preserved at the time of imaging, increasing the confidence of our findings on contact-dependent Treg suppression. These experiments lay the groundwork for using the superior Salsa6f reporter mouse in the same fashion, with the increased brightness of Salsa6f being a key advantage for future *in vivo* imaging.

The greatest interest for use of GECIs has always been in neuronal studies, as a sensitive and noninvasive means to detect action potentials and cell behavior. Our Salsa6f reporter mouse with fast response kinetics, high dynamic range, and ratiometric capability offers new possibilities for neuronal studies *in vivo*. Breeding of Salsa6f to neuronal Cre driver lines would grant the ability to differentiate between neuronal populations based on cell morphology and facilitate identification of target cells in the absence of signaling. We acknowledge there is a great deal of work required in characterization of the Salsa6f reporter mouse in the nervous system. Nevertheless, our aim is to provide a powerful new system for associating Ca^{2+} signaling with cellular activity, enabling previously inaccessible functional studies *in vivo* and *in vitro*.

4.4. Material and Methods

4.4.1 Mice

Ai38 mice containing the Cre-dependent GCaMP3 transgene (#014538), CD4-Cre mice expressing Cre recombinase driven by a *CD4* enhancer and promoter (#017336), PC::G5-tdT mice containing the GCaMP5G-IRES-tdTomao cassette under Cre-dependent control (#024477), R26ΦC31o mice expressing a codon-optimized phi-C31 recombinase (#007743), and Foxp3^{EGFP} mice expressing enhanced GFP along with Foxp3 (#006772) were all obtained from Jackson Laboratory and housed in a selective pathogen-free environment with sterile food and water in the animal housing facility at the University of California, Irvine.

4.4.2. Human T cell purification and nucleofection

Human PBMCs were isolated from blood of voluntary healthy donors by Histopaque-1077 (1.077 g/mL; Sigma, St. Louis, MO) density gradient centrifugation. Human CD3$^+$ T cells were isolated using the EasySep Human T Cell Isolation Kit (StemCell Technologies, Vancouver, Canada) according to manufacturer's instructions. The purity of isolated cells was confirmed to be >95% by flow cytometry. Purified cells were rested overnight in complete RPMI, then transfected by nucleofection (Lonza, Walkersville, MD), using the Human T Cell Nucleofector Kit with high-viability “U-014” protocol for primary human T cells. GCaMP6f was transfected as indicated. Human T cells were used for experiments 24-48 hr after transfection.

4.4.3 Targeted transgenesis of Salsa6f into the *Rosa26* locus

This work was performed by the Transgenic Mouse Facility (TMF) at UC Irvine under the supervision of Managing Director Jon Neumann. In short, a CAG-loxP-STOP-loxP-Salsa6f-WPRE-pA targeting cassette containing a neomycin resistance gene was inserted between *Rosa26* homology arms, then linearized and electroporated into JM8.N4 ES cells. Insertion events was selected by neomycin resistance, and homologous recombination at the *Rosa26* locus was screened via Southern blot. Correctly targeted ES cells were injected into blastocysts and implanted to produce chimeric mice expressing the Salsa6f transgene. Chimeric mice will be bred to homozygosity using the R26ΦC31o strain to remove the neomycin resistance gene flanked by AttB and AttP sites in the original transgenic cassette, and to produce F1 founders carrying the allele for Salsa6f at the *Rosa26* locus.

4.4.4 Mouse T cell purification and activation

$CD4^+$ T cells were isolated from spleen and lymph nodes of 8-12 week old mice by negative selection using the EasySep Mouse T cell Isolation Kit from StemCell Technologies, and $CD25^+$ regulatory T cells (Tregs) were purified by positive selection using the CD25 MicroBead Kit from Miltenyi Biotec, or depleted from purified $CD4^+$ T cells to prepare $CD4^+CD25^-$ conventional T cells (Tcons). For activation assays, 35 mm chambered coverglass (MatTek Corp) were coated with 1 μg/mL of αCD3 and αCD28 antibodies (Tonbo Biosciences) in PBS for 1 hr at 37°C, then washed before mouse T cells were dropped onto chambers in complete RPMI with 30 U/mL recombinant mouse IL-2

(BioLegend). For co-culture assays, purified Foxp3-EGFP Tregs were first activated for 24 hr in the same manner but in 100 U/mL IL-2, before mixing with freshly purified Tcons and plated again onto platebound αCD3/28 in complete RPMI with 30 U/mL IL-2. Activated T cells were taken for imaging directly in chambered coverglass, without any perturbation or washing of activation media.

4.4.5 Flow cytometry

Cells were analyzed using a LSRII with FACSDiva software (Becton Dickinson), and anti-mouse CD4 and CD8 antibodies were obtained from eBioscience. Spleen from Salsa6f$^{+/-}$ CD4-Cre$^{+/-}$ mice were collected and made into single-cell suspensions with 70 μm nylon cell strainers (BD Falcon). Splenocytes were first blocked in PBS with 10% FCS and 2 mM EDTA for 15 min, then stained with conjugated mAbs for 20-30 min. Unbound Abs were removed by two washes with 1% FCS and 2 mM EDTA in PBS, and cells were resuspended for flow cytometry. Cells were gated for appropriate forward and side scatter, and Salsa6f^{+} T cells were identified by tdTomato fluorescence. For measuring Salsa6f dynamic range, cells were first treated for 10 min with 10 μM ionomycin in Ca^{2+}-free solution, then run on flow cytometry and the final Ca^{2+} concentration was adjusted to 2 mM. Salsa6f ratio was calculated by FlowJo Kinetics tool using GCaMP6f fluorescence over tdTomato fluorescence.

4.4.5 Confocal microscopy

For imaging GECI-expressing mouse T cells *in vitro*, we used the self-contained Olympus Fluoview FV10i-LIV, with 473 nm and 559 nm diode lasers for excitation and a 60x phase contrast water immersion objective (NA 1.2). The FV10i-LIV contains a built-in incubator set to 37 °C, together with a Tokai-Hit stagetop incubator to maintain local temperature and humidity. T cells were imaged in the same activation media from co-cultures and mounted at least half an hour before imaging to allow for equilibration. Cells were imaged at 20-sec intervals for 20-30 min, and the data analyzed using Imaris software. Fluorescence intensity from green and red channels was measured using Spots analysis, and Salsa6f ratio was calculated by total green fluorescence over total red fluorescence. For measurements of Ca^{2+} signaling in 5G-tdT-expressing T cell activation assays, the area under the curve of GCaMP5G/tdTomato ratio was calculated using Prism software, then divided by the total time of each recording.

CHAPTER 5: Imaging regulatory T cell dynamics and CTLA4-mediated suppression of T cell priming

(Matheu et al. 2015)

In this chapter, I performed the experiments and made the figures for **5.S4** and **5.S5**, and assisted in editing and revising the manuscript.

5.1 Introduction

Regulatory T cells (Tregs) expressing the Foxp3 transcription factor constitute a critical component of peripheral immune homeostasis and tolerance. Several autoimmune and inflammatory pathologies in humans are associated with functional defects in Tregs, and depletion of Tregs in experimental animals leads to systemic autoimmune and allergic disease accompanied by unchecked lymphoproliferation (Wildin and Freitas 2005; van der Vliet and Nieuwenhuis 2007; Huter et al. 2008; Sakaguchi et al. 2008). Expression of an inhibitory member of the immunoglobulin super-family, cytotoxic T lymphocyte antigen 4 (CTLA4) by Tregs is critical for their function. The loss of Treg-specific CTLA4 expression or treatment with a blocking antibody lead to potentially lethal T-cell mediated autoimmune pathology (Tivol et al. 1995; Waterhouse et al. 1995; Takahashi et al. 2000; Wing et al. 2008). Moreover, polymorphisms in human CTLA4 are linked to the development of autoimmune diseases, including type I diabetes and primary progressive multiple sclerosis (Gough et al. 2005). Although it is now established that Tregs and their expression of CTLA4 are both indispensable for the maintenance of immune homeostasis (Takahashi et al. 2000; Tang et al.

2004; Huter et al. 2008; Wing et al. 2008), the underlying cellular and molecular mechanisms of CTLA4-mediated suppression are not well understood (Schmidt et al. 2012). In vitro studies of APC-free T cell cultures have demonstrated that Tregs directly suppress both $CD4^+$ and $CD8^+$ T cell proliferation in a contact-dependent, antigen-independent manner (Thornton and Shevach 2000; Piccirillo and Shevach 2001). However, *in vivo* data are lacking on how endogenous Tregs interact with antigen-presenting cells (APC) and conventional T cells (Tconvs).

Two-photon (2P) microscopy allows detailed observation and analysis of the spatio-temporal choreography of live cell-cell interactions within the native tissue environment of the lymph node, secondary lymphoid organs and peripheral tissues (Miller et al. 2002; Germain et al. 2012). In the lymph node, naive $CD4^+$ T cells exhibit three distinct phases of behavior in relation to dendritic cells (DCs) during initiation of an immune response (Miller et al. 2004): 1) dynamic scanning with transient interactions with antigen-bearing DCs; 2) formation of dynamic clusters in which multiple T cells stop migrating freely and form stable contacts with DCs; and 3) disengagement of T cells from DCs, followed by swarming behavior and subsequent antigen-specific T cell proliferation. Previous 2P imaging studies have investigated Treg-induced suppression during T cell priming either by addition of *in vitro*-separated $CD4^+$ $CD25^+$ T cells (Mempel et al. 2006; Tadokoro et al. 2006; Tang et al. 2006; Angiari et al. 2013; Tomiyama et al. 2013) or by diphtheria toxin-induced depletion of Tregs (Pace et al. 2012). Notably, no previous studies have imaged endogenous Tregs in the context of both Tconvs and DCs. Simultaneous and direct imaging of endogenous Tregs

together with naïve T cells and dendritic cells would permit insight into the cellular behavior and *in vivo* mechanisms that underlie immunoregulation.

Here, using 2P microscopy of lymph nodes from Foxp3^{EGFP} mice, we have characterized the dynamics of unperturbed, endogenous Tregs interacting with Tconv and with DCs under steady-state conditions; in the presence of LPS-activated DCs as a model for inflammation; and during antigen-specific CD4 T cell priming. We further demonstrate the crucial involvement of CTLA4-B7 interactions in determining cellular dynamics among Tregs, conventional T cells, and DCs in vivo.

5.2 Results

5.2.1 Imaging regional differences in Treg dynamics

To visualize endogenous Treg cells, we screened mouse strains that express fluorescent proteins specific to Tregs, and identified Foxp3^{EGFP} mice as optimal for 2P imaging. Developed by Haribhai *et al*., Foxp3^{EGFP} mice contain a bicistronic Foxp3-EGFP gene that induces reliable co-expression of EGFP and Foxp3 in *bona fide* endogenous Tregs (Haribhai et al. 2007). EGFP^{+} Tregs were clearly visualized by 2-photon imaging of explanted lymph nodes without exogenous labeling or adoptive transfer (**Figure 5.1a**). Mapping the distribution of Tregs with respect to CFP^{+} CD19^{+} B cells and CMTMR-labeled CD4^{+} CD25^{-} T (Tconv) cells revealed that Tregs are abundant in the T cell zone, and are also present at lower density within B cell follicles and in the sub-capsular space (**Figure 5.1b**). Time-lapse images of Tregs and associated tracks indicated little or no active exchange between

follicle and adjacent T-zone (**Figure 5.1c**). Their basal motility characteristics, morphology, and choreography clearly differed between locations within the lymph node. Mean velocities of Tregs in the T cell zone (14.6 ± 0.2 μm/min) were significantly higher than follicular Tregs (12.9 ± 0.1 μm/min, $p < 0.001$). Near or at the capsule, Tregs migrated more slowly (9.5 ± 0.2 μm/min; **Figure 5.1d**), many along collagen fibers (**Figure 5.S1a**). The collagen-interacting Tregs migrated more slowly than other Tregs within 50 μm of the capsule (**Figure 5.S1b**). Deeper in the paracortex (>50 μm below the capsule), Tregs moved rapidly and extended cellular processes (**Figure 5.1e**). Within the T-cell zone, Tregs exhibited higher mean velocities (13.9 ± 0.17 μm/min) than colocalized Tconv cells (12.0 ± 0.2 μm/min, $p < 0.001$; **Figure 5.1f**). Moreover, Tregs extended longer cellular processes than colocalized Tconvs (**Figure 5.S1c**); and follicular Tregs were, on average, even more elongated (**Figure 5.S1d**). Close examination under steady-state conditions in the absence of antigen revealed cell-cell contacts between Treg and Tconv cells (**Figure 5.1g**).

In summary, under steady-state conditions two non-overlapping populations of Tregs explore the T-zone and the follicle. Follicular Tregs (fTregs) have been identified previously as $CD4^+$ $Foxp3^+$ cells expressing CXCR5 and Bcl6 (Chung et al. 2011; Linterman et al. 2011). Endogenous Tregs in the T cell zone are the most rapidly motile cells in the lymph node reported to date. In the remainder of this report, we focus on the dynamics of Tregs interacting with Tconvs and DCs in the Tzone.

5.2.2 Tregs engage resident DCs and Tconv cells

To image endogenous Tregs, resident DCs, and Tconvs simultaneously, we crossed Foxp3-EGFP male mice with CD11c-EYFP reporter female mice (Lindquist et al. 2004). In the resultant F1 heterozygote females, 50% of Foxp3$^+$ Tregs express EGFP (Haribhai et al. 2007), and EYFP is highly expressed in the lymph node-resident DCs. CMTMR-labeled Tconv cells were then adoptively transferred into these F1 mice, followed by lymph node imaging 24 hr after cells were allowed to equilibrate (**Figure 5.2a**). The highly dynamic endogenous Tregs (**Figure 5.2b,c**) interacted with CD11c-EYFP$^+$ resident DCs, forming transient contacts that lasted longer (3.3 ± 0.4 min) than interactions between Tconvs and DCs (2.5 ± 0.3 min, $p < 0.004$, **Figure 5.2d**). In the female heterozygous recipient population, only half of the Tregs are GFP$^+$; therefore, the actual mean frequency of Treg:DC contacts would be twice that observed (**Figure 5.2e**). Thus, a single DC makes contact with 8.6 ± 1.1 Tregs/hr. Given the mean frequency of contacts between endogenous Tregs and resident DCs and their average contact duration of 3.3 min, our measurements indicate that a lymph node-resident DC is in contact with at least one Treg for 28.4 min/hr – *i.e.*, nearly half of the time. Conventional CD4 T cells briefly interacted with Tregs under basal conditions, encountering up to 13.4 Tregs/hour (**Figure 5.2e**) for an average of 1:36 min:sec. Therefore, a single Tconv cell spends an average of 21.5 min/hr (36% of the time) in contact with endogenous Tregs. These results demonstrate that individual Tregs, although less abundant than Tconv cells, are highly active and frequently encounter both DCs and Tconv under basal conditions.

5.2.3 Activated migratory DCs are intercepted by Tregs

Resident DCs in the LN constitutively present low levels of self-antigens, and the TCR repertoire of Tregs is skewed toward self-antigen recognition (Hsieh et al. 2006; Pacholczyk et al. 2006). Accordingly, we sought to define the interactions between Tregs and activated, migratory DCs from the periphery. Subcutaneous injection of CMTMR-labeled LPS-activated bone marrow-derived DCs (LPS-DCs) into a Foxp3-EGFP animal followed by imaging at 24 hr revealed the highest density of DCs on and around collagen fibers just under the lymph node capsule (**Figure 5.3a**). In this region of the lymph node, Tregs readily interacted with and surrounded immigrant DCs, while forming both brief and extended LPS-DC:Treg contacts (**Figure 5.3b**). Strikingly, some Tregs established long-lived (up to 40 min) contacts with LPS-DCs near the capsule (**Figure 5.3c,d**).

To investigate LPS-DCs and Tregs in the presence of antigen-specific T cells, we transferred labeled OTII cells (**Figure 5.3e**) and observed that LPS-DCs were surrounded by endogenous Tregs (**Figure 5.3f**). Under these conditions, average Treg contact durations with LPS-DCs were significantly longer (**Figure 5.3g**; 5:53 ± 0:38, min:sec), as compared to both Tconv:LPS-DC (2:53 ± 0:22, min:sec) and basal Treg:DC interactions (3:14 ± 0:28, both $p < 0.001$; *cf.* **Figure 5.3g** and **Figure 5.2d**). Consistent with results from WT Tconv cells, endogenous Treg velocities were significantly higher than adoptively transferred OTII Tconv cells; however, endogenous Tregs slowed significantly as they interacted with LPS-DCs while OTII T cell velocities were unaltered (**Figure 5.3h**).

These results led us to examine whether the Treg:DC interactions visualized near the lymph node capsule may lead to the activation of endogenous Tregs (Wilson et al. 2004;

Idoyaga et al. 2013). Indeed, a higher percentage of CD4 T cells were $CD69^{+}Foxp3^{+}$ in animals injected with LPS-DCs, compared to control animals (**Figure 5.S2**). Contralateral lymph nodes also had an increased number of $CD69^{+}Foxp3^{+}$ cells. Our results thus demonstrate that endogenous Tregs interact with activated LPS-DCs draining into the lymph node from the periphery. Prolonged interactions take place near the capsule, and reduce Treg velocity significantly. We infer that such prolonged interactions with immigrant LPS-DCs lead to activation of endogenous Tregs.

5.2.4 Treg interactions with DC and Tconv during priming

To examine Treg behavior during an antigen-specific response, we imaged OTII Tconv cells, Ova-pulsed DCs (Ova-DCs), and Tregs at a critical point in T cell activation, 12 hr after the transfer of antigen-specific OTII Tconv cells (**Figure 5.4a**). This timing matches the initial formation of naïve $CD4^{+}$ T cell clusters around antigen-bearing DCs (phase II of T cell activation) (Miller et al. 2004). As expected, OTII Tconv cells formed clusters around Ova-DCs. We further observed that Tregs form dynamic contacts with both DCs and antigen-specific Tconv cells (**Figure 5.4b**). Although Tconv cells slowed as they interacted with Ova-DCs, no significant change in Treg velocity was observed compared to steady-state conditions (**Figure 5.4c** *cf.* **Figure 5.1d**). Treg contact histories illustrate that Tregs spent more time in contact with responding Tconv cells (**Figure 5.4d**, red bars), than with Ova-DCs (green bars); and were often in contact with both (blue bars). However, in several instances, Tregs transitioned from interacting with both the DC and responding T cell to maintain an interaction with the responding Tconv cell alone (**Figure 5.4e**). Therefore,

during T cell priming, Tregs engage dynamic clusters of DCs and Tconv cells making frequent, brief contacts but without significant slowing.

5.2.5 Blocking CTLA4 enhances clustering and limits Treg contacts

Cytotoxic T lymphocyte antigen 4 (CTLA4) expressed on Tregs is indispensable for maintenance of immune homeostasis, and treatment with a blocking antibody leads to T-cell-mediated autoimmune disease (Tivol et al. 1995; Waterhouse et al. 1995; Takahashi et al. 2000; Wing et al. 2008). Based on this, we examined the effect of blocking CTLA4 on the dynamics of Tregs during an antigen-specific T cell response. Using the T cell priming protocol of **Figure 5.4**, we injected antigen-primed Foxp3^{EGFP} mice with αCTLA4 or isotype control (ITC) antibody 30 min after transfer of OTII Tconvs and 4 hr before imaging (**Figure 5.5a**). OTII Tconv cell dynamics were visibly altered following αCTLA4 treatment. Stable clusters of OTII T cells formed around Ova-DCs, and Tregs were excluded from these clusters (**Figure 5.5b**), thereby reducing Treg interactions with DCs. αCTLA4 treatment enhanced Tconv cluster stability and prevented Tregs from making extensive DC contact, as indicated by tracks of Tregs and OTII Tconv cells (respectively, green and red, **Figure 5.5c**) and contact history maps (**Figure 5.5d**). In αCTLA4-treated animals, the percentage of OTII Tconv cells that remained in contact with an Ova-DC for over 20 min (stable contact) was significantly higher (**Figure 5.5e**). Indeed, OTII Tconv cell contacts with DCs were significantly longer on average in the presence of αCTLA4 ($p < 0.01$), whereas Treg interactions with Ova-DCs were not altered (**Figure 5.5f**). Collectively, these results indicate that OTII Tconv cell clustering around Ova-DCs is enhanced by blocking CTLA4.

5.2.6 CTLA4-B7 interactions contribute to Treg function

CTLA-4 is known to negatively regulate T cell responses through interactions with co-stimulatory B7 molecules, B7.1 (CD80) and B7.2 (CD86) on APCs (Teft et al. 2006). In vitro and in vivo studies have shown that Tregs can capture B7 ligands from DCs through a process of trans-endocytosis that requires CTLA4 on Tregs (Qureshi et al. 2011). To determine whether αCTLA4 treatment alters the expression of co-stimulatory ligands on DCs, we transferred LPS-DCs into recipients that were treated with control (ITC) or αCTLA4 antibodies. By flow cytometric analysis, CD80 and CD86 levels were unaffected by αCTLA4 treatment (**Figure 5.S3**). Although the expression of CD80 and CD86 has been studied most extensively in APCs, we confirm previous observations (Azuma et al. 1993; Prabhu Das et al. 1995; Greenfield et al. 1997) that Tconv cells also express CD86 and up-regulate CD80 and CD86 in vivo within 12-24 hr of priming (**Figure 5.S4a-d)**. Furthermore, after stimulation with anti-CD3/CD28 beads in vitro, CD80 and CD86 were upregulated in Tconv cells that had divided at least once, and elevated levels were retained through several divisions (**Figure 5.S4e**). CTLA4 expression was also increased on Tconv cells that had undergone at least one division and, as expected for activated T cells, CD69 expression was significantly increased in proliferating cells (**Figure 5.S5**).

Upregulation of the CTLA4 ligands CD80 and CD86 in Tconv cells suggested that suppressive CTLA4-B7 interactions may not be exclusive to Treg:DC partners, but may contribute to Treg:Tconv interactions. Using αCTLA4 blocking antibody and the same dosing protocol as in **Figure 5.5a**, we first confirmed a previous study (Read et al. 2006)

that OTII Tconv cells from the draining lymph nodes proliferated more in αCTLA4-treated animals than in isotype controls (**Figure 5.6a,b**). To complement our results using αCTLA antibody we then used a genetic approach to address whether Tregs mediate CD80/86-dependent Tconv interactions and suppression. We compared proliferation and Treg suppression of wild-type and CD80/86-double knockout Tconv cells in an APC-free in vitro system (to exclude the effect of Tregs on DCs) using anti-CD3 and anti-CD28 coated beads. WT and CD80/86 knockout Tconv cells proliferated comparably in response to αCD3/CD28 beads (**Figure 5.6c**). At a 1:1 ratio, WT Tregs inhibited proliferation of WT Tconvs by 48% ± 1.1% (mean ± SEM); however, Treg suppression was significantly reduced in CD80/86 knockout Tconv cells to 38% ± 1.7% (p=0.001, **Figure 5.6d**). Thus, the lack of CD80/CD86 makes Tconv cells less susceptible to suppression by Tregs.

5.2.7 CTLA4 stabilizes Treg interactions with Tconv cells

Collectively, the above results point toward an important functional role of Treg CTLA4 interactions with CD80/86 on Tconvs. To examine the choreography of these interactions, we compared Treg:Tconv interactions under control conditions (ITC) and following αCTLA4 treatment. In ITC-treated mice, it was clear that Tregs interacted extensively with Tconvs while also simultaneously interacting with DCs during antigen priming (**Figure 5.6e**). In contrast, during αCTLA4 treatment Tregs did not interact with Tconv in DC clusters (**Figure 5.6f**). To quantitatively analyze the role of CTLA4 in stabilizing T cell-T cell interactions, we measured contact durations under steady-state, inflammatory, and priming conditions. Steady-state Tconv:Treg cell contacts, although brief, were significantly

longer than Tconv:Tconv cell contacts (**Figure 5.6g**). Treg interaction times with Tconvs were prolonged in the presence of LPS-DCs, implying that inflammatory conditions may increase Tconv:Treg adhesion (**Figure 5.6g**). During antigen activation of OTII Tconv cells, Tconv:Treg interaction times were substantially increased; and notably, αCTLA4 treatment during priming reduced Tconv:Treg contact durations to steady-state values (**Figure 5.6h**). These results indicate that the stronger interactions between Tconv and Tregs during inflammation and priming are CTLA4-dependent.

In light of the high constitutive expression of CTLA4 by Tregs and induced expression of CTLA4 by Tconvs, as well as apparently conflicting evidence as to whether CTLA4 over-rides or has no effect on the TCR-induced stop-signal (Schneider et al. 2006; Fife et al. 2009), we also analyzed the effects of αCTLA4 treatment on OTII Tconv and Treg velocities under both steady-state and priming conditions. In the absence of cognate antigen, αCTLA4 treatment increased Treg velocity modestly without significantly altering Tconv cell velocity (**Figure 5.6i**). Under priming conditions, DC-interacting OTII Tconv velocities were reduced by αCTLA4 treatment, while at the same time Treg velocities were increased, relative to ITC treatment (**Figure 5.6j**). These results are consistent with the well-known observation that velocities are reduced by cellular interactions as cells cluster during priming (Miller et al. 2002; Miller et al. 2004).

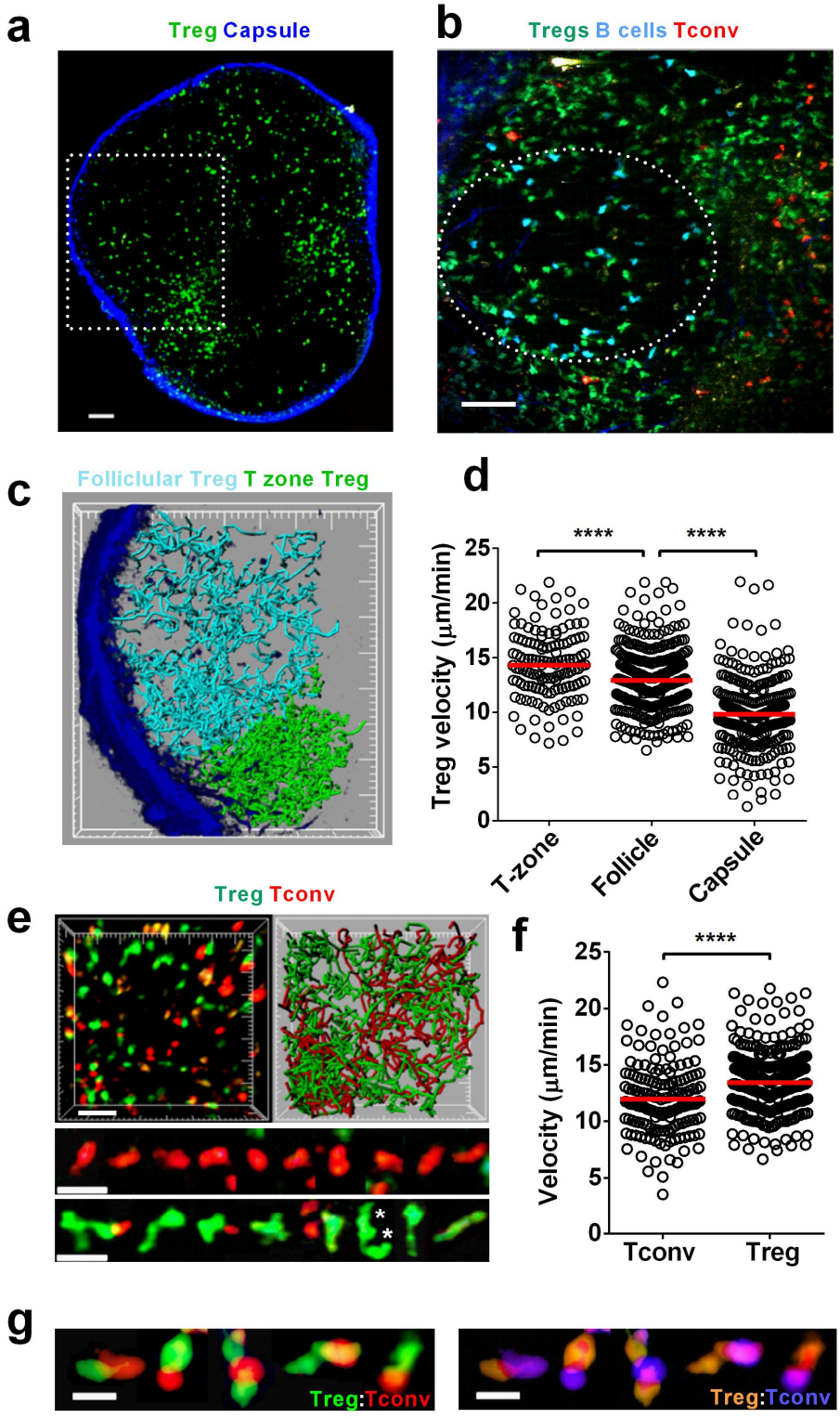

Figure 5.1. Endogenous Foxp3⁺ Treg regional behavior and interaction with Tconvs.

(**a**) Tregs in inguinal lymph node from a Foxp3^{EGFP} mouse under steady-state conditions. Green, EGFP^{+} endogenous Tregs; blue, second-harmonic collagen signal in capsular boundary. Single plane image, scale bar = 100 μm. White square represents area imaged in (**c**). (**b**) T-zone and follicular Tregs (both green), visualized 72 hr after adoptive transfer of CFP^{+}CD19^{+} B cells (blue) and CMTMR-labeled Tconv cells (red). Note Tregs colocalized with B cells within the dotted outline, and at higher density with Tconv cells throughout the T cell zone. Scale bar = 50 μm. (**c**) Non-overlapping populations of Tregs in the T-zone and the follicle. Treg movements represented by tracks within (light blue tracks) and outside the B cell follicle (bright green). Cells tracked over 29:38 (min:sec); 35 μm z stack, 50 μm tick marks. (**d**) Treg velocities in three regions of the lymph node. Each circle represents mean velocity in the T cell zone (n = 174 tracks); in the follicle (n = 397 tracks); and within 50 μm of the capsule (n = 343 tracks). Data pooled from 4 experiments. Open circles represent measurements from individual cell tracks; red bars indicate overall mean values; and p values are marked as * $p < 0.05$, ** $p < 0.01$, *** $p < 0.001$, and **** $p < 0.0001$ Mann–Whitney U test. (**e**) CMTMR-labeled Tconv cells adoptively transferred 24 hr before imaging and tracked with Tregs over 12 min. Still image (top left, scale bar = 30 μm) and corresponding tracks (top right) of Tconv cells (red) and Tregs (green) in the T-zone. Lower panels: magnified views of representative individual Tconv cells and endogenous Tregs (scale bars = 20 μm). Asterisks mark cellular processes. (**f**) Velocities of individual Tregs (n = 217 tracks) and Tconvs (n = 166 tracks) in the T-zone. Data pooled from 3 experiments. (**g**) Tconvs (red) and Tregs

(green) in the absence of antigen; right panel pseudocolored to highlight areas of contact; scale bars = 10 μm.

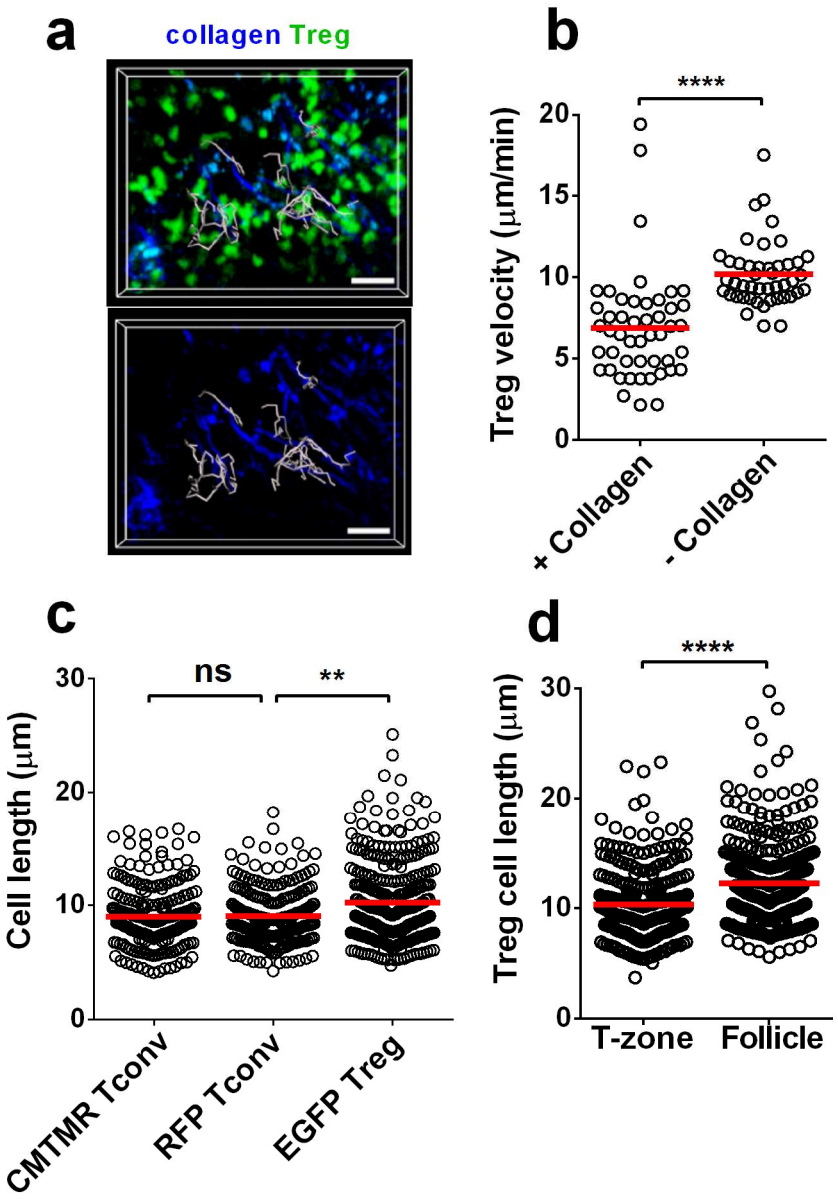

Figure 5.S1. Velocities of collagen-interacting Tregs and distinct regional Treg morphology.

(**a**) Tracks of Tregs (green) near the capsule (blue). Cell images removed in lower panel to highlight close association of some cells with collagen fibers, tracked over 5 min. Scale bar

= 30 μm. (**b**) Mean track velocities of Tregs when in contact with collagen (left), and not in contact (right). (**c**) Cell length of Treg and Tconv cells. To exclude the possibility of misinterpretation of cell size due to differences in cell labeling, we imaged endogenous Tregs together with either RFP^+ Tconv cells or CMTMR-labeled Tconv cells. Endogenous Tregs (n = 320) were significantly more elongated than either CMTMR-labeled (n = 237) or RFP-expressing $CD4^+CD25^-$ Tconv cells (n = 240). Data from 3 experiments. (**d**) Regional variation in Treg cell length. Follicular Tregs (n = 373) were more elongated than T-zone Tregs (n = 323). 4 experiments.

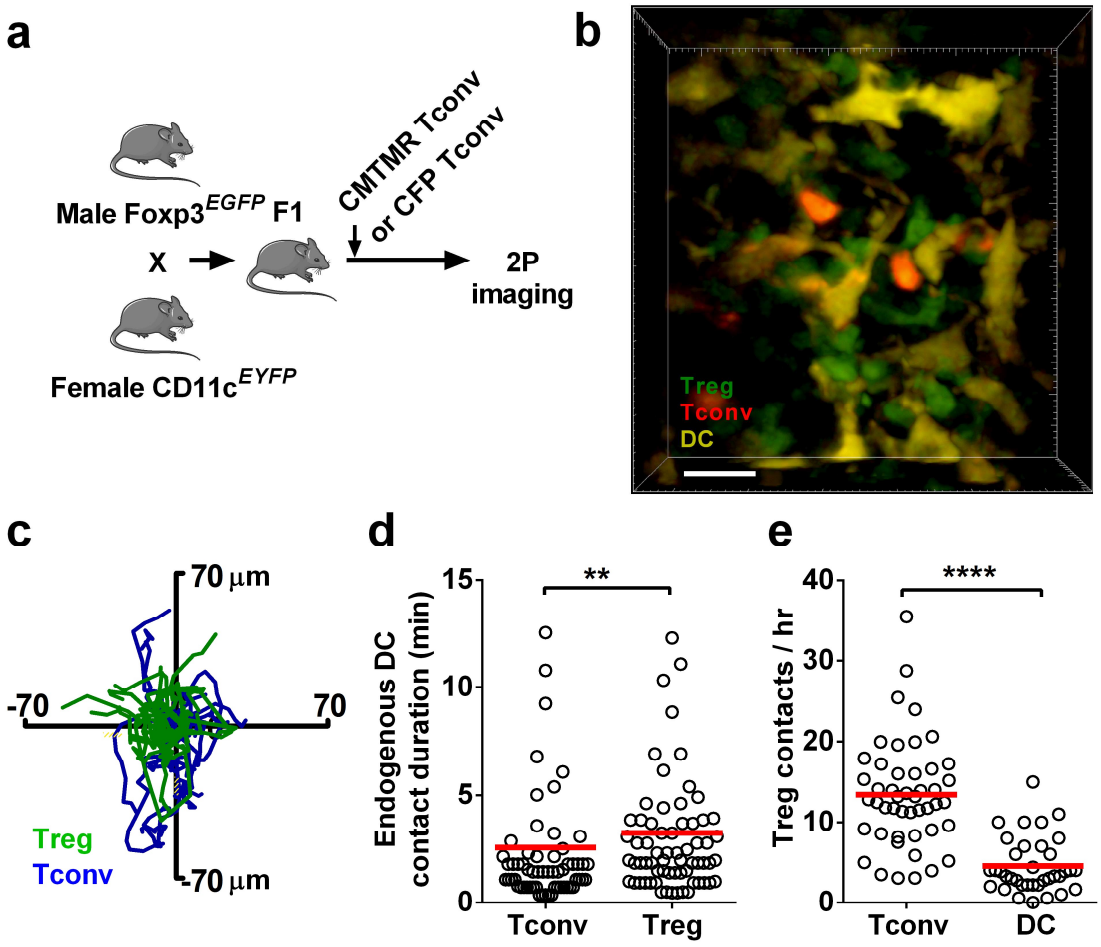

Figure 5.2. Tregs interact with LN-resident DCs.

(**a**) Experimental design to visualize endogenous Tregs together with resident DCs and Tconv cells. CMTMR-labeled Tconv cells from wild type C57Bl/6 mice, or CFP$^+$ Tconv cells from β-actin-CFP mice were adoptively transferred 12 hr or 4 days, respectively, prior to imaging, into F1 of Foxp3^{EGFP} x CD11c^{EYFP} mice. (**b**) Interactions among Tconv cells (red), resident DCs (yellow), and Tregs (green) under steady-state conditions. Scale bar = 20 μm. (**c**) Superimposed Treg (green) and Tconv (blue) tracks, z compressed and normalized to DC position at center (x, y, = 0, 0). Data from CFP$^+$ Tconv cells are shown;

similar results were obtained with CMTMR-labeled Tconv cells. Cells were tracked over 15:21 (min:sec). (**d**) Contact durations between cell pairs: Tconvs interacting with DCs (n = 61); Tregs interacting with DCs (n = 67). Data from CFP^+ Tconv cells are shown, and are also representative of results with CMTMR-labeled Tconv cells. 3 separate experiments, imaging duration >1 hr. (**e**) Observed contact frequencies with endogenous Tregs by labeled Tconvs (n = 47) and by resident DCs (n = 36). 2 experiments.

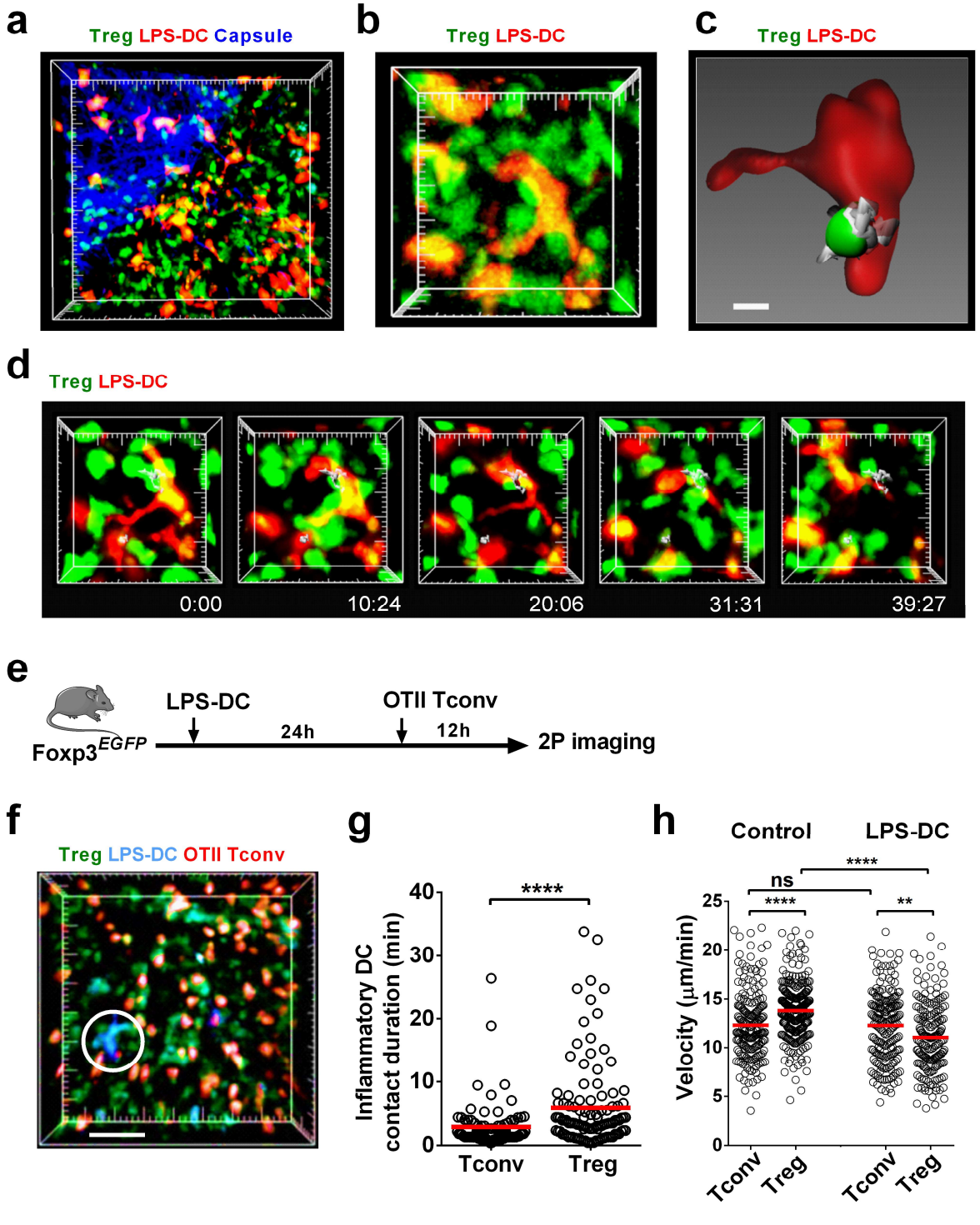

Figure 5.3. Tregs engage immigrant DCs near the lymph node capsule.

(**a**) LPS-activated CMTMR-labeled DCs (red) imaged in the draining inguinal lymph node 24 hr after subcutaneous injection into a Foxp3^{EGFP} mouse, showing immigrant DCs encountering and making contact with numerous endogenous Tregs (green) directly beneath the collagen capsule (blue) of the lymph node (major tick marks = 20 μm, 50 μm z-stack). (**b**) Close-up image of a DC (red) near the collagen capsule and its interactions with several Tregs (green). Major tick marks = 10 μm. (**c**) Space-filled rendering of the DC (red) from (**b**) and an associated Treg (green) with track (grey, 39:27 min:sec duration of imaging), showing the close association between Treg and DC (scale bar = 5 μm). (**d**) Time sequence (times shown in min:s) showing interactions of Tregs (green with grey tracks) engaging recently immigrated DCs (red). (**e**) Experimental design to examine the effect of LPS-activated DCs on OTII Tconv cells and Tregs. LPS-activated DCs from a ECFP mouse were injected into a Foxp3^{EGFP} mouse followed by adoptive transfer of CMTMR-labeled OTII Tconv cells at 24 hr and 2P imaging in the draining lymph node 12 hr later. (**f**) Snapshot showing adoptively transferred OTII Tconv cells (red), LPS activated DC (blue), and Tregs (green). Scale bar = 30 μm. (**g**) Contact durations of Tregs with LPS-DCs (n = 110 contacts) and Tconvs with LPS-DCs (88 contacts). Data pooled from 3 experiments each. (**h**) Effect of LPS-activated DCs on Treg velocities. Control velocities in the absence of LPS-DCs: Treg n = 296; OTII Tconv cells n = 213. In the presence of LPS DCs: OTII Tconv cell velocity did not change appreciably (p = 0.7, n = 207, Mann–Whitney U test) whereas Treg velocity was reduced (n = 193) Data pooled from 3 experiments each.

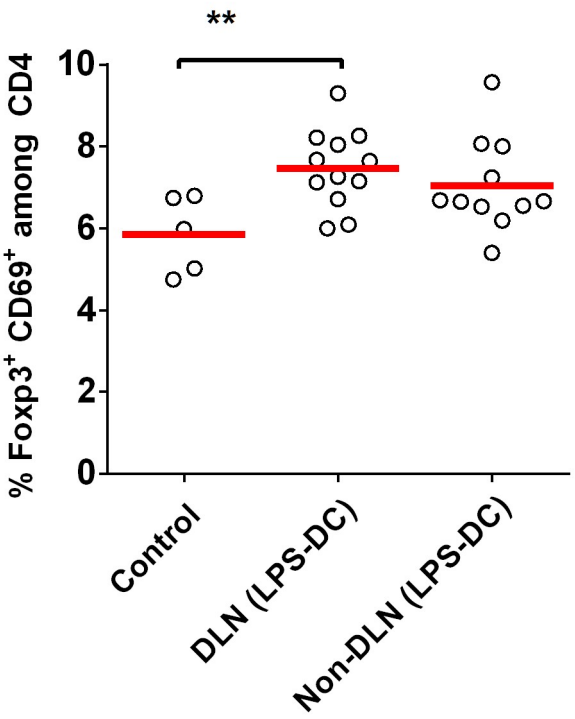

Figure 5.S2. Activated (LPS-treated) DCs induce activation of Tregs.

Draining lymph nodes of LPS-DCs injected mice contained a higher percentage of $CD69^{+}Foxp3^{+}$ Tregs as compared to PBS-injected control (** $p < 0.01$). Contralateral non-draining lymph nodes also showed a higher percentage of activated Tregs.

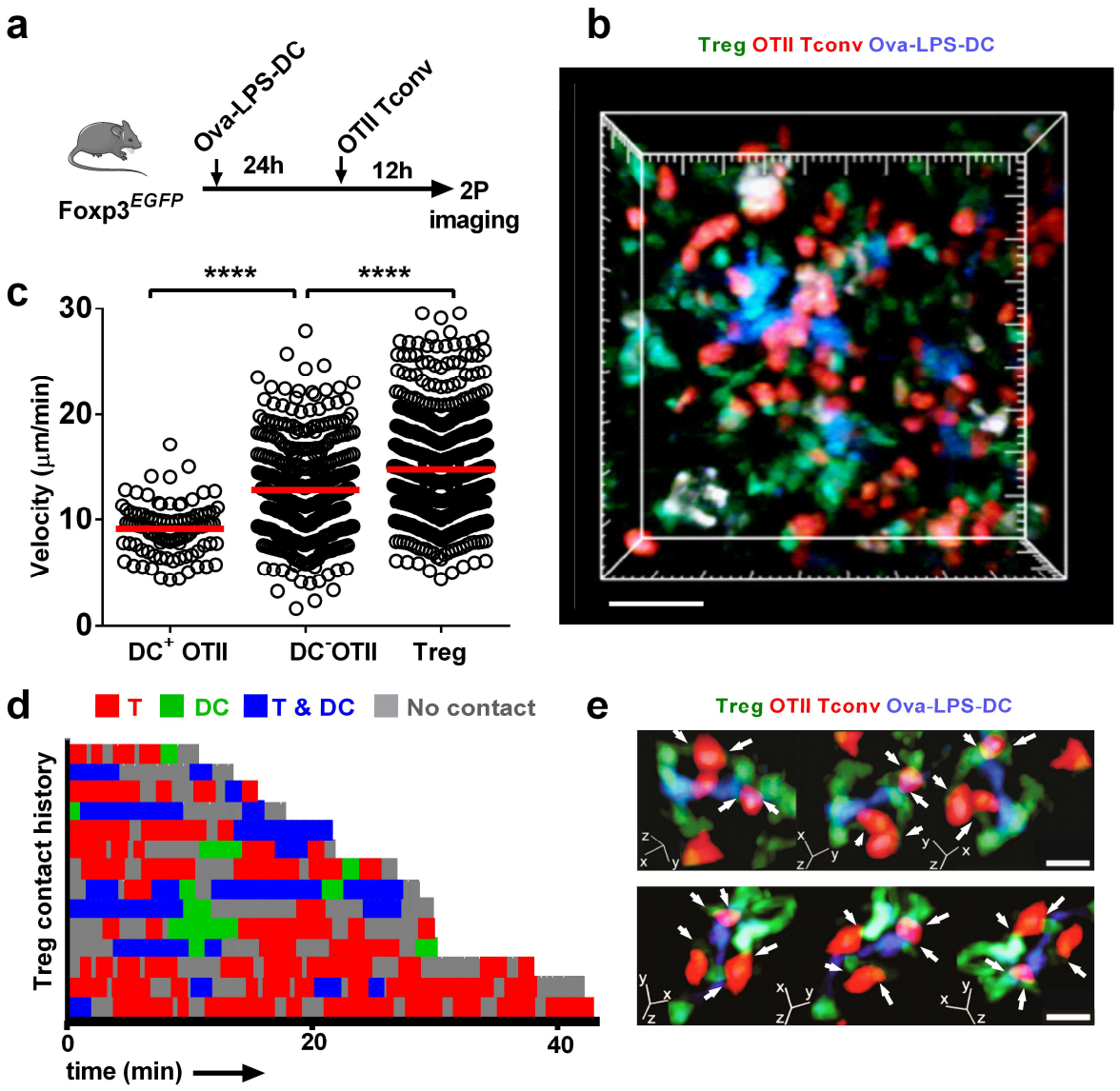

Figure 5.4. Dynamics of Tregs during antigen-specific Tconv priming.

(**a**) Experimental design to examine endogenous Treg behavior during an immune response. Ova-pulsed DCs were adoptively transferred into Foxp3^{EGFP} mice 24 hr prior to transfer of CMTMR-labeled OTII Tconv cells; imaging was performed 12 hr after OTII T cell transfer. (**b**) Tconv-DC clusters. Still image showing DCs (blue), OTII Tconv cells

(red), and Tregs (green). Scale bar = 50 μm. (**c**) Tconv and Treg velocities. Mean track velocities of OTII T cells were separated into those that interacted with a DC (DC^+ OTII, n = 99) and those that did not (DC^- OTII, n = 426). Treg velocities, n = 811. Data are pooled from 3 experiments. (**d**) Contact history map for 14 representative Tregs. Each horizontal bar represents times when a single Treg was alone (grey), in contact with a Tconv (red), in contact with a DC (blue), or in contact with DC:Tconv pairs (green). (**e**) Close-up images of Treg-Tconv cell contacts (white arrows) in the vicinity of a DC. The panel shows 3-way rotations at two time points, 67 sec apart. Scale bar = 10 μm.

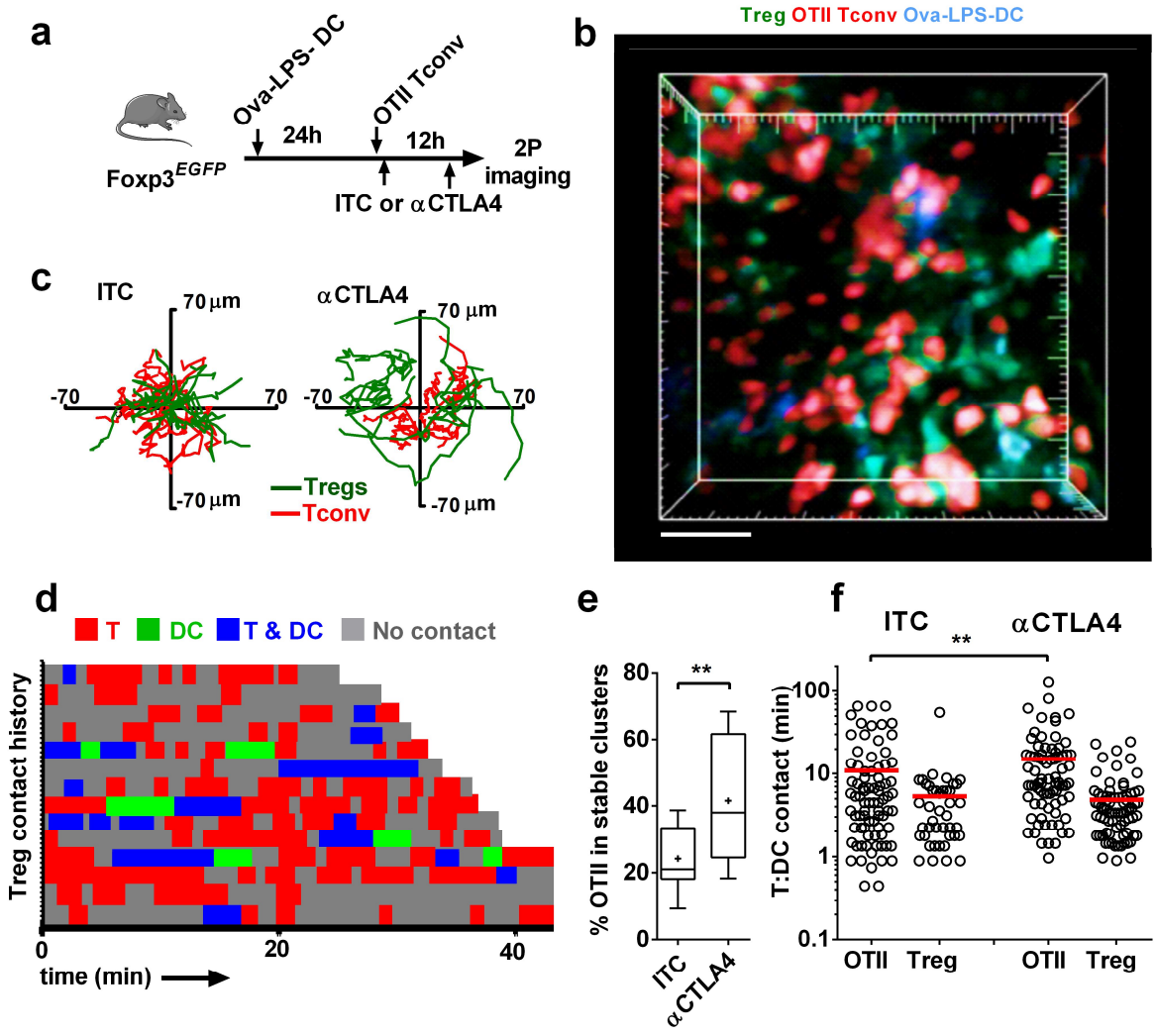

Figure 5.5. Tregs engage antigen-specific clusters of DCs and Tconv cells in a CTLA4-dependent manner.

(**a**) Experimental design to image the role of CTLA4-B7 in Treg interactions. Ova-pulsed DCs from ECFP mice were adoptively transferred into Foxp3^{EGFP} mice 24 hr prior to CMTMR-labeled OTII Tconv cells; imaging was performed 12 hr after OTII Tconv cell transfer. Animals received 150 μg of either ITC or αCTLA4, 30 min after adoptive transfer and 4 hr prior to imaging. (**b**) Still image showing DCs (blue), OTII Tconv cells (red), and

Tregs (green) in a node from αCTLA4-treated mouse. Scale bar = 50 μm. (**c**) Superimposed tracks of OTII T cells (red) and Tregs (green), with their origins normalized to the center of a DC. Cells were tracked for 10:14 min:sec. n = 21 for ITC and 34 for αCTLA4. (**d**) Treg contact history map. Each horizontal bar represents a single Treg, with contacts color coded as in **Figure 5.4d**. Note the shorter red and blue bars as compared to **Figure 5.4d**, indicating that Tregs spend less time interacting with Tconv cells and DCs in the presence of αCTLA4. (**e**) The percentage of OTII T cells in stable contact with a DC was increased by αCTLA4 treatment, compared to control (n = 21 and 14, respectively). 20 min imaging period minimum. (**f**) Tconv and Treg contact durations with antigen-bearing DCs. OTII Tconv:DC contact durations are increased in the presence of αCTLA4 (n = 78) relative to ITC control (n = 80). Treg:DC contact durations were shortened in the presence of αCTLA4 (n = 42) relative to ITC (n = 83).

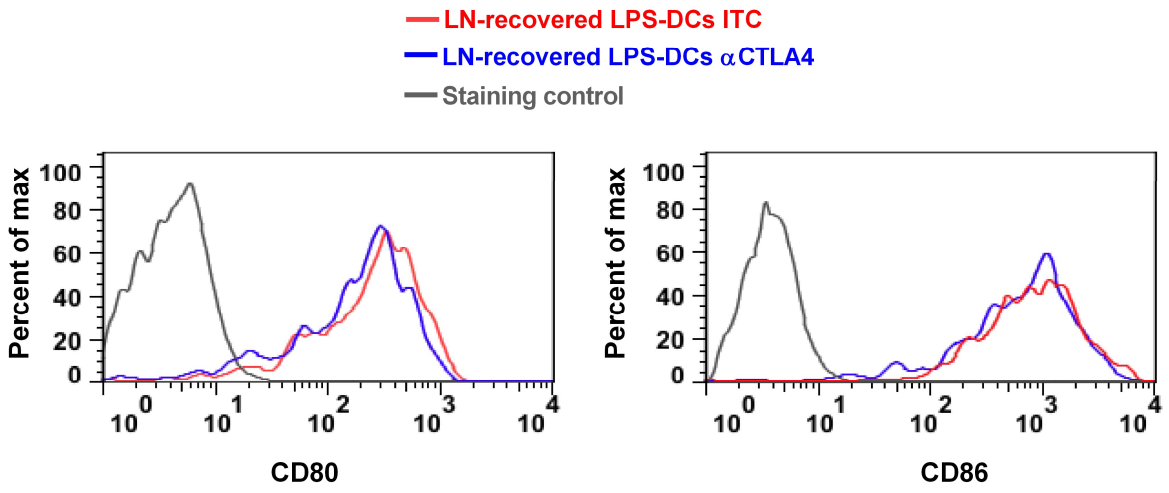

Figure 5.S3. Expression levels of CD80 and CD86 on LPS-DCs in vivo with and without αCTLA4 antibody treatment.

BMDCs were stimulated with LPS for 24 hr and labeled with CFSE before injection into the footpad of mice treated with ITC or αCTLA4 antibody. After 40 hr, popliteal LN were harvested and treated with collagenase (1mg/ml) and DNAse (50 μg/ml) for 45 min at 37° C to release the DCs. Representative histograms showing CD80 and CD86 expression in $CFSE^+$ DCs (2 independent experiments).

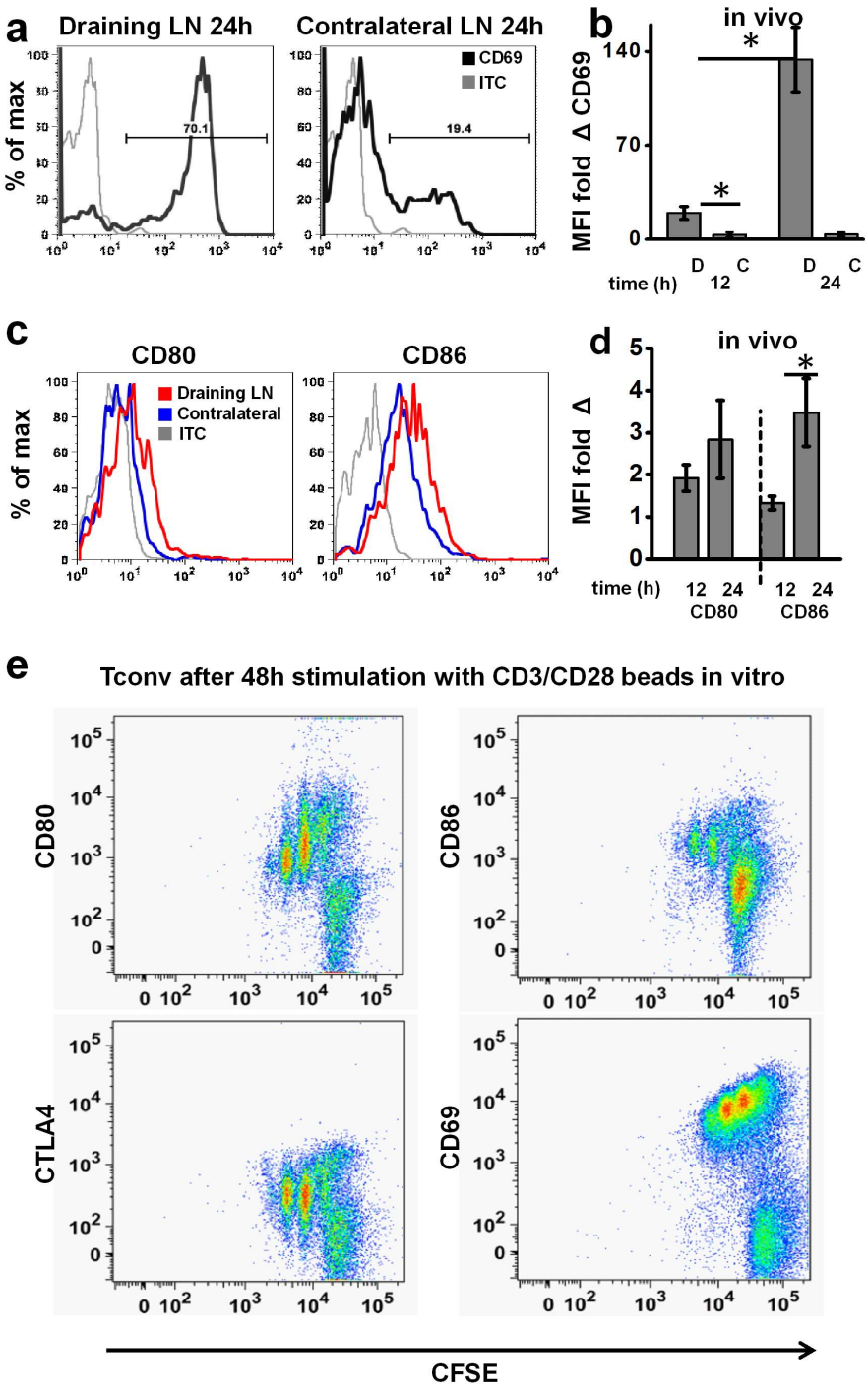

Figure 5.S4. Expression profiles of CD69, CD80 and CD86 on OTII Tcvon cells during priming.

(**a**) In vivo activation of OTII Tconv cells by Ova-pulsed DCs. CD69 expression is increased on OTII Tconv cells isolated from draining lymph node. Data are representative of 3 experiments. (**b**) Fold change in CD69 expression in vivo at 12 and 24 hr after OTII T cell transfer (36 and 48 hr after DC injection, respectively); CD69 is significantly increased in the draining lymph node (D) at 12 and 24 hr relative to the contralateral lymph node (C). (**c**) CD80 and CD86 expression is also increased in OTII T cells in the draining lymph node, relative to OTII T cells in the contralateral lymph node 24 hr after adoptive transfer, 48 hr after DC injection. Data are representative of 3 separate experiments. (**d**) Fold change in CD80 and CD86 expression in vivo 12 and 24 hr after adoptive transfer. CD80 and CD86 are nearly 2-fold higher on OTII T cells at 24 hr than at 12 hr after adoptive transfer. n = 4-7 separate experiments. (**e**) CFSE dilution and expression profiles of CD80, CD86, CTLA-4, and CD69 on Tconv stimulated with anti-CD3/CD28-coated beats for 48 hr. FACS plots are representative of 3 separate experiments.

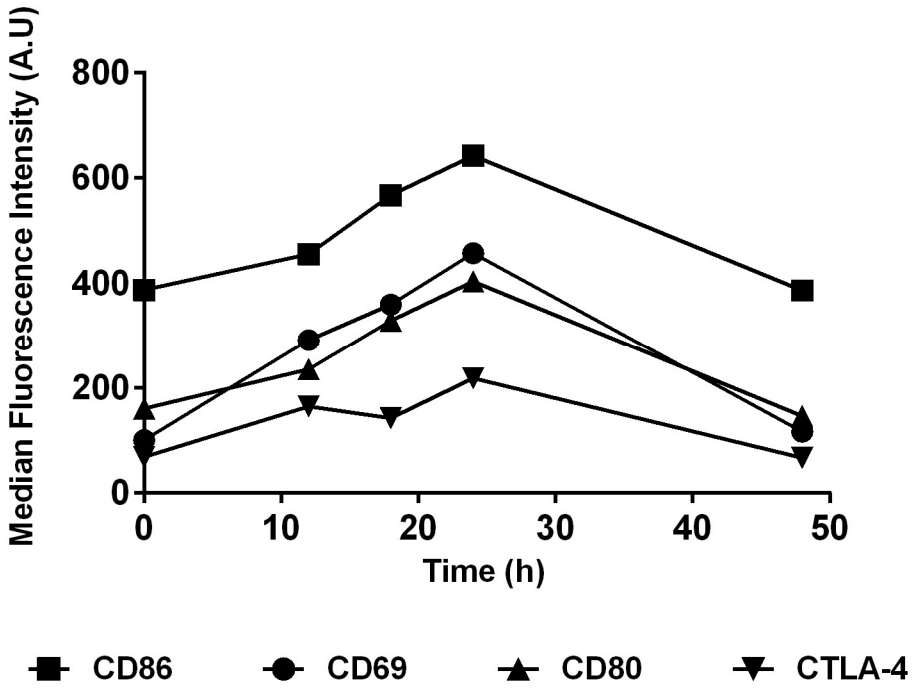

Figure 5.S5. Kinetics of expression profiles of CD86, CD80 and CD69 and CTLA-4 on T cells during activation.

CD4 T cells stimulated with anti-CD3/CD28-coated beads for 48 hr and analyzed for median of fluorescence intensity of surface markers at indicated time intervals is shown.

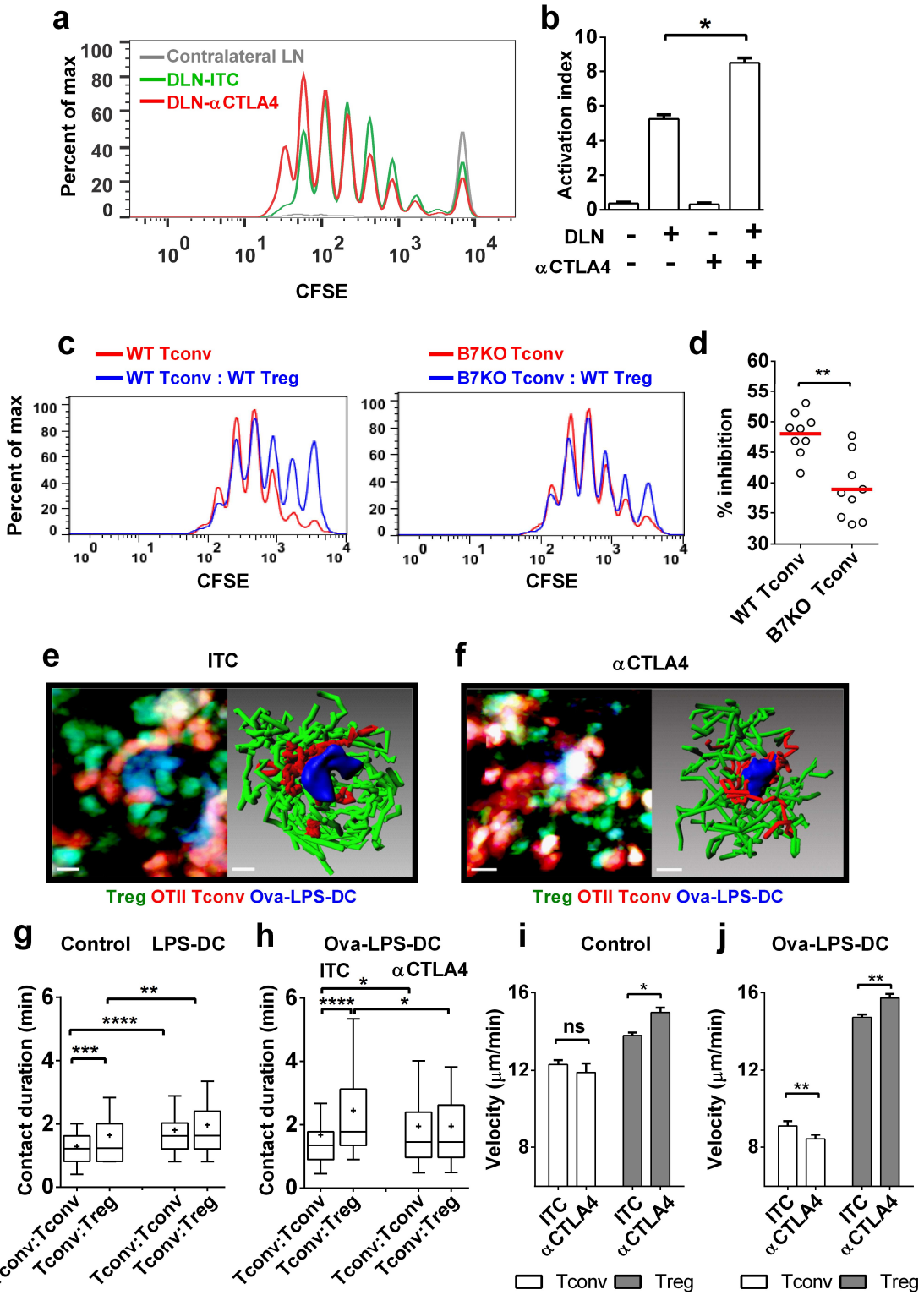

Figure 5.6. CTLA4 is critical for Tconv-Treg interactions during priming.

(**a**) CFSE dilution in OT-II Tconv cells 72 hr following transfer into WT mice primed with Ova-LPS pulsed DCs. Green and red lines for draining lymph node (DLN) of ITC- and αCTLA4-treated mice, respectively; grey line for contralateral LN with αCTLA4. (**b**) In vivo proliferation of OTII Tconv determined by CFSE dilution; data from 4-5 mice with αCTLA4 or ITC control treatment. (**c**) In vitro proliferation of Tconv (WT, left, and B7-KO, right) after stimulation with anti-CD3/28 Dynabeads with (blue) and without (red) WT Treg co-culture (1:1 ratio). (**d**) Inhibition of WT and B7-KO Tconv cell proliferation by WT Tregs; red bars indicate mean values, data pooled from two independent experiments. (**e**) Left: Ova-pulsed DCs (blue) interacting with OTII Tconvs (red) and Tregs (green) in a Foxp3^{EGFP} mouse. Right: tracks of Tconvs and Tregs that touched a DC at least once during imaging (20:55, min:sec); tracks normalized to DC position; scale bar = 10 μm. (**f**) Left: Ova-pulsed DCs (blue), OTII Tconvs (red), and Tregs (green) in Foxp3^{EGFP} mouse treated with αCTLA4. Right: tracks of Tconvs and Tregs that interacted with a DC (blue) at least once during imaging (20:33, min:sec). Scale bar = 10 μm. (**g**) Contact durations of OTII Tconvs in the absence and presence of LPS-DCs. Basal: Tconv:Tconv, n = 135; Tconv:Treg, n = 234. LPS-DCs present: Tconv:Tconv, n = 108; Tconv:Treg, n = 145. (**h**) Contact durations of OTII Tconvs in the presence of Ova-pulsed DCs after treatment with 150 μg isotype control (ITC) or αCTLA4 antibodies. ITC-treated: Tconv:Tconv, n = 101; Tconv:Treg, n = 108. αCTLA4-treated: Tconv:Tconv, n = 87; Tconv:Treg, n = 152. (**i**) Velocities of OTII Tconvs and Tregs under basal conditions after treatment with ITC or αCTLA4 antibodies. Tconv tracks: n = 268 (ITC) and 238 (αCTLA4); Treg tracks: n = 296 (ITC) and 213 (αCTLA4). (**j**) Velocities of OTII Tconvs and Tregs in

Ova-LPS-DC immunized mice after treatment with ITC or αCTLA4 antibodies. Tconv tracks: n = 99 (ITC) and 114 (αCTLA4). Treg tracks: n = 811 (ITC) and 305 (αCTLA4).

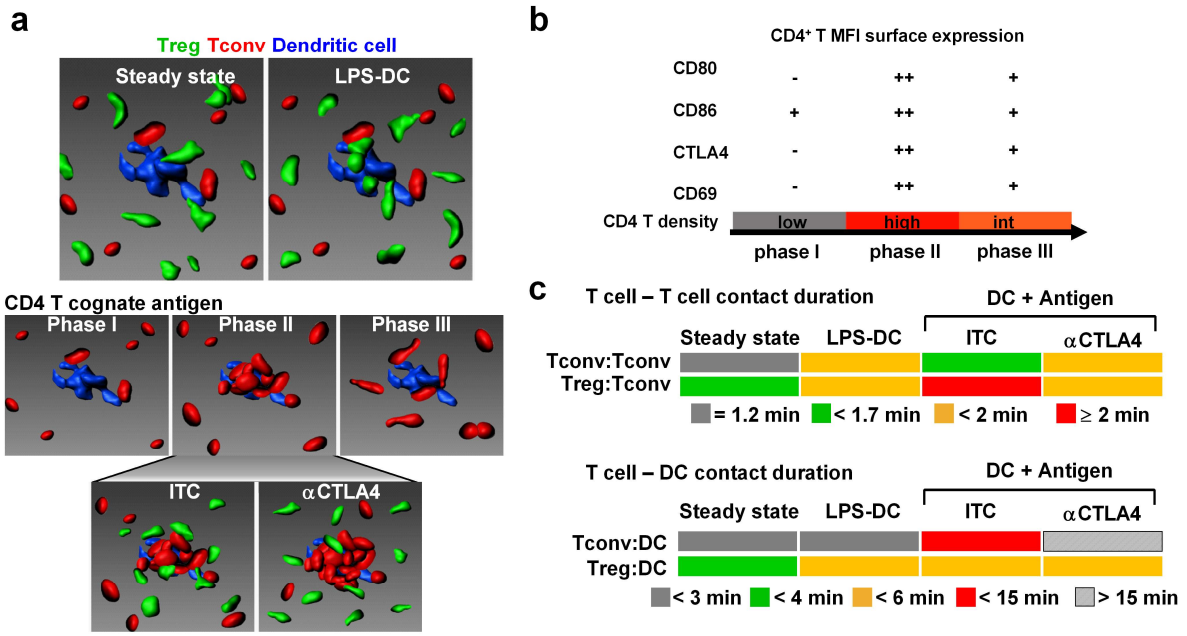

Figure 5.7. Summary of Treg, Tconv, and DC dynamics.

(**a**) Cellular choreography illustrating cell dynamics and the role of CTLA using cell shapes rendered from 2P images (Tregs, green; Tconv, red; DCs, blue). Panels represent steady-state conditions (top left); inflammation (LPS DC; top right); T cell priming in three phases (middle); Tregs interacting with clusters during phase II under normal priming conditions (labeled ITC for isotype control; bottom left) and in the presence of CTLA4-blocking antibody (labeled αCTLA4; bottom right). (**b**) Chart of relative surface expression by Tconv cells during T cell priming. CD4 density refers to the local concentration of antigen-specific T cells near antigen-presenting DCs during phase 2. (**c**) Color-coded diagram of measured contact durations among Tregs and Tconvs (top panel), and among T cells and DCs (bottom panel). Each change in contact duration (different colors) represents a significant difference of at least $p < 0.05$.

5.3 Discussion

Previous *in vitro* and *in vivo* studies have described both contact-dependent and chemokine-mediated mechanisms of suppression by Tregs (Paust and Cantor 2005; Sakaguchi et al. 2009; Schmidt et al. 2012). In this study, we employed 2P imaging to directly visualize and characterize the behavior of endogenous Tregs and their interactions with DCs and conventional T cells. Two non-overlapping populations of Tregs were observed in lymph node: one in the T cell zone, and one in the follicle. The follicular population was characterized by its position near the periphery of the lymph node, colocalization with B cells, and lack of exchange with Tregs in the T-zone as defined by colocalization with Tconv cells. Follicular Tregs have been previously described as being retained in the B cell follicle by expression of $CXCR5^+$ and high local concentrations of CXCL13 (Chung et al. 2011); and have been shown to regulate germinal center formation (Linterman et al. 2011). Here, we focus on T-zone Tregs that limit Tconv cell priming.

Several imaging studies used *in vitro*-expanded T cells to infer the effects of Tregs on Tconv cells in lymph node, but without a full consensus on mechanisms of immunoregulation (Mempel et al. 2006; Tadokoro et al. 2006; Angiari et al. 2013). Tadokoro *et al.* (Tadokoro et al. 2006) concluded that Tregs inhibit $CD4^+$ helper T cell interactions with DCs; Angiari *et al*. (Angiari et al. 2013) found that Treg inhibition of T cell:DC contacts and cluster formation was restricted to the late phases of activation; whereas Mempel *et al.* (Mempel et al. 2006) observed that the addition of Tregs did not affect the long duration interactions between $CD8^+$ cytotoxic T lymphocytes and antigen-presenting B cell targets. Tang *et al.* (Tang et al. 2006) imaged adoptively transferred antigen-specific $CD4^+CD25^+$

Tregs during immune response to islet antigen and concluded that DC-Treg interactions limit helper T cell activation. Recently, Pace *et al.* (Pace et al. 2012) indirectly demonstrated that Tregs suppress low-avidity $CD8^+$ responses to foreign antigens, showing that Treg depletion did not alter the long lasting APC-T cell interactions induced by high-affinity antigen, whereas short duration interactions induced by low affinity antigen were prolonged. While reporting the role of *Mst*1 kinase in Tregs, Tomiyama *et al.* (Tomiyama et al. 2013) suggested an alternative mechanism – that antigen-specific Tregs down-regulate co-stimulatory molecules on DCs but are unlikely to inhibit naïve T cell priming by physically competing for DCs. However, in that study (Tomiyama et al. 2013) 2P imaging was performed on sliced LN instead of intact or *in vivo* LN, raising caveats regarding damage to tissue architecture. Distinct from previous studies, our results provide evidence for direct physical interaction among endogenous Tregs with Tconv and APCs during an ongoing immune regulation in LN and further highlight the role of CTLA4 in coordinating these interactions. **Figure 5.7** depicts a summary of cellular choreography, surface markers, and cell interactions measured by contact durations under basal conditions, during inflammation, and during T cell priming.

Under basal conditions in the absence of antigen (**Figure 5.7a** top left), Tconv cells move rapidly and in a random-walk search for cognate antigen, sampling DCs with brief interactions (Miller et al. 2004). In the present study, we show that Tregs in the T cell zone migrate even faster than Tconv cells and engage both resident DCs and Tconv cells in frequent, brief contacts. Tregs have elongated processes, and contacts with Tconv are characterized by close apposition of membranes. Although Tregs constitute only 5-10% of

the total number of T cells in the lymph node, our data indicate that individual Tconvs and resident DCs interact directly with Tregs with high frequency, and are in contact with at least one Treg 36% and 47% of the time, respectively, under basal conditions.

During inflammation (**Figure 5.7a** top right), activated DCs from the periphery enter the lymph node via afferent lymphatics and encounter Tregs near the lymph node capsule. Activated DCs not pulsed with exogenous antigen up-regulate CD80 and CD86, and present self-antigens in the context of MHCII (Scheinecker et al. 2002; Wilson et al. 2004). We demonstrate that activated LPS-DCs form prolonged contacts with Tregs and that the presence of LPS-DCs causes a significant increase in the proportion of Tregs that are activated. The interactions of Tregs with LPS-activated DCs are reminiscent of prolonged CD4 T cell interactions with dermally-derived antigen-presenting DCs during priming (Miller et al. 2004).

When antigen is present on migratory DCs (**Figure 5.7a** bottom), the cellular dynamics undergo marked changes that can be divided into three phases as previously described (Miller et al. 2004). We show the dynamic behavior and physical interaction of Tregs with Tconvs and DCs during phase II (sustained contact). During this phase, regulatory T cells frequently interact with clusters of APC:Tconv but remain highly motile, suggesting that Tregs transiently scan these clusters. Our results complement a recent study reporting interaction behavior of antigen-specific Tregs with CTLs and APCs in a tumor model (Bauer et al. 2014). That study and our results suggest that APCs displaying peptide-MHC complexes and co-stimulatory molecules provide a platform for Tconv and Treg interaction. Mechanistically, Tregs have been proposed to regulate immune responses

by decreasing CD80 and CD86 on APCs in a CTLA-4 dependent manner, thus rendering APCs less potent for further activation of Tconv cells (Oderup et al. 2006; Onishi et al. 2008; Qureshi et al. 2011; Thauland et al. 2014). However, in our experiments, *in vivo* treatment with αCTLA4 did not alter expression of the co-stimulatory ligands, CD80 and CD86 in adoptively transferred and LN-recovered DCs. Several in vitro APC-free assays have shown that Tregs are capable of direct inhibition of Tconv cell activation in a contact-dependent and antigen-independent manner (Thornton and Shevach 1998; Thornton and Shevach 2000). We confirm this, and now provide direct evidence for CTLA4-dependent physical interactions between Treg:Tconv cells during immune activation in vivo. Coinciding with phase II of antigen-specific Tconv priming, when cognate Tconv cells interact stably with DCs and high-density Tconv:DC clusters form (8-16 hr), we show that Tconv cells increase their expression of CD80 and CD86 upon activation (**Figure 5.7b**), becoming potential targets for CTLA4-mediated interaction with Tregs. In the presence of blocking αCTLA4 antibody, Tregs appeared oblivious to both DCs and Tconvs, resulting in larger and more stable Tconv:DC clusters and contributing to enhanced T cell proliferation in vivo.

Contact-dependent suppression mediated by B7 molecules on activated T cells was previously proposed by Cantor and colleagues (Paust and Cantor 2005). CD86 is expressed by naïve $CD4^+$ T cells, and we demonstrate that both CD80 and CD86 are expressed by activated $CD4^+$ T cells. Using an *in vitro*, APC-free, genetic approach we show that lack of CD80 and CD86 expression on Tconvs renders them less susceptible to suppression by Tregs. Notably, Treg suppression is not completely abrogated, because multiple mechanisms for Treg suppression of Tconv cell priming may operate simultaneously

(Walker and Sansom 2011; Wing et al. 2011; Schmidt et al. 2012). Here, we show that CTLA4 on Tregs limits Tconv clustering around antigen-bearing DCs. We demonstrate that Tregs physically engage Tconv cells that have up-regulated CD80 and CD86. Indeed, we found that αCTLA4 treatment disrupts both Treg-Tconv and Treg-DC cell interactions at this early time point of T cell activation (**Figure 5.7c**). Moreover, T cell-T cell synapses have been reported to play a critical role in CD8 T cell differentiation through active exchange of cytokines during transient T-T synapse formation (Gerard et al. 2013). In line with a recent report on the role of CTLA-4 in stabilizing Treg synapses in vitro(Dilek et al. 2013), our study delineates an important functional role of Tregs to limit priming through CTLA4 interactions with upregulated B7 ligands on Tconv cells in vivo.

Finally, it has been suggested that CTLA4 may play a role in the inhibition of TCR-induced T cell stopping (Schneider et al. 2006; Lu et al. 2012), but this is controversial (Fife et al. 2009). In our hands, treatment with αCTLA4 increased steady-state Treg motility while having no effect on Tconv motility. During antigen-specific immune activation, treatment with αCTLA4 again enhanced Treg motility, but antigen-specific Tconv exhibited a significant decrease in velocity while forming stable clusters with DCs. Considering the role of CTLA4 in stabilizing Treg immune-synapses (Dilek et al. 2013), local exclusion of Tregs when CTLA4 is blocked could contribute to enhanced Tconv-cell clustering adjacent to DCs.

5.4 Materials and Methods

5.4.1 Mice, cell-labeling and reagents

Mice were housed in a clean, pathogen-free facility. Animal care and protocols were reviewed and approved by Institutional Animal Care and Use Committee of the University of California, Irvine and the animal ethics committee of Ghent University (ethical committee number 2013-015), in accordance with European guidelines (directive 2010/63/EU; Belgian Royal Decree of 6 April 2010). Male mice from the C57Bl/6 background were used at 8-12 weeks of age in donor/recipient experiments. $Foxp3^{EGFP}$ mice expressing enhanced GFP along with Foxp3 were obtained from Jackson Laboratories (Stock Number 006772). The CD11c-EYFP mouse strain expressing enhanced YFP on the CD11c promoter (Lindquist et al. 2004) was a kind gift of M. Nussenzweig (The Rockefeller University, New York, NY). $Foxp3^{EGFP}$ male mice were crossed with $CD11c^{EYFP}$ female mice to generate F1 heterozygote females. Other mouse strains included β-actin-CFP (Stock Number 004218), T-cell receptor transgenic ova-IA^b-specific OTII mice (Stock Number 004194), $CD80^{-/-}$ $CD86^{-/-}$ mice (Stock Number 003610) and wild type C57Bl/6 mice (Stock Number 000664) were purchased from Jackson Laboratories. Cell labeling was performed by suspending 4-6 million cells in 4 ml of RPMI-1640 at 37° C, quenching and washing twice with RPMI-1640 containing 10% FBS (Gibco). Tconv cells were labeled with 10 μM CMTMR for 30 min; for proliferation assays, OTII Tconv cells were labeled with 1.6 μM CFSE for 7 min; in some analyzed videos (not shown) DCs were labeled blue with 40 μM CMF_2HC for 40 min (Molecular Probes, CellTrace™ series). The following antibodies were purchased from BioLegend and were used at 0.2 μg/ml for flow cytometry and 100 μg per animal for

in vivo blocking: anti-mouse CTLA4 (clone 9H10, Syrian hamster IgG), ITC (hamster IgG), anti-mouse CD4 (clone GK1.5), APC-conjugated anti-mouse Vα2 (clone B20.1), anti-mouse CD69, anti-mouse CD62L, anti-mouse CD80 (clone 16-10A1), and anti-mouse CD86 (clone GL1). All adoptive transfers were performed under anesthesia and mild restraint, via tail-vein injection (T cells) or by subcutaneous injection (DCs) near a draining lymph node.

5.4.2 Dendritic cell culture and Tconv proliferation assays

Bone marrow-derived dendritic cells (BMDCs) for 2P imagining were generated as described (Matheu et al. 2008). Briefly, marrow was extracted from the femur of 6-10 weeks old mice and cultured in non-tissue culture treated polystyrene dishes for 9-10 days (Corning™) using RPMI 1640 (Lonza™) supplemented with 1% L-glutamine, 10% fetal calf serum (FCS; Hyclone Inc.), 100 units/ml penicillin, 100 µg/ml streptomycin, 2-βME and GM-CSF, IL-4 and TNFα, as previously described (Matheu et al. 2008). For *in vivo* proliferation assays IL-4 and TNFα were excluded to enhance antigen uptake during Ova-pulsing. For activated DCs and antigen-specific T-DC interaction imaging studies, DCs were treated with LPS (100 ng/ml) alone or with LPS + Ova (100 µg/ml) for 12-24 hr prior to harvest and injection. $CD4^{+}CD25^{-}$ T cells (Tconv) were isolated from spleen and lymph nodes of 6-10 week old mice using negative selection (Miltenyi Biotec and StemCell Technologies). For APC-free *in vitro* proliferation, CFSE-labeled WT Tconv cells were co-cultured with anti-CD3/CD28 coated dynabeads (Life Technologies®) at 1:1 ratio according to the manufacturer's protocol. Tregs were added to Tconv at 1:1 ratio for suppression assays. CFSE dilution in live cells (Fixable Viability Dye eFluor® 780 negative gating;

eBioscience) was analyzed using BD LSRII flow cytometer. For measuring the effects of αCTLA4 on *in vivo* proliferation, 2 x 10^6 Ova-pulsed DCs were injected s.c. into the footpad of WT mice; after 18 hr, 3 x 10^6 CFSE-labeled OTII Tconv cells were injected intravenously; popliteal lymph nodes were collected on day 3 of Tconv cell transfer; LN from the contralateral hind limb served as immunization control. CFSE dilution in single cells was analyzed by gating on $V\alpha2^+$ $CFSE^+$ population. Activation Indices (AI) were calculated using Equation 1, as described (Sen et al. 2008), where M values correspond to the number of cell divisions assessed by CFSE dilution.

Equation 1:
$$AI = \frac{M_9 + \frac{127}{128}M_8 + \frac{63}{64}M_7 + \frac{31}{32}M_6 + \frac{15}{16}M_5 + \frac{7}{8}M_4 + \frac{3}{4}M_3 + \frac{1}{2}M_2}{\frac{1}{128}M_8 + \frac{1}{64}M_7 + \frac{1}{32}M_6 + \frac{1}{16}M_5 + \frac{1}{8}M_4 + \frac{1}{4}M_3 + \frac{1}{2}M_2 + M_1}$$

5.4.3 2-Photon Imaging

All images were acquired with excitation wavelengths between 890 and 910 nM. Two imaging systems were used. The primary system used is a custom-built 2-photon system based on an Olympus BX5 upright microscope, with excitation generated by a tunable Chameleon femtosecond laser (Coherent). 495 nm and 560 nm dichroic filters were arranged in series to separate blue, green and red signals, and images were collected as previously described (Matheu et al. 2012) at UC Irvine. EGFP and EYFP signals are separated using a 520 nm dichroic filter. Additional data were collected on a Zeiss inverted 710 2-photon system in the Inflammation Research Center (IRC), VIB-U Gent with a Zeiss SP 485 nm, LP 490 nm, LP 555 nm, BP 565-610 nm filter combination arranged in series

with blue, green and red PMTs. Both microscopes were fitted with either a 20x (NA = 0.95), 25x (NA = 1.05), or 60x (NA = 1.1) water-immersion objectives, and equipped with 3 PMTs, peristaltic heated perfusion systems (Warner Instruments), thermocouple-based temperature sensors placed next to the tissue. All imaging was carried out on lymph nodes maintained at 37˚ ± 0.5˚C and superfused with RPMI-1640 and medical grade carbogen gas (95% O_2 and 5% CO_2). Size and velocity comparisons of endogenous Foxp3-eGFP T cells from each microscope were analyzed separately and found to be nearly identical with no significant variation.

5.4.4 Data Analysis

All image analysis was performed using Imaris software (Bitplane) version 6.5-7.2. Cells were tracked manually and contact durations were measured with 3D rotation to verify contacts. Stable contact formation was defined as any OTII T cell that remained in contact with one DC for a minimum of 20 min. Displayed images in the all figures are maximal intensity projections through the z-axis ('top view'; 50-70 μm depth in this panel) of x-y-z stacks. Flow-cytometry was performed on either a BD LSRII (UC-Irvine and VIB-UGent) or BD LSR-Fortessa (VIB-UGent) and analyzed using FlowJo. Figures were generated using Graphpad Prism and OriginPro8. Statistical analysis was performed using Mann Whitney test (unpaired sample, nonparametric); p values are marked in figures: * $p < 0.05$; ** $p < 0.01$; *** $p < 0.001$; and **** $p < 0.0001$.

CHAPTER 6: Conclusions

6.1 A novel ratiometric genetically encoded Ca^{2+} indicator and transgenic reporter mouse for Ca^{2+} imaging

Genetically encoded Ca^{2+} indicators were first introduced two decades ago, as a revolutionary method of using endogenously expressed fluorescent proteins to monitor Ca^{2+} signaling. It has only been in recent years that the performance of GECIs have caught up to the standards long held by synthetic small molecule indicators, enabling the use of GECIs without having to sacrifice Ca^{2+} sensitivity or dynamic range. We introduce Salsa6f, a novel GECI that combines ratiometric capability with the high performance of its GCaMP6f component, currently the fastest single fluorescent protein-based Ca^{2+} indicator. Salsa6f addresses a key weakness of single fluorescent protein-based GECIs, by enabling tracking of motile cells and identification of cell morphology even in the absence of Ca^{2+} signaling. We have then generated a transgenic reporter mouse with Cre-dependent expression of Salsa6f, further expanding the range of choices in the "Calcium Toolkit" for researchers to image Ca^{2+} signaling in specific cell types *in vivo*.

Despite the relatively simple modification of fusing GCaMP6f to tdTomato, this improvement of Salsa6f imparts powerful new capabilities for imaging Ca^{2+} *in vivo* and overcomes many limitations of currently available genetic probes. As demonstrated in our comparison with the PC::G5-tdT mouse, co-expression of a GCaMP variant with a separate tdTomato for labeling resulted in different localization of each fluorescent protein.

Although the total fluorescence of GCaMP5G and tdTomato from an entire cell could still be used to obtain a pseudo-ratiometric measure of cytosolic Ca^{2+} levels, such measurements have long been possible with small-molecule indicators, either directly with fura-2 or by combining two single wavelength indicators (Thomas et al. 2000). Salsa6f provides a true ratiometric measurement of Ca^{2+} levels with high brightness and a wide dynamic range that encompasses physiological Ca^{2+} signals over an entire order of magnitude. The Ca^{2+} affinity of Salsa6f is low enough to be unaffected by noise at resting Ca^{2+} levels, but still sensitive enough to detect spontaneous Ca^{2+} signaling events during T cell motility. This would enable Salsa6f to be used efficiently in a variety of different situations ranging from global cytosolic Ca^{2+} elevations induced by agonist stimulation to localized Ca^{2+} microdomains within dendritic spines (Chen et al. 2013).

In particular, it is when high spatial and temporal resolution are required that Salsa6f exceeds the capabilities of currently available methods. Genetic targeting of Salsa6f to defined subcellular locations such as within organelles or directly tagged unto target proteins would allow accurate and absolute measurement of local Ca^{2+} levels. For example, the FRET-based GECIs YC3.6 has been successfully targeted to the mitochondria, demonstrating agonist induced Ca^{2+} uptake, and to the plasma membrane, detecting Ca^{2+} entry specifically through PM channels but not from ER store release (Demaurex 2005; Loro et al. 2013). Since YC3.6 has a reported *in vitro* k_d of 250 nM, compared to 373 nM for GCaMP6f, it is conceivable that Salsa6f would perform just as well if targeted in the same manner (Nagai et al. 2004; Chen et al. 2013). The increased brightness and dynamic range of Salsa6f would allow for such localized Ca^{2+} measurements to be done *in vivo*, after

transient transfection or viral transduction of cells with new Salsa6f constructs. As we have already shown that RedGCaMP6f can perform as a fusion tag to Orai1 channels, this approach could be replicated with Salsa6f to enable greater two-photon capability, and be extended to other Ca^{2+} channels or Ca^{2+}-sensing proteins of interest.

The direct fusion of GCaMP6f and tdTomato in Salsa6f would allow for ratiometric imaging at the highest resolution, down to the single molecule level. This would be crucial in studies where Ca^{2+} influx from different sources need to be distinguished. For example, in glutamate-mediated neuronal excitotoxicity, it is currently unclear why Ca^{2+} entry through NMDA receptors is neurotoxic, whereas Ca^{2+} entry through voltage-gated Ca^{2+} channels is neuroprotective (Lai et al. 2014). Ca^{2+} influx from excitotoxic glutamate stimulation leads to mitochondrial Ca^{2+} uptake and subsequent mitochondrial production of reactive oxygen species, depolarization, and induction of neuronal cell death (Reynolds and Hastings 1995; White and Reynolds 1996; Stout et al. 1998). Salsa6f could be directly tagged to either NMDA receptors or voltage-gated Ca^{2+} channels, then combined with another GECI targeted to the mitochondria. This would allow for simultaneous visualization of the spatial and temporal dynamics for different sources of Ca^{2+} entry in relation to mitochondrial Ca^{2+} uptake and subsequent events leading to neuronal excitotoxicity.

Currently, viral transduction is the most popular method of expressing GECIs within various cell types, particularly for neurons and lymphocytes (Monahan and Samulski 2000; Zhang et al. 2007; Chen et al. 2013; Mues et al. 2013; Thestrup et al. 2014). Infection with viral constructs result in high expression levels over long periods of time, and specific cell

types can be targeted based on viral tropisms or cell-type-specific promoters (Davidson and Breakefield 2003; Shevtsova et al. 2005; Nathanson et al. 2009). However, viral infection of neurons within intact mouse brain is an invasive surgical procedure, and infection of lymphocytes requires a purified population of activated cells. Furthermore, viral transduction of neurons leads to variation in expression levels between neighboring cells and based on distance from the viral injection site (Tian et al. 2012; Chen et al. 2013). Over time, expression level of GECIs in virally transduced neurons continue to rise until they result in abnormal cell physiology and aberrant cell death, restricting imaging studies to a few weeks within infection (Akerboom et al. 2012; Zariwala et al. 2012).

Transgenic expression would overcome the limitations of viral transduction, and provide stable expression levels without the need for invasive procedures. In particular, the *Rosa26* locus is ubiquitously expressed and can permit insertion of an exogenous promoter to drive high expression with Cre-dependent control (Soriano 1999; Madisen et al. 2010). This strategy was used to establish a robust system of Cre-reporter mouse lines, expressing a variety of fluorescent probes including eGFP and tdTomato, as well as genetic Ca^{2+} indicators such as GCaMP3 and GCaMP6 (Zariwala et al. 2012; Madisen et al. 2015). When crossed to cell-type-specific Cre lines, our new Salsa6f reporter line allows for the expression of tdTomato to examine morphology of labeled cells, trace axonal projections, perform long-term *in vivo* imaging, and follow development and differentiation, combined with GCaMP6f to obtain a functional readout of cellular activity at the same time. Since the site of integration is known, off target side effects are avoided unlike previous randomly integrated transgenic GECI lines (Direnberger et al. 2012). Furthermore, since there is

already a growing online database for characterization of Cre crosses on the Allen Mouse Brian Atlas, any researcher interested in neuronal studies can first look up the expected pattern of expression before committing time and resources to establishing a new Cre cross with the Salsa6f reporter mouse.

6.2 A new role for Orai1 in regulating T cell motility

Ca^{2+} signaling through the store-operated Ca^{2+} channel, Orai1, is crucial for T cell activation and initiation of the immune response. Although we have previously shown that Orai1 function is essential for T cell homing to lymph nodes (Greenberg et al. 2013), a role in regulating T cell motility within lymph nodes has not been previously reported. Our findings expand the range of T cell functions regulated by Orai1 to include fine-tuning motility speed to enhance antigen search within confined environments. Furthermore, we show that this Orai1-dependent modulation arises through a previously unknown cell-intrinsic mechanism. This provides further support for the hypothesis that intrinsic and stochastic T cell motility patterns underlie immune surveillance in the lymph node.

The application of two-photon microscopy to immune imaging has enabled the tracking of lymphocyte trajectories within intact lymph nodes, revealing a highly active "random walk" pattern independent of pervasive chemokine gradients (Miller et al. 2002; Wei et al. 2003; Cahalan and Parker 2008). This stochastic motility of T cells, combined with dynamic processes extended by dendritic cells, enable efficient scanning of the T cell repertoire and rapid initiation of the immune response (Miller et al. 2004). In order to maintain proper immune surveillance, T cells must balance their high motility with the

need to thoroughly scan their surroundings. The T cell "STOP" signal was identified over two decades ago to be triggered by antigen recognition and elevated intracellular Ca^{2+} levels, but it is still unclear how such Ca^{2+} signals regulate basal T cell motility (Donnadieu et al. 1994; Negulescu et al. 1996; Dustin et al. 1997).

Recent studies have highlighted the accumulation of TRPM7 channels at the uropod of migrating T cells, where they are believed to trigger local Ca^{2+} signals and activate calpain-2 in the turnover of integrin adhesions (Svensson et al. 2010; Kuras et al. 2012). Although both studies excluded a role for Orai1 in modulating T cell motility, we believe the use of open field integrin-dependent motility assays does not replicate the confined physiological environment experienced by T cells within crowded lymph nodes, and thus does not represent the predominant mode of motility utilized by T cells *in vivo*. Our findings demonstrate a novel role for Orai1 in modulating T cell motility both *in vivo* within the lymph node and *in vitro* within microchannels, highlighting the need for faithful replication of physiological conditions in studying T cell motility. Furthermore, we show that Orai1 specifically alters the frequency of cell pauses without affecting the duration of pauses or the maximum and minimum cell velocity, and this modulation occurs *in vitro* even in the absence of extrinsic cell contacts. This selective alteration of timing is a hallmark of cell regulatory pathways, and identifies Orai1 as a potential candidate for the molecular trigger of spontaneous pauses during stochastic T cell motility. Specifically, the pauses triggered by Orai1 activity would limit the distance traveled by a T cell within the lymph node to ensure adequate scanning of local dendritic cells during immune surveillance.

6.3 Regulatory T cell dynamics within the lymph node

Tregs make up only a small subset of the total T cell population, and yet Tregs are essential for maintaining immune homeostasis, through mechanisms that remain incompletely defined. While several imaging studies have used *in vitro*-expanded T cells to infer the effects of Tregs on conventional T cells (Tcons) in lymph node, there has yet to be a full consensus on the mechanisms of immunoregulation (Mempel et al. 2006; Tadokoro et al. 2006; Angiari et al. 2013). We show for the first time, *in vivo* imaging of unperturbed, endogenous Tregs interacting with Tcons and dendritic cells. We demonstrate the crucial involvement of CTLA-4 in determining cellular dynamics among Tregs, Tcons, and dendritic cells *in vivo*. Distinct from previous studies, our results provide evidence for direct physical interaction among endogenous Tregs with Tcons and APCs during ongoing immune regulation within the lymph node.

Recent studies have implicated a contact dependent mechanism of Treg-mediated suppression, resulting in inhibition of Ca^{2+} signals in activating Tcons within 30 minutes of contact with Tregs (Schmidt et al. 2011; Schwarz et al. 2013). While the exact mechanism for this suppression remained unknown, another recent study provided a possible explanation by demonstrating trans-endocytosis of costimulatory molecules from APCs by CTLA-4 on T cells (Qureshi et al. 2011). Although Tregs demonstrated greater efficiency at depleting ligands from APCs than Tcons, the Qureshi et al. study did not analyze direct interactions between Tregs and Tcons. It is plausible that CTLA-4 or another yet unknown

receptor could be used by Tregs to capture molecular machinery on Tcons and selectively inhibit T cell activation.

As Orai1 is the main Ca^{2+} channel in T cells and is upregulated during activation (Lioudyno et al. 2008), Orai1 would be an attractive target for trans-endocytosis in a possible Treg-mediated mechanism of immune suppression. However, several experiments performed in the Cahalan lab have failed to show any consistent functional downregulation of Orai1 channel activity in either resting or activating Tcons, as a result of co-culture with preactivated Tregs (unpublished data). Only the experiments in **Chapter 4.2.5** were able to demonstrate a quantitative reduction in the intensity of Ca^{2+} signaling in Tcons activated overnight in the presence of preactivated Tregs. Such experiments were made possible by GECI-expressing T cells, so that cell activation could be measured through Ca^{2+} signaling even after overnight culture, without having to wash away any soluble factors in the culture media to load a synthetic small-molecule Ca^{2+} indicator. When Tcons were co-cultured with preactivated Tregs at physiological ratios, Tcons in direct contact with Tregs showed a greater reduction in Ca^{2+} signaling. As we cannot exclude the possibility of soluble factors secreted by Tregs at a low enough concentration to affect only Tcons in close proximity, the mechanism for this Treg-mediated suppression of Ca^{2+} signaling remains to be elucidated. Further studies utilizing our Salsa6f reporter mouse will be aimed at pinpointing whether the Treg-mediated suppression of Ca^{2+} signaling is a transient effect of suppressing Orai1 function, or a permanent effect of downregulating total number of Orai1 channels in Tcons. Furthermore, since no studies have evaluated the

in vivo effects of Tregs on Ca^{2+} signaling in resting and activating Tcons, it will be important to establish *in vivo* Ca^{2+} imaging studies, now made possible by the Salsa6f reporter mouse.

Understanding the mechanisms of Treg-mediated suppression, such as through CTLA-4 or inhibition of Ca^{2+} signaling, will be important in the key settings of cancer, HIV infection, and autoimmune disease. Antibodies that block CTLA-4 function to enhance immune responses are currently being evaluated as experimental therapies for antitumor immunity (Hoos et al. 2010). Ipilimumab and tremelimumab are two such CTLA-4 antibodies under clinical investigation in patients with metastatic melanoma (Callahan et al. 2010). Patients under CTLA-4 antibody treatment developed a range of immune related adverse events, the most significant of which was severe enterocolitis that was treatable with corticosteroids and/or anti-TNF therapy (Wolchok et al. 2010). Various independent studies have been unable to conclude whether positive clinical response to CTLA-4 antibody treatment was correlated with the frequency of tumor infiltrating Tregs (Comin-Anduix et al. 2008; Ribas et al. 2009). Subsequent studies have demonstrated that combination therapy of CTLA-4 blockade with other treatments, such as vaccination with irradiated GM-CSF secreting tumor cells or blocking the programmed cell death 1 (PD-1) receptor, to produce more rapid and deeper clinical tumor responses than monotherapy (Hodi et al. 2008; Wolchok et al. 2013; Tsai and Daud 2015). Thus, it will be important to evaluate endogenous T cell activity within tumor microenvironments and peripheral tissue, as well as interactions with tumor infiltrating Tregs, in order to gain a better understanding of the cellular response to different combinations of antitumor therapy.

6.4 Future Directions

The Salsa6f reporter mouse has only just been introduced, and there is still much to be done. While we have plans to use it extensively within the immune system, it must be thoroughly characterized to ensure transgenic expression of a Ca^{2+}-binding fluorescent indicator does not perturb cellular functions. So far, we have not noticed any gross abnormalities or behavior defects in Salsa6f mice or those crossed with CD4-Cre mice. As we begin to initiate collaborative efforts to widen the use of the Salsa6f mouse, we will also evaluate the use of Salsa6f in the nervous system, and compare it to currently use standards.

A key advantage of transgenic reporter mice is endogenous expression of a fluorescent marker and continued expression even after differentiation and repeated cell divisions. The Salsa6f mouse will allow us to differentiate fibroblasts or T cells into induced or activated cell types, and continue to track daughter cell populations over extended time periods. This is particularly useful in adoptive transfer protocols, when cells with distinguishable fluorescent labels can be injected into recipient animals, then imaged weeks or months after transfer. Transgenic expression allows for labeling of genetically defined neuronal populations, without the need for invasive surgeries, and tolerates repeated chronic imaging experiments. To facilitate the use of Salsa6f mice for neuronal studies, we will begin by breeding Salsa6f mice to CaMKIIa-Cre mice and Pvalb-2A-Cre mice for expression in neuronal subpopulations, and to CX3CR1-Cre mice for expression in microglial cells. Expression patterns will be evaluated in the resulting crosses, and the specific cell types now expressing Salsa6f will be used to measure cellular function in

standard assays. This data will be compared to what has been published for other GECI reporter mice to ensure the Salsa6f reporter mouse can match and exceed what is currently available.

In the context of scientific research, the development of new molecular probes, novel microscopies, and more relevant mouse models have led to incredible advances in understanding the underlying mechanisms of human disease and pathophysiology. Cloning of fluorescent proteins have allowed endogenous labeling of specific cell populations or subcellular organelles, and when combined with two-photon microscopy have allowed for visualization of the complex cellular choreography of lymphocytes within intact lymph nodes (Cahalan et al. 2002; Miller et al. 2002; Cahalan and Parker 2008). Mouse models replicating human conditions have been established for almost every aspect of disease, from cancer to diabetes to depression (Rosenthal and Brown 2007; Van Belle et al. 2009; Cheon and Orsulic 2011; Barkus 2013; Takao and Miyakawa 2015; Perlman 2016). The ability to simultaneously track specific cell types of interest while visualizing cell function as a readout of fluorescence provides enormous insight into the cellular dynamics and activation states in numerous disease models. The application of fluorescence imaging to clinics will bring about new probes and devices to enhance treatment options for patients. Labeling with fluorescent probes could better outline tumor margins to guide surgery (Nguyen and Tsien 2013), monitor pancreatic beta cell function directly *in vivo* for feedback of insulin delivery in diabetics, evaluate cardiomyocyte function for early detection and prevention of ischemic events, and aid in assessing neuronal function and recovery after stroke. Translation of basic research techniques to clinical applications

requires benchwork in the laboratory and the ability to envision and engineer new diagnostic instruments and implantable devices.

The universal prevalence of Ca^{2+} signaling will no doubt play an important role in understanding, diagnosing, and treating numerous diseases. As a future physician scientist, I look forward to playing a role in the incorporation of cellular Ca^{2+} sensors into the practice of medicine. It is already routine for specific immune cells to be purified from patient blood samples and evaluated for function by flow cytometric analysis of surface markers. Ca^{2+} indicators can be incorporated into assays to diagnose immunosuppression and autoimmunity, based on insight from well-characterized Ca^{2+} imaging studies using transgenic GECI mice. I am convinced that my training as a scientist will enable me to recognize new developments in basic science research and how they could apply to novel diagnostic methods in clinical medicine.

6.5 Final Remarks

Taken together, my thesis is the accumulation of developing a novel tool for Ca^{2+} imaging and applying it in the study of cellular function in the immune system. While my own interests lie in T cell function, it is my hope that the Salsa6f reporter mouse can be widely applied to studies in the nervous system, the cardiovascular system, the endocrine system, and beyond. By establishing a reliable transgenic reporter mouse with validated expression and function, we hope to lower the burden of entry and provide other scientists with a powerful new tool in associating cellular activity with morphology, position, and molecular profile. These insights can then be extended to elucidate the underlying mechanisms in

pathophysiology, and eventually, applied to develop new diagnostics and treatments of human disease.

BIBLIOGRAPHY

Akerboom, J., Carreras Calderon, N., Tian, L., Wabnig, S., Prigge, M., Tolo, J., Gordus, A., Orger, M. B., Severi, K. E., Macklin, J. J., Patel, R., Pulver, S. R., Wardill, T. J., Fischer, E., Schuler, C., Chen, T. W., Sarkisyan, K. S., Marvin, J. S., Bargmann, C. I., Kim, D. S., Kugler, S., Lagnado, L., Hegemann, P., Gottschalk, A., Schreiter, E. R. and Looger, L. L. (2013). Genetically encoded calcium indicators for multi-color neural activity imaging and combination with optogenetics. Front Mol Neurosci **6**: 2.

Akerboom, J., Chen, T. W., Wardill, T. J., Tian, L., Marvin, J. S., Mutlu, S., Calderon, N. C., Esposti, F., Borghuis, B. G., Sun, X. R., Gordus, A., Orger, M. B., Portugues, R., Engert, F., Macklin, J. J., Filosa, A., Aggarwal, A., Kerr, R. A., Takagi, R., Kracun, S., Shigetomi, E., Khakh, B. S., Baier, H., Lagnado, L., Wang, S. S., Bargmann, C. I., Kimmel, B. E., Jayaraman, V., Svoboda, K., Kim, D. S., Schreiter, E. R. and Looger, L. L. (2012). Optimization of a GCaMP calcium indicator for neural activity imaging. J Neurosci **32**(40): 13819-13840.

Angiari, S., Rossi, B., Piccio, L., Zinselmeyer, B. H., Budui, S., Zenaro, E., Della Bianca, V., Bach, S. D., Scarpini, E., Bolomini-Vittori, M., Piacentino, G., Dusi, S., Laudanna, C., Cross, A. H., Miller, M. J. and Constantin, G. (2013). Regulatory T cells suppress the late phase of the immune response in lymph nodes through P-selectin glycoprotein ligand-1. J Immunol **191**(11): 5489-5500.

Arnaudeau, S., Kelley, W. L., Walsh, J. V., Jr. and Demaurex, N. (2001). Mitochondria recycle Ca(2+) to the endoplasmic reticulum and prevent the depletion of neighboring endoplasmic reticulum regions. J Biol Chem **276**(31): 29430-29439.

Azuma, M., Yssel, H., Phillips, J. H., Spits, H. and Lanier, L. L. (1993). Functional expression of B7/BB1 on activated T lymphocytes. J Exp Med **177**(3): 845-850.

Babich, A. and Burkhardt, J. K. (2013). Coordinate control of cytoskeletal remodeling and calcium mobilization during T-cell activation. Immunol Rev **256**(1): 80-94.

Baird, G. S., Zacharias, D. A. and Tsien, R. Y. (1999). Circular permutation and receptor insertion within green fluorescent proteins. Proc Natl Acad Sci U S A **96**(20): 11241-11246.

Bajenoff, M., Egen, J. G., Koo, L. Y., Laugier, J. P., Brau, F., Glaichenhaus, N. and Germain, R. N. (2006). Stromal cell networks regulate lymphocyte entry, migration, and territoriality in lymph nodes. Immunity **25**(6): 989-1001.

Baksh, S. and Michalak, M. (1991). Expression of calreticulin in Escherichia coli and identification of its Ca2+ binding domains. J Biol Chem **266**(32): 21458-21465.

Barkus, C. (2013). Genetic mouse models of depression. Curr Top Behav Neurosci **14**: 55-78.

Bauer, C. A., Kim, E. Y., Marangoni, F., Carrizosa, E., Claudio, N. M. and Mempel, T. R. (2014). Dynamic Treg interactions with intratumoral APCs promote local CTL dysfunction. J Clin Invest **124**(6): 2425-2440.

Belan, P. V., Kostyuk, P. G., Snitsarev, V. A. and Tepikin, A. V. (1993). Calcium clamp in single nerve cells. Cell Calcium **14**(6): 419-425.

Berridge, M. J., Bootman, M. D. and Roderick, H. L. (2003). Calcium signalling: dynamics, homeostasis and remodelling. Nat Rev Mol Cell Biol **4**(7): 517-529.

Berridge, M. J., Lipp, P. and Bootman, M. D. (2000). The versatility and universality of calcium signalling. Nat Rev Mol Cell Biol **1**(1): 11-21.

Bhakta, N. R., Oh, D. Y. and Lewis, R. S. (2005). Calcium oscillations regulate thymocyte motility during positive selection in the three-dimensional thymic environment. Nat Immunol **6**(2): 143-151.

Bousso, P. and Robey, E. (2003). Dynamics of CD8+ T cell priming by dendritic cells in intact lymph nodes. Nat Immunol **4**(6): 579-585.

Brunkow, M. E., Jeffery, E. W., Hjerrild, K. A., Paeper, B., Clark, L. B., Yasayko, S. A., Wilkinson, J. E., Galas, D., Ziegler, S. F. and Ramsdell, F. (2001). Disruption of a new forkhead/winged-helix protein, scurfin, results in the fatal lymphoproliferative disorder of the scurfy mouse. Nat Genet **27**(1): 68-73.

Cahalan, M. D. and Chandy, K. G. (2009). The functional network of ion channels in T lymphocytes. Immunol Rev **231**(1): 59-87.

Cahalan, M. D. and Parker, I. (2005). Close encounters of the first and second kind: T-DC and T-B interactions in the lymph node. Semin Immunol **17**(6): 442-451.

Cahalan, M. D. and Parker, I. (2008). Choreography of cell motility and interaction dynamics imaged by two-photon microscopy in lymphoid organs. Annu Rev Immunol **26**: 585-626.

Cahalan, M. D., Parker, I., Wei, S. H. and Miller, M. J. (2002). Two-photon tissue imaging: seeing the immune system in a fresh light. Nat Rev Immunol **2**(11): 872-880.

Callahan, M. K., Wolchok, J. D. and Allison, J. P. (2010). Anti-CTLA-4 antibody therapy: immune monitoring during clinical development of a novel immunotherapy. Semin Oncol **37**(5): 473-484.

Calloway, N., Vig, M., Kinet, J. P., Holowka, D. and Baird, B. (2009). Molecular clustering of STIM1 with Orai1/CRACM1 at the plasma membrane depends dynamically on depletion of Ca2+ stores and on electrostatic interactions. Mol Biol Cell **20**(1): 389-399.

Campbell, D. J. and Koch, M. A. (2011). Phenotypical and functional specialization of FOXP3+ regulatory T cells. Nat Rev Immunol **11**(2): 119-130.

Chen, T. W., Wardill, T. J., Sun, Y., Pulver, S. R., Renninger, S. L., Baohan, A., Schreiter, E. R., Kerr, R. A., Orger, M. B., Jayaraman, V., Looger, L. L., Svoboda, K. and Kim, D. S. (2013). Ultrasensitive fluorescent proteins for imaging neuronal activity. Nature **499**(7458): 295-300.

Cheon, D. J. and Orsulic, S. (2011). Mouse models of cancer. Annu Rev Pathol **6**: 95-119.

Cho, W. and Stahelin, R. V. (2005). Membrane-protein interactions in cell signaling and membrane trafficking. Annu Rev Biophys Biomol Struct **34**: 119-151.

Chung, Y., Tanaka, S., Chu, F., Nurieva, R. I., Martinez, G. J., Rawal, S., Wang, Y. H., Lim, H., Reynolds, J. M., Zhou, X. H., Fan, H. M., Liu, Z. M., Neelapu, S. S. and Dong, C. (2011). Follicular regulatory T cells expressing Foxp3 and Bcl-6 suppress germinal center reactions. Nat Med **17**(8): 983-988.

Clapham, D. E. (2007). Calcium signaling. Cell **131**(6): 1047-1058.

Cobbold, P. H. and Rink, T. J. (1987). Fluorescence and bioluminescence measurement of cytoplasmic free calcium. Biochem J **248**(2): 313-328.

Comin-Anduix, B., Lee, Y., Jalil, J., Algazi, A., de la Rocha, P., Camacho, L. H., Bozon, V. A., Bulanhagui, C. A., Seja, E., Villanueva, A., Straatsma, B. R., Gualberto, A., Economou, J. S., Glaspy, J. A., Gomez-Navarro, J. and Ribas, A. (2008). Detailed analysis of immunologic effects of the cytotoxic T lymphocyte-associated antigen 4-blocking monoclonal antibody tremelimumab in peripheral blood of patients with melanoma. J Transl Med **6**: 22.

Davidson, B. L. and Breakefield, X. O. (2003). Viral vectors for gene delivery to the nervous system. Nat Rev Neurosci **4**(5): 353-364.

de Brito, O. M. and Scorrano, L. (2008). Mitofusin 2 tethers endoplasmic reticulum to mitochondria. Nature **456**(7222): 605-610.

De Stefani, D., Rizzuto, R. and Pozzan, T. (2016). Enjoy the Trip: Calcium in Mitochondria Back and Forth. Annu Rev Biochem **85**: 161-192.

Deluca, H. F. and Engstrom, G. W. (1961). Calcium uptake by rat kidney mitochondria. Proc Natl Acad Sci U S A **47**: 1744-1750.

Demaurex, N. (2005). Calcium measurements in organelles with Ca2+-sensitive fluorescent proteins. Cell Calcium **38**(3-4): 213-222.

Demuro, A. and Parker, I. (2006). Imaging single-channel calcium microdomains. Cell Calcium **40**(5-6): 413-422.

Dilek, N., Poirier, N., Hulin, P., Coulon, F., Mary, C., Ville, S., Vie, H., Clemenceau, B., Blancho, G. and Vanhove, B. (2013). Targeting CD28, CTLA-4 and PD-L1 costimulation differentially controls immune synapses and function of human regulatory and conventional T-cells. PLoS One **8**(12): e83139.

Direnberger, S., Mues, M., Micale, V., Wotjak, C. T., Dietzel, S., Schubert, M., Scharr, A., Hassan, S., Wahl-Schott, C., Biel, M., Krishnamoorthy, G. and Griesbeck, O. (2012). Biocompatibility of a genetically encoded calcium indicator in a transgenic mouse model. Nat Commun **3**: 1031.

Dixit, N., Yamayoshi, I., Nazarian, A. and Simon, S. I. (2011). Migrational guidance of neutrophils is mechanotransduced via high-affinity LFA-1 and calcium flux. J Immunol **187**(1): 472-481.

Dolmetsch, R. E. and Lewis, R. S. (1994). Signaling between intracellular Ca2+ stores and depletion-activated Ca2+ channels generates [Ca2+]i oscillations in T lymphocytes. J Gen Physiol **103**(3): 365-388.

Dolmetsch, R. E., Lewis, R. S., Goodnow, C. C. and Healy, J. I. (1997). Differential activation of transcription factors induced by Ca2+ response amplitude and duration. Nature **386**(6627): 855-858.

Donnadieu, E., Bismuth, G. and Trautmann, A. (1994). Antigen recognition by helper T cells elicits a sequence of distinct changes of their shape and intracellular calcium. Curr Biol **4**(7): 584-595.

Drobizhev, M., Makarov, N. S., Tillo, S. E., Hughes, T. E. and Rebane, A. (2011). Two-photon absorption properties of fluorescent proteins. Nat Methods **8**(5): 393-399.

Dustin, M. L., Bromley, S. K., Kan, Z., Peterson, D. A. and Unanue, E. R. (1997). Antigen receptor engagement delivers a stop signal to migrating T lymphocytes. Proc Natl Acad Sci U S A **94**(8): 3909-3913.

Dynes, J. L., Amcheslavsky, A. and Cahalan, M. D. (2016). Genetically targeted single-channel optical recording reveals multiple Orai1 gating states and oscillations in calcium influx. Proc Natl Acad Sci U S A **113**(2): 440-445.

Feske, S. (2007). Calcium signalling in lymphocyte activation and disease. Nat Rev Immunol **7**(9): 690-702.

Feske, S., Gwack, Y., Prakriya, M., Srikanth, S., Puppel, S. H., Tanasa, B., Hogan, P. G., Lewis, R. S., Daly, M. and Rao, A. (2006). A mutation in Orai1 causes immune deficiency by abrogating CRAC channel function. Nature **441**(7090): 179-185.

Fife, B. T., Pauken, K. E., Eagar, T. N., Obu, T., Wu, J., Tang, Q., Azuma, M., Krummel, M. F. and Bluestone, J. A. (2009). Interactions between PD-1 and PD-L1 promote tolerance by blocking the TCR-induced stop signal. Nat Immunol **10**(11): 1185-1192.

Gee, J. M., Smith, N. A., Fernandez, F. R., Economo, M. N., Brunert, D., Rothermel, M., Morris, S. C., Talbot, A., Palumbos, S., Ichida, J. M., Shepherd, J. D., West, P. J., Wachowiak, M., Capecchi, M. R., Wilcox, K. S., White, J. A. and Tvrdik, P. (2014). Imaging Activity in Neurons and Glia with a Polr2a-Based and Cre-Dependent GCaMP5G-IRES-tdTomato Reporter Mouse. Neuron **83**(5): 1058-1072.

Gee, K. R., Brown, K. A., Chen, W. N., Bishop-Stewart, J., Gray, D. and Johnson, I. (2000). Chemical and physiological characterization of fluo-4 Ca(2+)-indicator dyes. Cell Calcium **27**(2): 97-106.

Gerard, A., Khan, O., Beemiller, P., Oswald, E., Hu, J., Matloubian, M. and Krummel, M. F. (2013). Secondary T cell-T cell synaptic interactions drive the differentiation of protective CD8+ T cells. Nat Immunol **14**(4): 356-363.

Gerard, A., Patino-Lopez, G., Beemiller, P., Nambiar, R., Ben-Aissa, K., Liu, Y., Totah, F. J., Tyska, M. J., Shaw, S. and Krummel, M. F. (2014). Detection of rare antigen-presenting cells through T cell-intrinsic meandering motility, mediated by Myo1g. Cell **158**(3): 492-505.

Germain, R. N., Robey, E. A. and Cahalan, M. D. (2012). A decade of imaging cellular motility and interaction dynamics in the immune system. Science **336**(6089): 1676-1681.

Gossen, M. and Bujard, H. (1992). Tight control of gene expression in mammalian cells by tetracycline-responsive promoters. Proc Natl Acad Sci U S A **89**(12): 5547-5551.

Gough, S. C., Walker, L. S. and Sansom, D. M. (2005). CTLA4 gene polymorphism and autoimmunity. Immunol Rev **204**: 102-115.

Greenberg, M. L., Yu, Y., Leverrier, S., Zhang, S. L., Parker, I. and Cahalan, M. D. (2013). Orai1 function is essential for T cell homing to lymph nodes. J Immunol **190**(7): 3197-3206.

Greenfield, E. A., Howard, E., Paradis, T., Nguyen, K., Benazzo, F., McLean, P., Hollsberg, P., Davis, G., Hafler, D. A., Sharpe, A. H., Freeman, G. J. and Kuchroo, V. K. (1997). B7.2 expressed by T cells does not induce CD28-mediated costimulatory activity but retains CTLA4 binding: implications for induction of antitumor immunity to T cell tumors. J Immunol **158**(5): 2025-2034.

Grynkiewicz, G., Poenie, M. and Tsien, R. Y. (1985). A new generation of Ca2+ indicators with greatly improved fluorescence properties. J Biol Chem **260**(6): 3440-3450.

Haribhai, D., Lin, W., Relland, L. M., Truong, N., Williams, C. B. and Chatila, T. A. (2007). Regulatory T cells dynamically control the primary immune response to foreign antigen. J Immunol **178**(5): 2961-2972.

Hasan, M. T., Friedrich, R. W., Euler, T., Larkum, M. E., Giese, G., Both, M., Duebel, J., Waters, J., Bujard, H., Griesbeck, O., Tsien, R. Y., Nagai, T., Miyawaki, A. and Denk, W. (2004). Functional fluorescent Ca2+ indicator proteins in transgenic mice under TET control. PLoS Biol **2**(6): e163.

Hawkins, R. J., Piel, M., Faure-Andre, G., Lennon-Dumenil, A. M., Joanny, J. F., Prost, J. and Voituriez, R. (2009). Pushing off the walls: a mechanism of cell motility in confinement. Phys Rev Lett **102**(5): 058103.

Heim, N., Garaschuk, O., Friedrich, M. W., Mank, M., Milos, R. I., Kovalchuk, Y., Konnerth, A. and Griesbeck, O. (2007). Improved calcium imaging in transgenic mice expressing a troponin C-based biosensor. Nat Methods **4**(2): 127-129.

Heim, N. and Griesbeck, O. (2004). Genetically encoded indicators of cellular calcium dynamics based on troponin C and green fluorescent protein. J Biol Chem **279**(14): 14280-14286.

Hennig, G. W., Gould, T. W., Koh, S. D., Corrigan, R. D., Heredia, D. J., Shonnard, M. C. and Smith, T. K. (2015). Use of Genetically Encoded Calcium Indicators (GECIs) Combined with Advanced Motion Tracking Techniques to Examine the Behavior of Neurons and Glia in the Enteric Nervous System of the Intact Murine Colon. Front Cell Neurosci **9**: 436.

Hodi, F. S., Butler, M., Oble, D. A., Seiden, M. V., Haluska, F. G., Kruse, A., Macrae, S., Nelson, M., Canning, C., Lowy, I., Korman, A., Lautz, D., Russell, S., Jaklitsch, M. T., Ramaiya, N., Chen, T. C., Neuberg, D., Allison, J. P., Mihm, M. C. and Dranoff, G. (2008). Immunologic and clinical effects of antibody blockade of cytotoxic T lymphocyte-associated antigen 4 in previously vaccinated cancer patients. Proc Natl Acad Sci U S A **105**(8): 3005-3010.

Hogan, P. G., Chen, L., Nardone, J. and Rao, A. (2003). Transcriptional regulation by calcium, calcineurin, and NFAT. Genes Dev **17**(18): 2205-2232.

Hoos, A., Ibrahim, R., Korman, A., Abdallah, K., Berman, D., Shahabi, V., Chin, K., Canetta, R. and Humphrey, R. (2010). Development of ipilimumab: contribution to a new paradigm for cancer immunotherapy. Semin Oncol **37**(5): 533-546.

Hoth, M., Fanger, C. M. and Lewis, R. S. (1997). Mitochondrial regulation of store-operated calcium signaling in T lymphocytes. J Cell Biol **137**(3): 633-648.

Hou, X., Pedi, L., Diver, M. M. and Long, S. B. (2012). Crystal structure of the calcium release-activated calcium channel Orai. Science **338**(6112): 1308-1313.

Hsieh, C. S., Zheng, Y., Liang, Y., Fontenot, J. D. and Rudensky, A. Y. (2006). An intersection between the self-reactive regulatory and nonregulatory T cell receptor repertoires. Nat Immunol **7**(4): 401-410.

Huter, E. N., Punkosdy, G. A., Glass, D. D., Cheng, L. I., Ward, J. M. and Shevach, E. M. (2008). TGF-beta-induced Foxp3+ regulatory T cells rescue scurfy mice. Eur J Immunol **38**(7): 1814-1821.

Idoyaga, J., Fiorese, C., Zbytnuik, L., Lubkin, A., Miller, J., Malissen, B., Mucida, D., Merad, M. and Steinman, R. M. (2013). Specialized role of migratory dendritic cells in peripheral tolerance induction. J Clin Invest **123**(2): 844-854.

Jacobelli, J., Bennett, F. C., Pandurangi, P., Tooley, A. J. and Krummel, M. F. (2009). Myosin-IIA and ICAM-1 regulate the interchange between two distinct modes of T cell migration. J Immunol **182**(4): 2041-2050.

Jacobelli, J., Friedman, R. S., Conti, M. A., Lennon-Dumenil, A. M., Piel, M., Sorensen, C. M., Adelstein, R. S. and Krummel, M. F. (2010). Confinement-optimized three-dimensional T cell amoeboid motility is modulated via myosin IIA-regulated adhesions. Nat Immunol **11**(10): 953-961.

Ji, G., Feldman, M. E., Deng, K. Y., Greene, K. S., Wilson, J., Lee, J. C., Johnston, R. C., Rishniw, M., Tallini, Y., Zhang, J., Wier, W. G., Blaustein, M. P., Xin, H. B., Nakai, J. and Kotlikoff, M. I. (2004). Ca2+-sensing transgenic mice: postsynaptic signaling in smooth muscle. J Biol Chem **279**(20): 21461-21468.

Kar, P., Samanta, K., Kramer, H., Morris, O., Bakowski, D. and Parekh, A. B. (2014). Dynamic assembly of a membrane signaling complex enables selective activation of NFAT by Orai1. Curr Biol **24**(12): 1361-1368.

Khan, O., Headley, M., Gerard, A., Wei, W., Liu, L. and Krummel, M. F. (2011). Regulation of T cell priming by lymphoid stroma. PLoS One **6**(11): e26138.

Kirichok, Y., Krapivinsky, G. and Clapham, D. E. (2004). The mitochondrial calcium uniporter is a highly selective ion channel. Nature **427**(6972): 360-364.

Korkotian, E., Oni-Biton, E. and Segal, M. (2017). The role of the store-operated calcium entry channel Orai1 in cultured rat hippocampal synapse formation and plasticity. J Physiol **595**(1): 125-140.

Kretsinger, R. H. and Nockolds, C. E. (1973). Carp muscle calcium-binding protein. II. Structure determination and general description. J Biol Chem **248**(9): 3313-3326.

Krummel, M. F., Bartumeus, F. and Gerard, A. (2016). T cell migration, search strategies and mechanisms. Nat Rev Immunol **16**(3): 193-201.

Krummel, M. F., Friedman, R. S. and Jacobelli, J. (2014). Modes and mechanisms of T cell motility: roles for confinement and Myosin-IIA. Curr Opin Cell Biol **30C**: 9-16.

Kuras, Z., Yun, Y. H., Chimote, A. A., Neumeier, L. and Conforti, L. (2012). KCa3.1 and TRPM7 channels at the uropod regulate migration of activated human T cells. PLoS One **7**(8): e43859.

Lai, T. W., Zhang, S. and Wang, Y. T. (2014). Excitotoxicity and stroke: identifying novel targets for neuroprotection. Prog Neurobiol **115**: 157-188.

Lammermann, T., Bader, B. L., Monkley, S. J., Worbs, T., Wedlich-Soldner, R., Hirsch, K., Keller, M., Forster, R., Critchley, D. R., Fassler, R. and Sixt, M. (2008). Rapid leukocyte migration by integrin-independent flowing and squeezing. Nature **453**(7191): 51-55.

Lewis, R. S. (2001). Calcium signaling mechanisms in T lymphocytes. Annu Rev Immunol **19**: 497-521.

Lewit-Bentley, A. and Rety, S. (2000). EF-hand calcium-binding proteins. Curr Opin Struct Biol **10**(6): 637-643.

Lindquist, R. L., Shakhar, G., Dudziak, D., Wardemann, H., Eisenreich, T., Dustin, M. L. and Nussenzweig, M. C. (2004). Visualizing dendritic cell networks in vivo. Nat Immunol **5**(12): 1243-1250.

Linterman, M. A., Pierson, W., Lee, S. K., Kallies, A., Kawamoto, S., Rayner, T. F., Srivastava, M., Divekar, D. P., Beaton, L., Hogan, J. J., Fagarasan, S., Liston, A., Smith, K. G. and Vinuesa, C. G. (2011). Foxp3+ follicular regulatory T cells control the germinal center response. Nat Med **17**(8): 975-982.

Liou, J., Kim, M. L., Heo, W. D., Jones, J. T., Myers, J. W., Ferrell, J. E., Jr. and Meyer, T. (2005). STIM is a Ca2+ sensor essential for Ca2+-store-depletion-triggered Ca2+ influx. Curr Biol **15**(13): 1235-1241.

Lioudyno, M. I., Kozak, J. A., Penna, A., Safrina, O., Zhang, S. L., Sen, D., Roos, J., Stauderman, K. A. and Cahalan, M. D. (2008). Orai1 and STIM1 move to the immunological synapse and are up-regulated during T cell activation. Proc Natl Acad Sci U S A **105**(6): 2011-2016.

Llinas, R., Blinks, J. R. and Nicholson, C. (1972). Calcium transient in presynaptic terminal of squid giant synapse: detection with aequorin. Science **176**(4039): 1127-1129.

Llinas, R. and Nicholson, C. (1975). Calcium role in depolarization-secretion coupling: an aequorin study in squid giant synapse. Proc Natl Acad Sci U S A **72**(1): 187-190.

Lobbestael, E., Reumers, V., Ibrahimi, A., Paesen, K., Thiry, I., Gijsbers, R., Van den Haute, C., Debyser, Z., Baekelandt, V. and Taymans, J. M. (2010). Immunohistochemical detection of transgene expression in the brain using small epitope tags. BMC Biotechnol **10**: 16.

Loro, G., Ruberti, C., Zottini, M. and Costa, A. (2013). The D3cpv Cameleon reports Ca(2)(+) dynamics in plant mitochondria with similar kinetics of the YC3.6 Cameleon, but with a lower sensitivity. J Microsc **249**(1): 8-12.

Lu, Y., Schneider, H. and Rudd, C. E. (2012). Murine regulatory T cells differ from conventional T cells in resisting the CTLA-4 reversal of TCR stop-signal. Blood **120**(23): 4560-4570.

Luik, R. M., Wu, M. M., Buchanan, J. and Lewis, R. S. (2006). The elementary unit of store-operated Ca2+ entry: local activation of CRAC channels by STIM1 at ER-plasma membrane junctions. J Cell Biol **174**(6): 815-825.

Madisen, L., Garner, A. R., Shimaoka, D., Chuong, A. S., Klapoetke, N. C., Li, L., van der Bourg, A., Niino, Y., Egolf, L., Monetti, C., Gu, H., Mills, M., Cheng, A., Tasic, B., Nguyen, T. N., Sunkin, S. M., Benucci, A., Nagy, A., Miyawaki, A., Helmchen, F., Empson, R. M., Knopfel, T., Boyden, E. S., Reid, R. C., Carandini, M. and Zeng, H. (2015). Transgenic mice for intersectional targeting of neural sensors and effectors with high specificity and performance. Neuron **85**(5): 942-958.

Madisen, L., Zwingman, T. A., Sunkin, S. M., Oh, S. W., Zariwala, H. A., Gu, H., Ng, L. L., Palmiter, R. D., Hawrylycz, M. J., Jones, A. R., Lein, E. S. and Zeng, H. (2010). A robust and high-throughput Cre reporting and characterization system for the whole mouse brain. Nat Neurosci **13**(1): 133-140.

Malli, R., Frieden, M., Osibow, K. and Graier, W. F. (2003). Mitochondria efficiently buffer subplasmalemmal Ca2+ elevation during agonist stimulation. J Biol Chem **278**(12): 10807-10815.

Mank, M., Reiff, D. F., Heim, N., Friedrich, M. W., Borst, A. and Griesbeck, O. (2006). A FRET-based calcium biosensor with fast signal kinetics and high fluorescence change. Biophys J **90**(5): 1790-1796.

Mank, M., Santos, A. F., Direnberger, S., Mrsic-Flogel, T. D., Hofer, S. B., Stein, V., Hendel, T., Reiff, D. F., Levelt, C., Borst, A., Bonhoeffer, T., Hubener, M. and Griesbeck, O. (2008). A genetically encoded calcium indicator for chronic in vivo two-photon imaging. Nat Methods **5**(9): 805-811.

Marchant, J. S., Stutzmann, G. E., Leissring, M. A., LaFerla, F. M. and Parker, I. (2001). Multiphoton-evoked color change of DsRed as an optical highlighter for cellular and subcellular labeling. Nat Biotechnol **19**(7): 645-649.

Matheu, M. P., Othy, S., Greenberg, M. L., Dong, T. X., Schuijs, M., Deswarte, K., Hammad, H., Lambrecht, B. N., Parker, I. and Cahalan, M. D. (2015). Imaging regulatory T cell dynamics and CTLA4-mediated suppression of T cell priming. Nat Commun **6**: 6219.

Matheu, M. P., Sen, D., Cahalan, M. D. and Parker, I. (2008). Generation of bone marrow derived murine dendritic cells for use in 2-photon imaging. J Vis Exp(17).

Matheu, M. P., Su, Y., Greenberg, M. L., Blanc, C. A., Parker, I., Scott, D. W. and Cahalan, M. D. (2012). Toll-like receptor 4-activated B cells out-compete Toll-like receptor 9-activated B cells to establish peripheral immunological tolerance. Proc Natl Acad Sci U S A **109**(20): E1258-1266.

Matheu, M. P., Su, Y., Greenberg, M. L., Blanc, C. A., Parker, I., Scott, D. W. and Cahalan, M. D. (2012). Toll-like receptor 4-activated B cells out-compete Toll-like receptor 9-activated B cells to establish peripheral immunological tolerance. Proceedings of the National Academy of Sciences of the United States of America **109**(20): E1258-1266.

Maus, M., Cuk, M., Patel, B., Lian, J., Ouimet, M., Kaufmann, U., Yang, J., Horvath, R., Hornig-Do, H. T., Chrzanowska-Lightowlers, Z. M., Moore, K. J., Cuervo, A. M. and Feske, S. (2017). Store-Operated Ca2+ Entry Controls Induction of Lipolysis and the Transcriptional Reprogramming to Lipid Metabolism. Cell Metab.

McCombs, J. E. and Palmer, A. E. (2008). Measuring calcium dynamics in living cells with genetically encodable calcium indicators. Methods **46**(3): 152-159.

Mempel, T. R., Henrickson, S. E. and Von Andrian, U. H. (2004). T-cell priming by dendritic cells in lymph nodes occurs in three distinct phases. Nature **427**(6970): 154-159.

Mempel, T. R., Pittet, M. J., Khazaie, K., Weninger, W., Weissleder, R., von Boehmer, H. and von Andrian, U. H. (2006). Regulatory T cells reversibly suppress cytotoxic T cell function independent of effector differentiation. Immunity **25**(1): 129-141.

Miller, M. J., Hejazi, A. S., Wei, S. H., Cahalan, M. D. and Parker, I. (2004). T cell repertoire scanning is promoted by dynamic dendritic cell behavior and random T cell motility in the lymph node. Proc Natl Acad Sci U S A **101**(4): 998-1003.

Miller, M. J., Safrina, O., Parker, I. and Cahalan, M. D. (2004). Imaging the single cell dynamics of CD4+ T cell activation by dendritic cells in lymph nodes. J Exp Med **200**(7): 847-856.

Miller, M. J., Wei, S. H., Parker, I. and Cahalan, M. D. (2002). Two-photon imaging of lymphocyte motility and antigen response in intact lymph node. Science **296**(5574): 1869-1873.

Minta, A., Kao, J. P. and Tsien, R. Y. (1989). Fluorescent indicators for cytosolic calcium based on rhodamine and fluorescein chromophores. J Biol Chem **264**(14): 8171-8178.

Miyawaki, A., Llopis, J., Heim, R., McCaffery, J. M., Adams, J. A., Ikura, M. and Tsien, R. Y. (1997). Fluorescent indicators for Ca2+ based on green fluorescent proteins and calmodulin. Nature **388**(6645): 882-887.

Miyazaki, S., Shirakawa, H., Nakada, K. and Honda, Y. (1993). Essential role of the inositol 1,4,5-trisphosphate receptor/Ca2+ release channel in Ca2+ waves and Ca2+ oscillations at fertilization of mammalian eggs. Dev Biol **158**(1): 62-78.

Mohamed, T. M., Abou-Leisa, R., Baudoin, F., Stafford, N., Neyses, L., Cartwright, E. J. and Oceandy, D. (2013). Development and characterization of a novel fluorescent indicator protein PMCA4-GCaMP2 in cardiomyocytes. J Mol Cell Cardiol **63**: 57-68.

Monahan, P. E. and Samulski, R. J. (2000). Adeno-associated virus vectors for gene therapy: more pros than cons? Mol Med Today **6**(11): 433-440.

Montero, M., Alonso, M. T., Carnicero, E., Cuchillo-Ibanez, I., Albillos, A., Garcia, A. G., Garcia-Sancho, J. and Alvarez, J. (2000). Chromaffin-cell stimulation triggers fast millimolar mitochondrial Ca2+ transients that modulate secretion. Nat Cell Biol **2**(2): 57-61.

Moreau, H. D., Lemaitre, F., Garrod, K. R., Garcia, Z., Lennon-Dumenil, A. M. and Bousso, P. (2015). Signal strength regulates antigen-mediated T-cell deceleration by distinct mechanisms to promote local exploration or arrest. Proc Natl Acad Sci U S A **112**(39): 12151-12156.

Mosier, D. E., Gulizia, R. J., Baird, S. M. and Wilson, D. B. (1988). Transfer of a functional human immune system to mice with severe combined immunodeficiency. Nature **335**(6187): 256-259.

Mrass, P., Petravic, J., Davenport, M. P. and Weninger, W. (2010). Cell-autonomous and environmental contributions to the interstitial migration of T cells. Semin Immunopathol **32**(3): 257-274.

Mues, M., Bartholomaus, I., Thestrup, T., Griesbeck, O., Wekerle, H., Kawakami, N. and Krishnamoorthy, G. (2013). Real-time in vivo analysis of T cell activation in the central nervous system using a genetically encoded calcium indicator. Nat Med **19**(6): 778-783.

Nagai, T., Yamada, S., Tominaga, T., Ichikawa, M. and Miyawaki, A. (2004). Expanded dynamic range of fluorescent indicators for Ca(2+) by circularly permuted yellow fluorescent proteins. Proc Natl Acad Sci U S A **101**(29): 10554-10559.

Nakai, J., Ohkura, M. and Imoto, K. (2001). A high signal-to-noise Ca(2+) probe composed of a single green fluorescent protein. Nat Biotechnol **19**(2): 137-141.

Nakamura, K., Zuppini, A., Arnaudeau, S., Lynch, J., Ahsan, I., Krause, R., Papp, S., De Smedt, H., Parys, J. B., Muller-Esterl, W., Lew, D. P., Krause, K. H., Demaurex, N., Opas, M. and Michalak, M. (2001). Functional specialization of calreticulin domains. J Cell Biol **154**(5): 961-972.

Nakayama, S. and Kretsinger, R. H. (1994). Evolution of the EF-hand family of proteins. Annu Rev Biophys Biomol Struct **23**: 473-507.

Nathanson, J. L., Yanagawa, Y., Obata, K. and Callaway, E. M. (2009). Preferential labeling of inhibitory and excitatory cortical neurons by endogenous tropism of adeno-associated virus and lentivirus vectors. Neuroscience **161**(2): 441-450.

Negulescu, P. A., Krasieva, T. B., Khan, A., Kerschbaum, H. H. and Cahalan, M. D. (1996). Polarity of T cell shape, motility, and sensitivity to antigen. Immunity **4**(5): 421-430.

Negulescu, P. A., Shastri, N. and Cahalan, M. D. (1994). Intracellular calcium dependence of gene expression in single T lymphocytes. Proc Natl Acad Sci U S A **91**(7): 2873-2877.

Neher, E. and Augustine, G. J. (1992). Calcium gradients and buffers in bovine chromaffin cells. J Physiol **450**: 273-301.

Nguyen, Q. T., Callamaras, N., Hsieh, C. and Parker, I. (2001). Construction of a two-photon microscope for video-rate Ca(2+) imaging. Cell Calcium **30**(6): 383-393.

Nguyen, Q. T. and Tsien, R. Y. (2013). Fluorescence-guided surgery with live molecular navigation--a new cutting edge. Nat Rev Cancer **13**(9): 653-662.

Oderup, C., Cederbom, L., Makowska, A., Cilio, C. M. and Ivars, F. (2006). Cytotoxic T lymphocyte antigen-4-dependent down-modulation of costimulatory molecules on dendritic cells in CD4+ CD25+ regulatory T-cell-mediated suppression. Immunology **118**(2): 240-249.

Oh-hora, M. and Rao, A. (2008). Calcium signaling in lymphocytes. Curr Opin Immunol **20**(3): 250-258.

Onishi, Y., Fehervari, Z., Yamaguchi, T. and Sakaguchi, S. (2008). Foxp3+ natural regulatory T cells preferentially form aggregates on dendritic cells in vitro and actively inhibit their maturation. Proc Natl Acad Sci U S A **105**(29): 10113-10118.

Pace, L., Tempez, A., Arnold-Schrauf, C., Lemaitre, F., Bousso, P., Fetler, L., Sparwasser, T. and Amigorena, S. (2012). Regulatory T cells increase the avidity of primary CD8+ T cell responses and promote memory. Science **338**(6106): 532-536.

Pacholczyk, R., Ignatowicz, H., Kraj, P. and Ignatowicz, L. (2006). Origin and T cell receptor diversity of Foxp3+CD4+CD25+ T cells. Immunity **25**(2): 249-259.

Palmer, A. E., Giacomello, M., Kortemme, T., Hires, S. A., Lev-Ram, V., Baker, D. and Tsien, R. Y. (2006). Ca2+ indicators based on computationally redesigned calmodulin-peptide pairs. Chem Biol **13**(5): 521-530.

Paredes, R. M., Etzler, J. C., Watts, L. T., Zheng, W. and Lechleiter, J. D. (2008). Chemical calcium indicators. Methods **46**(3): 143-151.

Parker, I., Choi, J. and Yao, Y. (1996). Elementary events of InsP3-induced Ca2+ liberation in Xenopus oocytes: hot spots, puffs and blips. Cell Calcium **20**(2): 105-121.

Paust, S. and Cantor, H. (2005). Regulatory T cells and autoimmune disease. Immunol Rev **204**: 195-207.

Perez Koldenkova, V. and Nagai, T. (2013). Genetically encoded Ca(2+) indicators: properties and evaluation. Biochim Biophys Acta **1833**(7): 1787-1797.

Perlman, R. L. (2016). Mouse models of human disease: An evolutionary perspective. Evol Med Public Health **2016**(1): 170-176.

Petrie, R. J., Doyle, A. D. and Yamada, K. M. (2009). Random versus directionally persistent cell migration. Nat Rev Mol Cell Biol **10**(8): 538-549.

Piccirillo, C. A. and Shevach, E. M. (2001). Cutting edge: control of CD8+ T cell activation by CD4+CD25+ immunoregulatory cells. J Immunol **167**(3): 1137-1140.

Porumb, T., Yau, P., Harvey, T. S. and Ikura, M. (1994). A calmodulin-target peptide hybrid molecule with unique calcium-binding properties. Protein Eng **7**(1): 109-115.

Prabhu Das, M. R., Zamvil, S. S., Borriello, F., Weiner, H. L., Sharpe, A. H. and Kuchroo, V. K. (1995). Reciprocal expression of co-stimulatory molecules, B7-1 and B7-2, on murine T cells following activation. Eur J Immunol **25**(1): 207-211.

Prakriya, M., Feske, S., Gwack, Y., Srikanth, S., Rao, A. and Hogan, P. G. (2006). Orai1 is an essential pore subunit of the CRAC channel. Nature **443**(7108): 230-233.

Quintana, A., Pasche, M., Junker, C., Al-Ansary, D., Rieger, H., Kummerow, C., Nunez, L., Villalobos, C., Meraner, P., Becherer, U., Rettig, J., Niemeyer, B. A. and Hoth, M. (2011). Calcium microdomains at the immunological synapse: how ORAI channels, mitochondria and calcium pumps generate local calcium signals for efficient T-cell activation. EMBO J **30**(19): 3895-3912.

Qureshi, O. S., Zheng, Y., Nakamura, K., Attridge, K., Manzotti, C., Schmidt, E. M., Baker, J., Jeffery, L. E., Kaur, S., Briggs, Z., Hou, T. Z., Futter, C. E., Anderson, G., Walker, L. S. and Sansom, D. M. (2011). Trans-endocytosis of CD80 and CD86: a molecular basis for the cell-extrinsic function of CTLA-4. Science **332**(6029): 600-603.

Rao, A. and Hogan, P. G. (2009). Calcium signaling in cells of the immune and hematopoietic systems. Immunol Rev **231**(1): 5-9.

Read, S., Greenwald, R., Izcue, A., Robinson, N., Mandelbrot, D., Francisco, L., Sharpe, A. H. and Powrie, F. (2006). Blockade of CTLA-4 on CD4+CD25+ regulatory T cells abrogates their function in vivo. J Immunol **177**(7): 4376-4383.

Reynolds, I. J. and Hastings, T. G. (1995). Glutamate induces the production of reactive oxygen species in cultured forebrain neurons following NMDA receptor activation. J Neurosci **15**(5 Pt 1): 3318-3327.

Ribas, A., Comin-Anduix, B., Economou, J. S., Donahue, T. R., de la Rocha, P., Morris, L. F., Jalil, J., Dissette, V. B., Shintaku, I. P., Glaspy, J. A., Gomez-Navarro, J. and Cochran, A. J. (2009). Intratumoral immune cell infiltrates, FoxP3, and indoleamine 2,3-dioxygenase in patients with melanoma undergoing CTLA4 blockade. Clin Cancer Res **15**(1): 390-399.

Ridgway, E. B. and Ashley, C. C. (1967). Calcium transients in single muscle fibers. Biochem Biophys Res Commun **29**(2): 229-234.

Rizzuto, R., De Stefani, D., Raffaello, A. and Mammucari, C. (2012). Mitochondria as sensors and regulators of calcium signalling. Nat Rev Mol Cell Biol **13**(9): 566-578.

Rizzuto, R., Pinton, P., Carrington, W., Fay, F. S., Fogarty, K. E., Lifshitz, L. M., Tuft, R. A. and Pozzan, T. (1998). Close contacts with the endoplasmic reticulum as determinants of mitochondrial Ca2+ responses. Science **280**(5370): 1763-1766.

Romoser, V. A., Hinkle, P. M. and Persechini, A. (1997). Detection in living cells of Ca2+-dependent changes in the fluorescence emission of an indicator composed of two green fluorescent protein variants linked by a calmodulin-binding sequence. A new class of fluorescent indicators. J Biol Chem **272**(20): 13270-13274.

Roos, J., DiGregorio, P. J., Yeromin, A. V., Ohlsen, K., Lioudyno, M., Zhang, S., Safrina, O., Kozak, J. A., Wagner, S. L., Cahalan, M. D., Velicelebi, G. and Stauderman, K. A. (2005). STIM1, an essential and conserved component of store-operated Ca2+ channel function. J Cell Biol **169**(3): 435-445.

Rosenthal, N. and Brown, S. (2007). The mouse ascending: perspectives for human-disease models. Nat Cell Biol **9**(9): 993-999.

Rubtsov, Y. P., Rasmussen, J. P., Chi, E. Y., Fontenot, J., Castelli, L., Ye, X., Treuting, P., Siewe, L., Roers, A., Henderson, W. R., Jr., Muller, W. and Rudensky, A. Y. (2008). Regulatory T cell-derived interleukin-10 limits inflammation at environmental interfaces. Immunity **28**(4): 546-558.

Sakaguchi, S., Wing, K., Onishi, Y., Prieto-Martin, P. and Yamaguchi, T. (2009). Regulatory T cells: how do they suppress immune responses? Int Immunol **21**(10): 1105-1111.

Sakaguchi, S., Yamaguchi, T., Nomura, T. and Ono, M. (2008). Regulatory T cells and immune tolerance. Cell **133**(5): 775-787.

Schaff, U. Y., Dixit, N., Procyk, E., Yamayoshi, I., Tse, T. and Simon, S. I. (2010). Orai1 regulates intracellular calcium, arrest, and shape polarization during neutrophil recruitment in shear flow. Blood **115**(3): 657-666.

Scheinecker, C., McHugh, R., Shevach, E. M. and Germain, R. N. (2002). Constitutive presentation of a natural tissue autoantigen exclusively by dendritic cells in the draining lymph node. J Exp Med **196**(8): 1079-1090.

Schmidt, A., Oberle, N. and Krammer, P. H. (2012). Molecular mechanisms of treg-mediated T cell suppression. Front Immunol **3**: 51.

Schmidt, A., Oberle, N., Weiss, E. M., Vobis, D., Frischbutter, S., Baumgrass, R., Falk, C. S., Haag, M., Brugger, B., Lin, H., Mayr, G. W., Reichardt, P., Gunzer, M., Suri-Payer, E. and Krammer, P. H. (2011). Human regulatory T cells rapidly suppress T cell receptor-induced Ca(2+), NF-kappaB, and NFAT signaling in conventional T cells. Sci Signal **4**(204): ra90.

Schneider, H., Downey, J., Smith, A., Zinselmeyer, B. H., Rush, C., Brewer, J. M., Wei, B., Hogg, N., Garside, P. and Rudd, C. E. (2006). Reversal of the TCR stop signal by CTLA-4. Science **313**(5795): 1972-1975.

Schwarz, A., Schumacher, M., Pfaff, D., Schumacher, K., Jarius, S., Balint, B., Wiendl, H., Haas, J. and Wildemann, B. (2013). Fine-tuning of regulatory T cell function: the role of calcium signals and naive regulatory T cells for regulatory T cell deficiency in multiple sclerosis. J Immunol **190**(10): 4965-4970.

Sen, D., Deerinck, T. J., Ellisman, M. H., Parker, I. and Cahalan, M. D. (2008). Quantum dots for tracking dendritic cells and priming an immune response in vitro and in vivo. PLoS One **3**(9): e3290.

Shaner, N. C., Lin, M. Z., McKeown, M. R., Steinbach, P. A., Hazelwood, K. L., Davidson, M. W. and Tsien, R. Y. (2008). Improving the photostability of bright monomeric orange and red fluorescent proteins. Nat Methods **5**(6): 545-551.

Shevtsova, Z., Malik, J. M., Michel, U., Bahr, M. and Kugler, S. (2005). Promoters and serotypes: targeting of adeno-associated virus vectors for gene transfer in the rat central nervous system in vitro and in vivo. Exp Physiol **90**(1): 53-59.

Shimomura, O., Johnson, F. H. and Saiga, Y. (1962). Extraction, purification and properties of aequorin, a bioluminescent protein from the luminous hydromedusan, Aequorea. J Cell Comp Physiol **59**: 223-239.

Shultz, L. D., Schweitzer, P. A., Christianson, S. W., Gott, B., Schweitzer, I. B., Tennent, B., McKenna, S., Mobraaten, L., Rajan, T. V., Greiner, D. L. and et al. (1995). Multiple defects in innate and adaptive immunologic function in NOD/LtSz-scid mice. J Immunol **154**(1): 180-191.

Soriano, P. (1999). Generalized lacZ expression with the ROSA26 Cre reporter strain. Nat Genet **21**(1): 70-71.

Stout, A. K., Raphael, H. M., Kanterewicz, B. I., Klann, E. and Reynolds, I. J. (1998). Glutamate-induced neuron death requires mitochondrial calcium uptake. Nat Neurosci **1**(5): 366-373.

Strack, R. L., Strongin, D. E., Bhattacharyya, D., Tao, W., Berman, A., Broxmeyer, H. E., Keenan, R. J. and Glick, B. S. (2008). A noncytotoxic DsRed variant for whole-cell labeling. Nat Methods **5**(11): 955-957.

Svensson, L., McDowall, A., Giles, K. M., Stanley, P., Feske, S. and Hogg, N. (2010). Calpain 2 controls turnover of LFA-1 adhesions on migrating T lymphocytes. PLoS One **5**(11): e15090.

Svoboda, K., Denk, W., Kleinfeld, D. and Tank, D. W. (1997). In vivo dendritic calcium dynamics in neocortical pyramidal neurons. Nature **385**(6612): 161-165.

Szabadkai, G., Bianchi, K., Varnai, P., De Stefani, D., Wieckowski, M. R., Cavagna, D., Nagy, A. I., Balla, T. and Rizzuto, R. (2006). Chaperone-mediated coupling of endoplasmic reticulum and mitochondrial Ca2+ channels. J Cell Biol **175**(6): 901-911.

Tadokoro, C. E., Shakhar, G., Shen, S., Ding, Y., Lino, A. C., Maraver, A., Lafaille, J. J. and Dustin, M. L. (2006). Regulatory T cells inhibit stable contacts between CD4+ T cells and dendritic cells in vivo. J Exp Med **203**(3): 505-511.

Takahashi, T., Tagami, T., Yamazaki, S., Uede, T., Shimizu, J., Sakaguchi, N., Mak, T. W. and Sakaguchi, S. (2000). Immunologic self-tolerance maintained by CD25(+)CD4(+) regulatory T cells constitutively expressing cytotoxic T lymphocyte-associated antigen 4. J Exp Med **192**(2): 303-310.

Takao, K. and Miyakawa, T. (2015). Genomic responses in mouse models greatly mimic human inflammatory diseases. Proc Natl Acad Sci U S A **112**(4): 1167-1172.

Tallini, Y. N., Ohkura, M., Choi, B. R., Ji, G., Imoto, K., Doran, R., Lee, J., Plan, P., Wilson, J., Xin, H. B., Sanbe, A., Gulick, J., Mathai, J., Robbins, J., Salama, G., Nakai, J. and Kotlikoff, M. I. (2006). Imaging cellular signals in the heart in vivo: Cardiac expression of the high-signal Ca2+ indicator GCaMP2. Proc Natl Acad Sci U S A **103**(12): 4753-4758.

Tang, Q., Adams, J. Y., Tooley, A. J., Bi, M., Fife, B. T., Serra, P., Santamaria, P., Locksley, R. M., Krummel, M. F. and Bluestone, J. A. (2006). Visualizing regulatory T cell control of autoimmune responses in nonobese diabetic mice. Nat Immunol **7**(1): 83-92.

Tang, Q., Boden, E. K., Henriksen, K. J., Bour-Jordan, H., Bi, M. and Bluestone, J. A. (2004). Distinct roles of CTLA-4 and TGF-beta in CD4+CD25+ regulatory T cell function. Eur J Immunol **34**(11): 2996-3005.

Tang, S., Wong, H. C., Wang, Z. M., Huang, Y., Zou, J., Zhuo, Y., Pennati, A., Gadda, G., Delbono, O. and Yang, J. J. (2011). Design and application of a class of sensors to monitor Ca2+

dynamics in high Ca2+ concentration cellular compartments. Proc Natl Acad Sci U S A **108**(39): 16265-16270.

Taylor, C. W., Rahman, T., Tovey, S. C., Dedos, S. G., Taylor, E. J. and Velamakanni, S. (2009). IP3 receptors: some lessons from DT40 cells. Immunol Rev **231**(1): 23-44.

Teft, W. A., Kirchhof, M. G. and Madrenas, J. (2006). A molecular perspective of CTLA-4 function. Annu Rev Immunol **24**: 65-97.

Thauland, T. J., Koguchi, Y., Dustin, M. L. and Parker, D. C. (2014). CD28-CD80 Interactions Control Regulatory T Cell Motility and Immunological Synapse Formation. J Immunol.

Thestrup, T., Litzlbauer, J., Bartholomaus, I., Mues, M., Russo, L., Dana, H., Kovalchuk, Y., Liang, Y., Kalamakis, G., Laukat, Y., Becker, S., Witte, G., Geiger, A., Allen, T., Rome, L. C., Chen, T. W., Kim, D. S., Garaschuk, O., Griesinger, C. and Griesbeck, O. (2014). Optimized ratiometric calcium sensors for functional in vivo imaging of neurons and T lymphocytes. Nat Methods.

Thomas, D., Tovey, S. C., Collins, T. J., Bootman, M. D., Berridge, M. J. and Lipp, P. (2000). A comparison of fluorescent Ca2+ indicator properties and their use in measuring elementary and global Ca2+ signals. Cell Calcium **28**(4): 213-223.

Thornton, A. M. and Shevach, E. M. (1998). CD4+CD25+ immunoregulatory T cells suppress polyclonal T cell activation in vitro by inhibiting interleukin 2 production. J Exp Med **188**(2): 287-296.

Thornton, A. M. and Shevach, E. M. (2000). Suppressor effector function of CD4+CD25+ immunoregulatory T cells is antigen nonspecific. J Immunol **164**(1): 183-190.

Tian, L., Hires, S. A. and Looger, L. L. (2012). Imaging neuronal activity with genetically encoded calcium indicators. Cold Spring Harb Protoc **2012**(6): 647-656.

Tian, L., Hires, S. A., Mao, T., Huber, D., Chiappe, M. E., Chalasani, S. H., Petreanu, L., Akerboom, J., McKinney, S. A., Schreiter, E. R., Bargmann, C. I., Jayaraman, V., Svoboda, K. and Looger, L. L. (2009). Imaging neural activity in worms, flies and mice with improved GCaMP calcium indicators. Nat Methods **6**(12): 875-881.

Tivol, E. A., Borriello, F., Schweitzer, A. N., Lynch, W. P., Bluestone, J. A. and Sharpe, A. H. (1995). Loss of CTLA-4 leads to massive lymphoproliferation and fatal multiorgan tissue destruction, revealing a critical negative regulatory role of CTLA-4. Immunity **3**(5): 541-547.

Tomiyama, T., Ueda, Y., Katakai, T., Kondo, N., Okazaki, K. and Kinashi, T. (2013). Antigen-specific suppression and immunological synapse formation by regulatory T cells require the Mst1 kinase. PLoS One **8**(9): e73874.

Tsai, K. K. and Daud, A. I. (2015). Nivolumab plus ipilimumab in the treatment of advanced melanoma. J Hematol Oncol **8**: 123.

Tsien, R. Y. (1981). A non-disruptive technique for loading calcium buffers and indicators into cells. Nature **290**(5806): 527-528.

Tsien, R. Y. (1989). Fluorescent probes of cell signaling. Annu Rev Neurosci **12**: 227-253.

Tsien, R. Y., Pozzan, T. and Rink, T. J. (1982). Calcium homeostasis in intact lymphocytes: cytoplasmic free calcium monitored with a new, intracellularly trapped fluorescent indicator. J Cell Biol **94**(2): 325-334.

Vaeth, M., Yang, J., Yamashita, M., Zee, I., Eckstein, M., Knosp, C., Kaufmann, U., Karoly Jani, P., Lacruz, R. S., Flockerzi, V., Kacskovics, I., Prakriya, M. and Feske, S. (2017). ORAI2 modulates store-operated calcium entry and T cell-mediated immunity. Nat Commun **8**: 14714.

Van Belle, T. L., Taylor, P. and von Herrath, M. G. (2009). Mouse Models for Type 1 Diabetes. Drug Discov Today Dis Models **6**(2): 41-45.

van der Vliet, H. J. and Nieuwenhuis, E. E. (2007). IPEX as a result of mutations in FOXP3. Clin Dev Immunol **2007**: 89017.

Vasington, F. D. and Murphy, J. V. (1962). Ca ion uptake by rat kidney mitochondria and its dependence on respiration and phosphorylation. J Biol Chem **237**: 2670-2677.

Vig, M., Beck, A., Billingsley, J. M., Lis, A., Parvez, S., Peinelt, C., Koomoa, D. L., Soboloff, J., Gill, D. L., Fleig, A., Kinet, J. P. and Penner, R. (2006). CRACM1 multimers form the ion-selective pore of the CRAC channel. Curr Biol **16**(20): 2073-2079.

von Andrian, U. H. and Mackay, C. R. (2000). T-cell function and migration. Two sides of the same coin. N Engl J Med **343**(14): 1020-1034.

Vorndran, C., Minta, A. and Poenie, M. (1995). New fluorescent calcium indicators designed for cytosolic retention or measuring calcium near membranes. Biophys J **69**(5): 2112-2124.

Waite, J. C., Vardhana, S., Shaw, P. J., Jang, J. E., McCarl, C. A., Cameron, T. O., Feske, S. and Dustin, M. L. (2013). Interference with Ca(2+) release activated Ca(2+) (CRAC) channel function delays T-cell arrest in vivo. Eur J Immunol **43**(12): 3343-3354.

Walker, L. S. and Sansom, D. M. (2011). The emerging role of CTLA4 as a cell-extrinsic regulator of T cell responses. Nat Rev Immunol **11**(12): 852-863.

Waterhouse, P., Penninger, J. M., Timms, E., Wakeham, A., Shahinian, A., Lee, K. P., Thompson, C. B., Griesser, H. and Mak, T. W. (1995). Lymphoproliferative disorders with early lethality in mice deficient in Ctla-4. Science **270**(5238): 985-988.

Wei, S. H., Parker, I., Miller, M. J. and Cahalan, M. D. (2003). A stochastic view of lymphocyte motility and trafficking within the lymph node. Immunol Rev **195**: 136-159.

Wei, S. H., Safrina, O., Yu, Y., Garrod, K. R., Cahalan, M. D. and Parker, I. (2007). Ca2+ signals in CD4+ T cells during early contacts with antigen-bearing dendritic cells in lymph node. J Immunol **179**(3): 1586-1594.

White, R. J. and Reynolds, I. J. (1996). Mitochondrial depolarization in glutamate-stimulated neurons: an early signal specific to excitotoxin exposure. J Neurosci **16**(18): 5688-5697.

Wildin, R. S. and Freitas, A. (2005). IPEX and FOXP3: clinical and research perspectives. J Autoimmun **25 Suppl**: 56-62.

Williams, R. J. (2006). The evolution of calcium biochemistry. Biochim Biophys Acta **1763**(11): 1139-1146.

Wilson, N. S., El-Sukkari, D. and Villadangos, J. A. (2004). Dendritic cells constitutively present self antigens in their immature state in vivo and regulate antigen presentation by controlling the rates of MHC class II synthesis and endocytosis. Blood **103**(6): 2187-2195.

Wing, J. B. and Sakaguchi, S. (2012). Multiple treg suppressive modules and their adaptability. Front Immunol **3**: 178.

Wing, K., Onishi, Y., Prieto-Martin, P., Yamaguchi, T., Miyara, M., Fehervari, Z., Nomura, T. and Sakaguchi, S. (2008). CTLA-4 control over Foxp3+ regulatory T cell function. Science **322**(5899): 271-275.

Wing, K., Yamaguchi, T. and Sakaguchi, S. (2011). Cell-autonomous and -non-autonomous roles of CTLA-4 in immune regulation. Trends Immunol **32**(9): 428-433.

Wolchok, J. D., Kluger, H., Callahan, M. K., Postow, M. A., Rizvi, N. A., Lesokhin, A. M., Segal, N. H., Ariyan, C. E., Gordon, R. A., Reed, K., Burke, M. M., Caldwell, A., Kronenberg, S. A., Agunwamba, B. U., Zhang, X., Lowy, I., Inzunza, H. D., Feely, W., Horak, C. E., Hong, Q., Korman, A. J., Wigginton, J. M., Gupta, A. and Sznol, M. (2013). Nivolumab plus ipilimumab in advanced melanoma. N Engl J Med **369**(2): 122-133.

Wolchok, J. D., Neyns, B., Linette, G., Negrier, S., Lutzky, J., Thomas, L., Waterfield, W., Schadendorf, D., Smylie, M., Guthrie, T., Jr., Grob, J. J., Chesney, J., Chin, K., Chen, K., Hoos, A., O'Day, S. J. and Lebbe, C. (2010). Ipilimumab monotherapy in patients with pretreated advanced melanoma: a randomised, double-blind, multicentre, phase 2, dose-ranging study. Lancet Oncol **11**(2): 155-164.

Woolf, E., Grigorova, I., Sagiv, A., Grabovsky, V., Feigelson, S. W., Shulman, Z., Hartmann, T., Sixt, M., Cyster, J. G. and Alon, R. (2007). Lymph node chemokines promote sustained T lymphocyte motility without triggering stable integrin adhesiveness in the absence of shear forces. Nat Immunol **8**(10): 1076-1085.

Wu, M. M., Covington, E. D. and Lewis, R. S. (2014). Single-molecule analysis of diffusion and trapping of STIM1 and Orai1 at endoplasmic reticulum-plasma membrane junctions. Mol Biol Cell **25**(22): 3672-3685.

Yamaguchi T, W. J., Sakaguchi S. (2011). Two modes of immune suppression by Foxp3(+) regulatory T cells under inflammatory or non-inflammatory conditions. Semin Immunol **23**(6): 424-430.

Yanez, M., Gil-Longo, J. and Campos-Toimil, M. (2012). Calcium binding proteins. Adv Exp Med Biol **740**: 461-482.

Yeromin, A. V., Zhang, S. L., Jiang, W., Yu, Y., Safrina, O. and Cahalan, M. D. (2006). Molecular identification of the CRAC channel by altered ion selectivity in a mutant of Orai. Nature **443**(7108): 226-229.

Zariwala, H. A., Borghuis, B. G., Hoogland, T. M., Madisen, L., Tian, L., De Zeeuw, C. I., Zeng, H., Looger, L. L., Svoboda, K. and Chen, T. W. (2012). A Cre-dependent GCaMP3 reporter mouse for neuronal imaging in vivo. J Neurosci **32**(9): 3131-3141.

Zhang, F., Aravanis, A. M., Adamantidis, A., de Lecea, L. and Deisseroth, K. (2007). Circuit-breakers: optical technologies for probing neural signals and systems. Nat Rev Neurosci **8**(8): 577-581.

Zhang SL, Y. A., Zhang XH, Yu Y, Safrina O, Penna A, Roos J, Stauderman KA, Cahalan MD. (2006). Genome-wide RNAi screen of Ca(2+) influx identifies genes that regulate Ca(2+) release-activated Ca(2+) channel activity. Proc Natl Acad Sci USA **103**(24): 9357-9362.

Zhang, S. L., Yu, Y., Roos, J., Kozak, J. A., Deerinck, T. J., Ellisman, M. H., Stauderman, K. A. and Cahalan, M. D. (2005). STIM1 is a Ca2+ sensor that activates CRAC channels and migrates from the Ca2+ store to the plasma membrane. Nature **437**(7060): 902-905.

Zhao, Y., Araki, S., Wu, J., Teramoto, T., Chang, Y. F., Nakano, M., Abdelfattah, A. S., Fujiwara, M., Ishihara, T., Nagai, T. and Campbell, R. E. (2011). An expanded palette of genetically encoded Ca(2)(+) indicators. Science **333**(6051): 1888-1891.

Zou, J., Hofer, A. M., Lurtz, M. M., Gadda, G., Ellis, A. L., Chen, N., Huang, Y., Holder, A., Ye, Y., Louis, C. F., Welshhans, K., Rehder, V. and Yang, J. J. (2007). Developing sensors for real-time measurement of high Ca2+ concentrations. Biochemistry **46**(43): 12275-12288.